UNIVERSITY OF CALIFORNIA

Santa Barbara

Roles of the Unfolded Protein Response in the Mammalian Cell Cycle

A Thesis submitted in partial satisfaction of the

requirements for the degree Master of Arts

in Molecular, Cellular and Developmental Biology

by

Sabrina C. Solley

Committee in charge

Professor Diego Acosta-Alvear, Chair

Professor Kathy Foltz

Professor Brooke Gardner

September 2020

The thesis of Sabrina C. Solley is approved.

_____
Kathy Foltz

_____
Brooke Gardner

_____
Diego Acosta-Alvear, Committee Chair

June 2020

Roles of the Unfolded Protein Response in the Mammalian Cell Cycle

by

Sabrina C. Solley

ACKNOWLEDGEMENTS

First and foremost, I'd like to take the opportunity to thank my PI and committee chair Dr. Diego Acosta-Alvear. Your support, guidance and mentorship throughout my time in your lab have cultivated my scientific curiosity and dramatically altered how I not only approach scientific challenges, but my own life. Your patience in teaching me how to dissect and address biological questions has been invaluable. To Dr. Carolina Arias, thank you for serving as such an excellent role model and bonus mentor. I cherish all of our late-night chats and will take all your advice and anecdotes to heart in the future. To Dr. Max Wilson, I am grateful for the scientific engagement, advice and support. And to my committee members Dr. Kathy Foltz and Dr. Brooke Gardner, thank you for all of the helpful comments, constructive feedback and guidance in writing this story.

I am grateful to Dr. Francesca Zappa, Soham Chowdhury, Lauren Hocker, TJ Sears and Lotte Russo, whom all in some shape or form helped contribute to the work presented in this thesis. The combined effort of all these people, especially Franci, helped me to bring the project from my mind into reality. An additional thank you to research specialist Dr. Fritzi-Braig Karzig for her molecular biology guidance, support and friendship. I am also thankful for the entirety of the Acosta-Alvear lab not mentioned above, including Dr. Jose Carlos Ponce Rojas, Nerea Muniozguren, Mike Costello, and Taivan Batjargal. The collaborative environment and feedback provided in subgroup meetings, lab meetings and lab retreats were crucial in progressing my work.

To Dr. Chris Richardson and Cassidy Arnold, I am thankful for your technical support, insight, knowledge and access to flow cytometry and FACS instruments which were necessary to this work.

A big thank you to my friends in the MCDB department, Duncan, Guillermo, Chinmay, Kevin, Cat, and Michelle. Thank you for engaging in science with me and providing me opportunities to thoroughly enjoy my time as a graduate student in Santa Barbara. I will greatly miss all of you and the time we spent together working late in the lab, grabbing dinner, or both in succession.

Thank you to my special friend Chris Kirby, who has been my rock of support throughout my master's studies. I am so appreciative of your love and encouragement as I navigated the winding turns of this work.

Finally, I would like to dedicate this work to my family: my mom, my dad, Amanda, Sean, Savta, Mormor, Morfar, and all my family in Denmark. Thank you for supporting my dreams to pursue science and for being there for me, always. Without you this work would not be feasible.

ABSTRACT

Roles of the Unfolded Protein Response in the Mammalian Cell Cycle

by

Sabrina C. Solley

Throughout the cell cycle, genome duplication is coordinated with the multiplication and growth of organelles, which requires membrane biosynthesis at the endoplasmic reticulum (ER). By this reasoning, ER growth and increased ER function would be a pre-requisite for cell division. Because the unfolded protein response (UPR)—a fundamental homeostatic mechanism that maintains ER integrity—increases the size and protein-processing capacity of the ER, I reasoned that it may oversee ER physiology during the cell cycle. To investigate ER growth and activation of the UPR during the cell cycle, I optimized and characterized a well-described fluorescent reporter of cell cycle progression, known as the FAST-FUCCI system. This live-cell reporter enabled me to separate G_1 and S/G_2 cell populations by fluorescence activated cell sorting (FACS). My data show that mammalian cells increased in size and granularity during interphase. These hallmarks were correlated with an increase in ER-resident protein content, suggesting that the ER enlarges in preparation for cell division. Moreover, I found that inhibition of IRE1 via pharmacological agents delayed progression through the G_1/S boundary. While

investigating a plausible mechanism that could regulate UPR activity during the cell cycle, I identified PKMYT1, an ER- and Golgi apparatus-associated G_2/M cell cycle checkpoint kinase, in a candidate-based approach. I found that IRE1 activity is suppressed by PKMYT1, suggesting that PKMYT1 exerts regulatory control over IRE1 prior to cell division. Preliminary data suggests that PKMYT1 and IRE1 do not physically interact, which suggests regulation via an unidentified intermediate or a transcriptomic regulation by downstream transcription factors, such as XBP1s. Taken together, my results provide evidence to suggest that mammalian cells engage a physiological UPR involving IRE1 signaling during cell cycle progression.

TABLE OF CONTENTS

LIST OF FIGURES

I. Introduction

Progression through the cell cycle requires integration of information about genome integrity, nutrient availability, cell size, and organelle content at discrete cell cycle checkpoints to ensure successful cell division and organelle inheritance. The endoplasmic reticulum (ER) is a structurally complex organelle that performs critical cellular functions, including protein folding and maturation, lipid and membrane biogenesis, and maintenance of calcium homeostasis. In addition, the ER serves as a hub for organellar intercommunication as it interacts with all organelles in the cell. Despite these fundamental biological roles, the mechanisms controlling ER growth and inheritance during the cell cycle have been largely overlooked. The unfolded protein response (UPR) is a fundamental homeostatic mechanism that oversees ER integrity and adjusts ER function according to the needs of the cell. A role for the UPR in cytokinesis has been described in budding yeast, and activation of the UPR results in delayed cell cycle progression in mammalian cells. However, the precise roles of the UPR in regulating the cell cycle of mammalian cells are unknown. Here I provide background information on the mammalian cell cycle and its regulation, on the ER structure and function, and provide links between ER physiology and cell cycle progression in mammalian cells.

A. The mammalian cell cycle

Cell division requires coordination of many signaling events to compute a single output: to divide or not to divide. Cells integrate information from intracellular and extracellular cues to decide how and if they will make the commitment to divide (Campisi and D'Adda Di Fagagna, 2007; Hernandez-Segura et al., 2018). Cell division can yield daughter cells of different sizes by asymmetric division or equivalent sizes by symmetric division. Both types of cell division have inherent physiological importance. Asymmetric divisions are required for establishing cellular identities during differentiation, whereas symmetric divisions play a role in the maintenance of cell pools (Shahriyari and Komarova, 2013).

Many signaling networks intersect at the cell cycle, including responses to DNA damage, oxidative stress, nutrient sensing, and cell size control. This vast signaling network interconnectivity underscores the highly complex regulation of the cell cycle (Ishikawa K., 2007; Macip et al., 2006; Rohde et al., 2001). Deviations of this multilayered regulatory control result in disease, as occurs in cancer when cells fail to control cell cycle progression (Hanahan and Robert, 2011). Often times, cancer driver mutations occur in cell cycle-related genes (Collins et al., 1997). However, they can also occur in genes not directly related to the cell cycle, giving rise to non-oncogene addiction; for example, reliance on genes that control signaling pathways that respond to hypoxia and nutrient deprivation, which can give tumors a growth advantage before the onset of angiogenesis (Dewhirst et al., 2008; Solimini et al., 2007). Therefore, a detailed understanding how signaling pathways

intersect with regulatory components of the cell cycle is essential if we are to understand how these connections become dysregulated in cancer.

1. Cell cycle regulation

The mammalian cell cycle is comprised of four stages: G_1 (Gap 1), S (Synthesis), G_2 (Gap 2), and M (Mitosis) (Alberts et al., 2004) **(Figure 1).** Each of these stages is characterized by well-established molecular events that ensure dividing cells give rise to two viable daughter cells (Alberts et al., 2004). In G_1, the cell monitors internal and external stimuli prior to committing to cell division (Gérard and Goldbeter, 2014; Sherr, 1994). These stimuli are of varied nature. For example, in the context of development, spatial organization and contact inhibition can alter proliferative outcome (Gérard and Goldbeter, 2014). In early G_1 the cell evaluates nutritional status and growth factor availability, which will be essential prior to division (Alberts et al., 2004). If appropriate conditions are not met at this so-called 'restriction point', cells enter quiescence, also known as G_0, a reversible state where they can remain dormant until conditions favorable to division arise (Pardee, 1974).

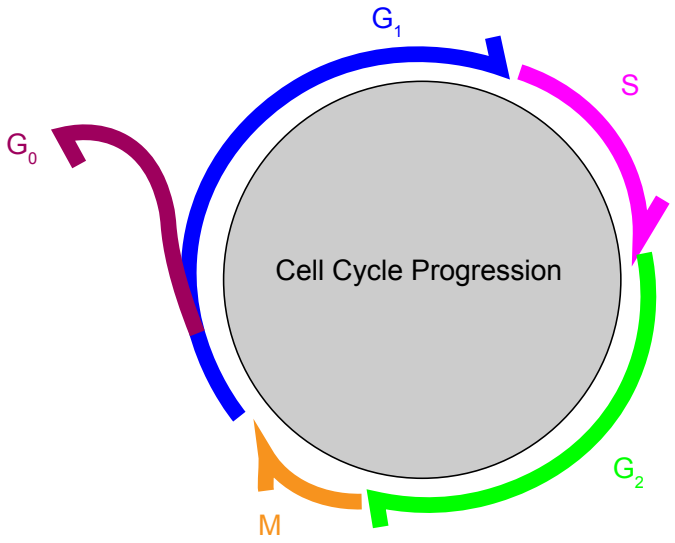

Figure 1. The mammalian cell cycle. Stages of the cell cycle, also indicating where cells enter quiescence if nutrient conditions are not met.

Once all conditions permissive to division are met in G_1, cells proceed to S phase. In S phase, the cell duplicates its genome and scans for errors in DNA replication to ensure the genome is copied with fidelity (Alberts et al., 2004). Following DNA replication, the cell enters G_2, where it continues to grow while it monitors genome integrity (Smits and Medema, 2001). The main requirement for cells to transition from G_2 to M is proper duplication of the genome (Nurse, 1994). However, recent work reveals the importance of G_2 in preparing other cellular components, such as the plasma membrane, for partitioning prior to mitosis (Denz et al., 2017). The transition between G_2 and M requires preparation for fragmentation of the nuclear envelope and rearrangement of the cytoskeleton which is required to segregate chromatids during mitosis (Smits and Medema, 2001). Mitosis thus relies on interconnections between cytoskeleton and chromosomes. However, it also requires organelles to partition amongst the two daughter cells. The M phase is comprised of five steps: prophase, metaphase, anaphase and telophase, and culminates with cytokinesis. During prophase, the chromatids condense. Formation of the mitotic spindle in metaphase allows for segregation of the chromatids in anaphase. Reformation of two daughter nuclei in telophase is coupled to a complete segregation of all cellular components by cytokinesis (McIntosh, 2016). With such distinct cellular events occurring in each phase of the cell cycle, it thus follows that that each phase must be clearly demarcated at a molecular level. Indeed, each phase of the cell cycle is characterized by the oscillating expression of specific proteins known as cyclins (Malumbres and Barbacid, 2001). (**Figure 2**).

Cyclins are proteins that activate cyclin-dependent kinases (CDKs), which drive progression through the cell cycle (Kobayashi et al., 1992; Lees and Harlow, 1993). Each cyclin/CDK complex is specific to a temporal state in the cell cycle and regulates the cellular events necessary in order to progress to the next phase (Gerard and Goldbeter, 2009; Meyerson and Harlow, 1994). The G_1 stage of the cell cycle is governed by the actions of Cyclin D1/CDK4 or Cyclin D1/CDK6 (Satyanarayana and Kaldis, 2009). Cyclin D1 expression is induced when adequate space and nutrients are available (Assoian and Schwartz, 2001; Schwartz and Assoian, 1996). The Cyclin D1/CDK complexes phosphorylate the retinoblastoma tumor suppressor protein (Rb), which in turn derepresses the E2F transcription factors (Kato et al., 1993; Satyanarayana and Kaldis, 2009; Weinberg, 1995). E2Fs drive transcription of cyclins E and A, which are required for entry into S phase (Jeffrey et al., 1995; Sherr, 1996). Cyclins E and A complex with CDK2 to activate the DNA replication machinery (Coverley et al., 2002). Following complete replication of the genome and even after entrance into G_2, cyclin A, together with CDK1 continues to promote progression through the cell cycle, and induces the expression of cyclin B (Jeffrey et al., 1995). The cyclin B/CDK1 complex is also known as the maturation promoting factor (MPF), as it promotes entrance into mitosis (Maller et al., 1989).

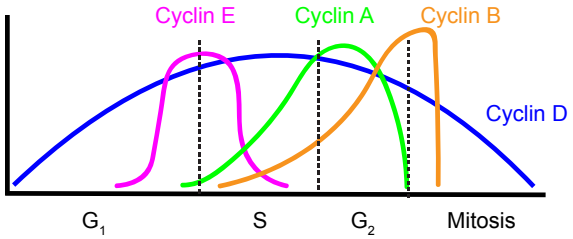

Figure 2. Mammalian cyclin expression. Expression patterns of each of the cyclins over the cell cycle.

Coordination of cyclin expression to ensure the formation of correct cyclin/CDK complexes at precise stages of the cell cycle involves multiple layers of regulation. Such regulatory control is exerted by CDK inhibitors. There are two families of CDK inhibitors, the INK4 derived CDK inhibitors and Cip/Kip inhibitors (Besson et al., 2008). INK4 and Cip/Kip inhibitors bind cyclin/CDK complexes to inactivate the kinase activity of CDKs (Hunter and Pines, 1994). Both families of CDK inhibitors are often activated in response to stress, such as viral infection or DNA damage (Besson et al., 2008; Gartel and Tyner, 1999; Sherr and Roberts, 1999). The INK4 family of CDK inhibitors each inhibit specific cyclin/CDK complexes, while the Cip/Kip inhibitors are more promiscuous. For example, INK4-derived CDK inhibitors are specific to Cyclin D/CDK4 or Cyclin D/CDK6 complexes, whereas $p21^{cip}$ inhibits multiple different cyclin/CDK complexes (Cánepa et al., 2007; Hunter and Pines, 1994).

Another layer of regulation of cell cycle progression depends on phosphorylation of the CDKs in the cyclin/CDK complex (Morgan, 1995). The best-known example of this mode of regulation is the regulation of the cyclin B/CDK1 complex by the kinases CAK, Wee1 and PKMYT1. Upon entrance into G_2, the cyclin B/CDK1 complex is targeted by CAK, which phosphorylates threonine 161 in CDK1 (Ducommun et al., 1991). Phosphorylation at Thr161 is necessary for the MPF to initiate mitosis (Fesquet et al., 1993). However, CDK1 can also be phosphorylated to prevent mitotic entry. The main CDK1 kinases acting to prevent entry into mitosis belong to the Wee1 family of kinases, which is comprised of Wee1, Wee1B and PKMYT1 (Schmidt et al., 2017a). Wee1 kinases phosphorylate

CDK1 in the cyclin B/CDK1 complex arresting cells at the G_2/M boundary upon genotoxic stress (Liu et al., 1997a; Russell and Nurse, 1987). If the stress can be resolved, cdc25 phosphatases dephosphorylate CDK1 and restore the cyclin B/CDK1 complex to its activate state, promoting progression through mitosis (Hoffmann, 2000). CAK, Wee1 and PKMYT1 exert regulatory control over the G_2/M transition, constituting a checkpoint that enables cells to ensure genome integrity prior to mitosis.

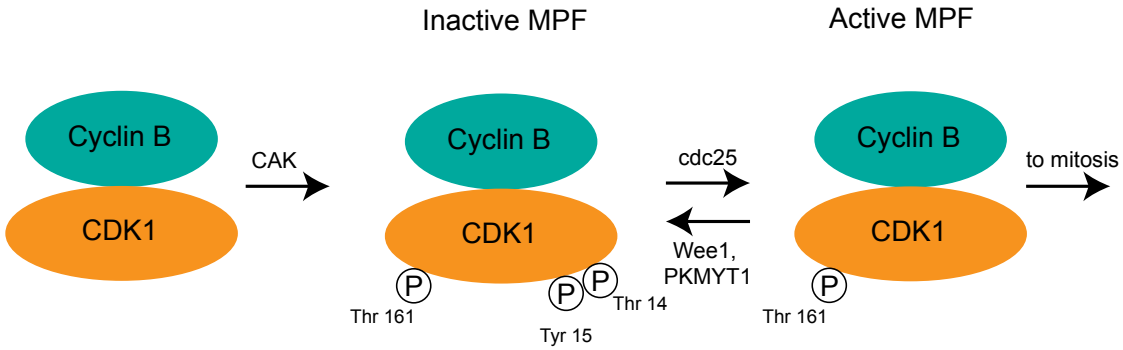

Figure 3. Regulation of the G_2/M transition by CDK1 kinases. CAK is a CDK1-activating kinase that promotes entrance to mitosis by phosphorylating CDK1 at Thr-161. Wee1 and PKMYT1 kinases are inhibitory CDK1 kinases that prevent mitotic entry by phosphorylating at Tyr 15 (both) and Thr14 (PKMYT1). The phosphatase cdc25 removes the inhibitory phosphorylation modifications to allow mitotic entry.

2. Cell size and organelles throughout the cell cycle

Successful cell divisions require that each daughter cell inherits enough material—genome and organelles—to propagate on its own (Warren and Wickner, 1996). This process requires enlargement of the cell and duplication of its contents prior to partitioning of cellular components at mitosis (Warren and Wickner, 1996).

Cell size is a crucial factor in determining cell division in prokaryotes and single cell eukaryotes, as well as in animal cells (Fantes and Nurse, 1977; Killander and Zetterberg, 1965a, b). Two models describing cell sizing exist, the 'adder' model and the 'sizer' model. The adder model suggests that regardless of starting point, cells balance the mass gained and the mass lost as a function of cell division (Conlon and Raff, 2003). The sizer model suggests that cells actively sense their size and accommodate cell growth to their current needs (Lloyd, 2013). Regardless, it has remained elusive how cells detect their size and integrate this information into signaling pathways such as the ones that govern cell division. Previous observations suggest that size uniformity of cells in populations can be explained by cell size sensing mechanisms that increase the growth rate of small cells and decrease the growth rate of large cells (Ginzberg et al., 2018). However, other observations show that increases in cell volume are independent of a cell's 'birth' size (Cadart et al., 2018).

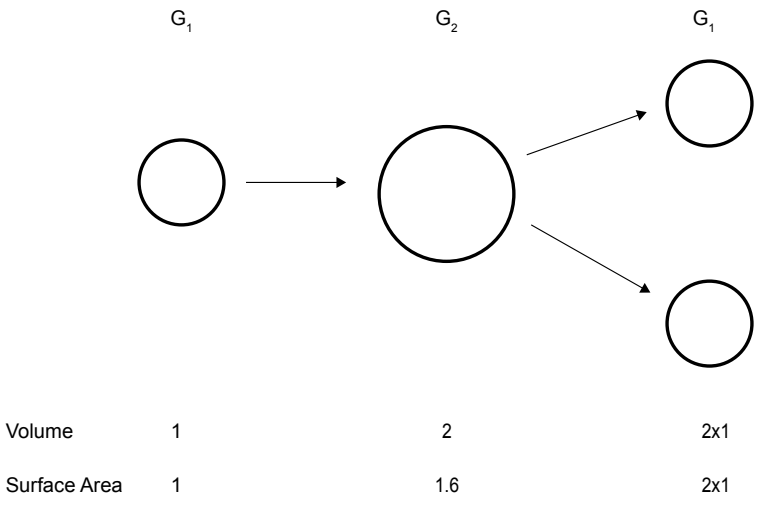

Figure 4. Proposed model for cellular growth. Model proposed by Graham et al, 1973 for plasma membrane assembly and growth during the cell cycle.

Duplication of the genome is essential for cell division. Therefore, the cell cycle phases have been defined taking this event as a benchmark (see **Figure**

1). By first principles, the duplication of the genome suggests that other components of the cell also duplicate. Indeed, a duplication of cellular contents was observed early on by microscopy and analysis of plasma membrane composition (protein, carbohydrate and lipid content), and has since been a source for multiple investigations (Graham et al., 1973; Wilson, 1947) (**Figure 4**). For organelles in multiple copies, stochastic models of organelle inheritance ensure that approximately equipartitioning occurs (Birky, 1983; Warren and Wickner, 1996). Partitioning of endosomes and lysosomes is ordered, and also follows a stochastic model (Bergeland et al., 2001). However, single-copy organelles, such as the Golgi apparatus or the ER, require fragmentation prior to partitioning. In contrast to multiple copy organelles, it has been shown that post fragmentation, the Golgi apparatus is able to associate with the mitotic spindle in an ordered model of division (Shima et al., 1998). The reassembly of the Golgi apparatus post-mitosis has been mechanistically linked to the cell cycle kinase PKMYT1, whose regulatory control on the MPF might enable suppression of MPF immediately following mitosis (Nakajima et al., 2008b).

Cells employ numerous cell-cycle checkpoints to ensure faithful duplication and inheritance of the genome (Ishikawa K., 2007). There is growing evidence that the same or additional checkpoints are employed to ensure the accurate partitioning of single-copy organelles, such as the Golgi-apparatus (Colanzi et al., 2007). Considering the intimate connection between the ER and the Golgi apparatus, it is surprising that an ‘ER checkpoint’ has not been described.

B. The endoplasmic reticulum

1. Structure of the endoplasmic reticulum

The ER is the largest, single contiguous organelle in the eukaryotic cell (Alberts et al., 2004). Two topological domains of the ER are recognized, the nuclear envelope (NE), which separates the genomic content of the cell from the cytoplasm, and the peripheral ER (Hetzer et al., 2005). The NE is a double lipid bilayer with an inner nuclear membrane (INM) facing the nucleus and an outer nuclear membrane (ONM) that is contiguous with the peripheral ER (Hetzer et al., 2005). The INM displays distinct biochemical and biophysical features that enable interactions with nuclear lamina and anchoring of chromatin (Gerace et al., 1978). The INM and ONM interconnect at the nuclear pores, highly regulated macromolecular assemblies that establish gates that allow transport of cellular components in and out of the nucleus (Franke et al., 1981; Kabachinski and Schwartz, 2015). The INM and ONM differ in their protein composition. INM protein content is established by selective retention mechanisms, whereas the ONM has a protein composition that is similar to that of the peripheral ER (Ellenberg et al., 1997; Gerace and Burke, 1988; Newport and Forbes, 1987; Soullam and Worman, 1995).

The peripheral ER can be further subdivided structurally into sheets, which are flat cisternae that are typically associated with many ribosomes, and tubules, which are branching tube-like structures that interconnect the ER throughout the cell (Shibata et al., 2010; Shibata et al., 2006). The interconnections between ER sheets have been described as ‘helical ramps’ that maximize functional surface

area of the ER (Terasaki et al., 2013). By contrast to ER sheets, ER tubules tend to not associate with ribosomes, which originally led to sheets and tubules to be classified as the rough and smooth ER, respectively (Shibata et al., 2006). Despite differing morphologies, the thickness between the lipid bilayers in both tubular and cisternal structures remains consistent, which suggest dynamic structural interchange can occur (West et al., 2011). The location, quantity, and organization of sheets and tubules varies by cell type. For example, in dedicated secretory cells, such as plasma cells making antibodies, the ER network is extended and consists mostly of ribosome-studded sheets (Gass, 2004; Kirk et al., 2010). In hepatocytes, the ER network is largely tubular, as they need to accommodate for increased lipid production for lipoprotein complexes, which mostly occurs in ER regions not studded with ribosomes (Alberts et al., 2004; Loud, 1968).

Because of its large size, the ER establishes physical and functional contact sites with many other organelles and cellular structures, including mitochondria, endosomes, peroxisomes, the plasma membrane, the cytoskeleton and even membrane-less organelles. These contact sites control a wide array of cellular functions that are critical for coordinating cellular and organellar growth. For example, both the ER and mitochondria function to generate lipids for the cell (Jelsema and Morré, 1978). Contact sites between the ER and mitochondria might serve as a bridge for lipid intermediates during lipid biogenesis (Kornmann et al., 2009). Other work also highlights the importance of ER-mitochondrial contacts in mitochondria division (Friedman et al., 2011). Similar to what has been observed in mitochondria, the ER can also spatiotemporally control endosome fission (Rowland

et al., 2014). ER-peroxisome contact sites are important in ensuring peroxisomal inheritance in budding yeast (Knoblach et al., 2013). The ER also contacts the plasma membrane, which is implicated in phosphatidylinositol signaling and calcium ion exchange (Manford et al., 2012). ER-plasma membrane contact sites also engage filamin A to maintain calcium reserves and assist in cell motility (Urra et al., 2018; van Vliet et al., 2017). In addition, the ER is intimately associated with microtubules and these ER-microtubule contacts are important for ER growth and organization, even though they are dispensable for formation of the ER network *in vitro*. (Dreier and Rapoport, 2000; Terasaki, 1986). The peripheral ER can associate with microtubules by three mechanisms, all of which might be important for a variety of cellular functions (Waterman-Storer and Salmon, 1998). The ER can slide along the length of microtubules, move at a fixed association point with microtubules, or associate with microtubule tips via the 'tip attachment complex (TAC) mechanism' (Waterman-Storer and Salmon, 1998). Even though microtubule dynamics can alter ER morphology (Terasaki, 1986) and despite the aforementioned physical associations, the physiological roles ER-microtubule contacts remain unexplored. More recently, an association between the ER and membrane-less organelles, including p-bodies and stress granules, has been described (Lee et al., 2020) The ER is also closely interconnected with the Golgi apparatus in the secretory pathway. The ER Golgi intermediate compartment (ERGIC) is a transitional compartment between the ER and Golgi as proteins get modified and processed for export from the ER to the Golgi apparatus (Appenzeller-Herzog, 2006).

The structure and dynamics of the ER are altered during mitosis to accommodate for genome and organelle inheritance. NE envelope breakdown during mammalian mitotic prophase is important for segregation of chromatids into daughter cells (Güttinger et al., 2009). Mechanisms of peripheral ER fragmentation and partitioning are yet to be described, but the mitotic structure of the ER has been a source of debate. Opposing lines of thought existed regarding whether the ER was primarily composed of tubules or sheets during mitosis. However, recent work suggests that the ER is primarily composed of sheets during mitosis (Anderson and Hetzer, 2008; Lu et al., 2009; Lu et al., 2011; Puhka et al., 2007). Changes in ER morphology during mitosis are accompanied by changes in ER protein localization. Proteins that primarily localize and promote formation of tubules are equally distributed in the ER during mitosis (Lu et al., 2009). In agreement with this notion, proteins that localize to the INM also are not restricted to a specified location during mitosis (Anderson and Hetzer, 2008; Lu et al., 2009). Mechanisms by which ER structure is modulated during mitosis have not been well explored, and homogeneity in ER protein localization during mitosis has been the focus of only a few studies. Evidence suggests REEP3/4, which functions to promote tubule formation, undergo phosphorylation during mitosis which suppresses their activity and enables the transition between tubules and sheets necessary for fragmentation of the ER (Schlaitz et al., 2013). Work involving CLIMP63, which functions to promote sheet formation, shows that mitotic phosphorylation might serve to prevent ER association with microtubules (Vedrenne, 2005). More work is required to understand the regulation and the implications of structural changes of the ER

during mitosis, and how these changes impact fragmentation, correct partitioning and reformation of the ER upon mitotic exit.

2. Functions of the endoplasmic reticulum

The vast size and interconnectivity of the ER with almost every single organelle suggest the ER may be a fundamental signaling hub which coordinates many cellular processes. The ER is the first compartment of the endomembrane system, and the site of protein folding for all proteins that comprise the secretory apparatus (Alberts et al., 2004). Proteins destined to the endomembrane system are targeted to the ER by hydrophobic N-terminal signal peptides (Blobel and Dobberstein, 1975). These peptides are recognized by the signal recognition particle SRP, which pauses translation and recruits the translating ribosome to the ER membrane via SRP-SRP receptor interactions (Walter and Blobel, 1982). Docking on the ER protein translocator (the Sec61 complex) displaces the SRP, allowing the ribosome to resume translation while simultaneously driving translocation into the ER lumen via the Sec61 complex in a process known as co-translational translocation (Walter and Blobel, 1981). This process is responsible for synthesis of about one third of the total proteome (Uhlén et al., 2015). The ER also ensures correct folding of all proteins that enter the secretory pathway via chaperones and protein folding enzymes, or ‘foldases’ (Braakman and Hebert, 2013). Proteins that do not fold correctly are targeted for degradation via a process known as ER-associated degradation (ERAD) (Qi et al., 2017).

The ER is also the site of lipid biogenesis and it harbors lipid metabolism enzymes that are essential for biogenesis of lipids found in all cellular membranes, including phosphatidylcholine, phosphatidylserine, phosphatidylethanolamine, phosphatidylinositol, basic sphingolipids and cholesterol (Jacquemyn et al., 2017). Lipid heterogeneity across biological membranes lends itself to specialized signaling by generating different biophysical properties depending on lipid composition, such as the case for the lipid raft (Munro, 2003). In addition to membrane biogenesis, the ER also is the site of lipid droplet formation, which are lipid monolayer enclosed vesicles that stock neutral lipids which can be used as energy stores (Olzmann and Carvalho, 2019).

Calcium ions are key regulators of essential signaling events in multicellular organisms, including muscle contraction in skeletal cells and neurotransmitter release in neurons (Koch, 1990; Mulkey and Zucker, 1991). The ER functions as a calcium reserve for the cell and is able to release calcium ions when cytosolic levels are depleted (Carreras-Sureda et al., 2018; Marchi et al., 2018). If levels of calcium in the cytosol are too high, ER transmembrane proteins known as SERCA pumps drive calcium reuptake into the ER (Chemaly et al., 2018; Periasamy and Kalyanasundaram, 2007).

3. The unfolded protein response

The unfolded protein response (UPR) is a collection of signaling pathways that constantly monitors and adjusts ER function according to need (Walter and Ron, 2011). The mammalian UPR is comprised of three signaling branches governed by

transmembrane sensor proteins, IRE1, PERK, and ATF6, which detect protein folding and lipid bilayer imbalances in the ER (Walter and Ron, 2011) (**Figure 5**). The activation of these sensors is largely thought to be fine-tuned by reversible association and dissociation with the ER chaperone BiP (Bakunts et al., 2017; Kopp et al., 2019; Shen et al., 2005) . BiP, which is induced by the UPR, provides a feedback loop to adjust the UPR threshold and control adaptation to ER stress (Vitale et al., 2019). Each UPR stress sensor transmits signals from inside the lumen of the ER to the nucleus via upregulation of transcription factors (Walter and Ron, 2011). Together, these transcription factors reprogram gene expression, allowing the cell to increase the ER protein processing and degradative capacities, as well as by physical expansion of the ER (Travers et al., 2000).

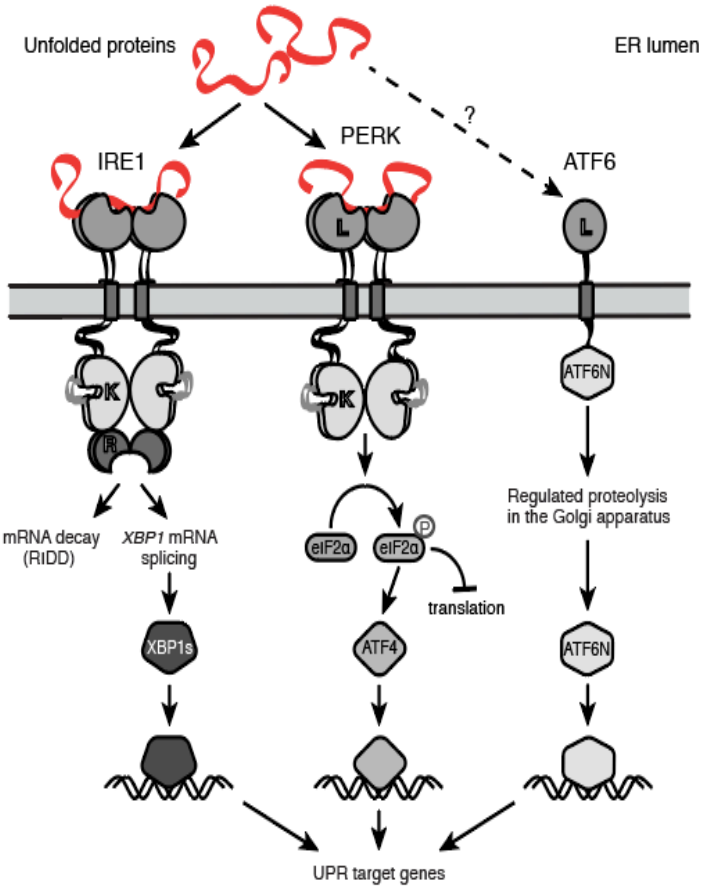

Figure 5. The mammalian UPR. Figure adapted from CSHL review. (Karagoz et al., 2019)

IRE1, the most ancestral of the UPR sensors is a bifunctional kinase/endoRNase and is conserved from yeast to animals (Cox et al., 1993). IRE1 possesses a sensor domain in the lumen of the ER which detects unfolded proteins by direct binding (Credle et al., 2005; Karagöz et al., 2017). It has also been proposed that reversible dissociation of the ER chaperone BiP from IRE1's lumenal domain fine-tunes its activity (Pincus et al., 2010). Upon detection of unfolded proteins, IRE1 oligomerizes in the plane of the membrane, leading to trans-autophosphorylation and allosteric activation of the RNase domain (Korennykh et al., 2009). IRE1's RNase activity cleaves 7-mer loop hairpins that conform to the consensus CNGNNGN motif (Gonzalez et al., 1999; Korennykh et al., 2011). In its best understood mechanism, mammalian IRE1 excises an unconventional intron from the *XBP1* mRNA generating a frameshift that allows translation of a potent transcription factor, *XBP1s* ("s" for spliced) (Uemura et al., 2009). Both IRE1 and mRNA structure contribute to catalysis, as intron junction cleavage and intron ejection require conformational changes in an RNA "zipper" structure (Peschek et al., 2015). The resulting exons are joined by the tRNA ligase RTCB (Kosmaczewski et al., 2014; Lu et al., 2014b). XBP1s upregulates genes involved in almost every aspect of ER function, such as chaperones, foldases, translocation machinery, and genes involved in ERAD (Lee et al., 2003). Upregulation of these genes increases the folding capacity of the ER, allowing the cell to cope with unfolded protein stress (Calfon et al., 2002; Lee et al., 2003).However, XBP1s also drives the expression of many other genes, including some involved in DNA damage and repair (Acosta-Alvear et al., 2007). Overexpression of XBP1s also enlarges the ER, which

together with upregulation of chaperones and foldases, increases the ER protein folding capacity (Sriburi et al., 2004).

Metazoan IRE1 also cleaves ER-bound mRNAs in a process known as Regulated IRE1-Dependent Decay of mRNAs, or RIDD (Hollien and Weissman, 2006). RIDD is thought to alleviate protein folding load in the ER by degrading mRNAs encoding ER clients (Hollien et al., 2009). However, this view of a passive degradative mechanism has been challenged recently. RIDD of a single mRNA, encoding the lysosome trafficking factor *Blos1* is sufficient to increase the cell's protein turnover capacity by repositioning lysosomes and resolving protein aggregation (Bae et al., 2019). Additionally, new results show RIDD of *Ppp2r1a* and *Ruvbl1,* two mRNAs encoding DNA repair proteins, hinting at specific RIDD mechanisms that serve purposes other than relieving secretory load (Dufey et al., 2020).

Recent work reports that IRE1 is able to detect perturbations in lipid homeostasis via its transmembrane domain (Halbleib et al., 2017; Volmer et al., 2013). In this mechanism, IRE1 senses lipid bilayer stress via distortion of its amphipathic transmembrane helix within the lipid bilayer (Halbleib et al., 2017). In yeast, mutations in phosphatidylcholine synthesis genes have been shown to activate IRE1 via lipid bilayer stress (Jonikas et al., 2009). Interestingly, IRE1 activation by lipid bilayer stress or by unfolded proteins leads to differential transcriptional programs (Ho et al., 2020).

PERK is a stress sensor kinase that, like IRE1, oligomerizes in the plane of the membrane and auto-phosphorylates upon detection of unfolded proteins

(Harding et al., 1999). PERK also phosphorylates the alpha subunit of the eukaryotic translation initiation factor 2 (eIF2a) (Marciniak et al., 2006; Prostko et al., 1993). PERK is one of four stress sensor kinases in the integrated stress response (ISR), which is a central homeostatic mechanism that regulates protein synthesis according to need. The other three ISR kinases are PKR, GCN2, and HRI, which detect double-stranded RNA (PKR), amino acid deprivation (GCN2), and heme deficiency, oxidative stress and mitochondrial stress (HRI) (Costa-Mattioli and Walter, 2020). All ISR kinases converge on the phosphorylation of the alpha subunit of the translation initiation factor eIF2, which is required to initiate protein synthesis (Naveau et al., 2013). Phosphorylation of eIF2a leads to a global translation attenuation, which is paradoxically coupled to the selective translation of mRNAs that contain regulatory upstream open reading frames in their 5' UTRs, such as *ATF4* (Vattem and Wek, 2004). ATF4 is a bZIP transcription factor that upregulates many genes involved in increasing the biosynthetic capacity of the cell, but also the pro-apoptotic transcription factor CHOP (Han et al., 2013b).

Unlike IRE1 and PERK, which are kinases, ATF6 is a membrane tethered transcription factor (Yoshida, 1998). Even though the exact mechanism of ATF6 activation is still unknown, current evidence suggest it acts as a redox sensor (Nadanaka et al., 2007). Activation of ATF6 requires trafficking to the Golgi apparatus, where it undergoes proteolytic cleavage by resident S1P and S2P proteases (Haze et al., 1999; Ye et al., 2000). This regulated intramembrane proteolysis releases the cytosolic half of ATF6 (ATF6-N, for N-terminal) from the membrane (Yoshida, 1998). ATF6-N is a bZIP transcription factor that upregulates

UPR target genes, which include XBP1 and ER chaperones, such as BiP (Lee, 2002). Combinatorial regulation of UPR target genes by heterodimerization of ATF6-N and XBP1s transcription factors amplifies the pro-survival stress response through upregulation of genes involved in protein folding, ERAD and lectin folding (Shoulders et al., 2013; Yamamoto et al., 2007).

If ER stress cannot be mitigated, the UPR initiates apoptosis through upregulation of death receptor 5 (DR5) by CHOP, downstream of PERK (Lu et al., 2014a). Induction of the DR5 mRNA by CHOP is counterbalanced by its degradation by RIDD (Lu et al., 2014a). This mechanism establishes a molecular clock controlled by opposing actions of IRE1 (pro-survival) and PERK (pro-apoptotic) (Lu et al., 2014a).

The UPR is known to be dysregulated in disease. The activity of the UPR is impaired in type II diabetes, where secretory pancreatic cells rely heavily on a functional UPR to maintain insulin secretion (Scheuner et al., 2001). Neurodegenerative diseases such as Huntington's disease, amyotrophic lateral sclerosis (ALS), Parkinson's disease (PD) and Alzheimer's disease also show a dysregulated UPR (Duran-Aniotz et al., 2014; Hashida et al., 2012; Hetz and Mollereau, 2014; Matus et al., 2013; Roussel et al., 2013; Vidal and Hetz, 2012). The importance of UPR in the health of secretory cells leads to sensitivity to increased ER stress in cancers of secretory cells, such as multiple myeloma (Harnoss et al., 2019). Constitutive stress in multiple myeloma cells is mediated by overexpression of the IRE1/XBP1 axis of the UPR and apoptotic signaling is suppressed, enabling multiple myeloma cells to proliferate in a tumorigenic capacity

(Harnoss et al., 2019). This makes multiple myeloma cells a suitable model system to study dysregulation of the UPR in the context of cell growth and cell cycle progression.

C. Potential roles of the UPR in the cell cycle

As noted above, cellular stress activates 'go' 'no-go' sensors of cell cycle progression. ER stress is able to induce cell cycle arrest, and activation of the UPR in NIH 3T3 cells reduces the levels of cyclin D1 through the translational suppression enforced by PERK (Brewer and Diehl, 2000). Other studies have shown that depletion of cyclin D1 alone upon PERK activation is not sufficient to induce cell cycle arrest. Activation of the UPR in PERK deficient cells leads to arrest at the G_1/S boundary, and in the fruit fly, CHK1 activity was shown to be necessary to overcome the cell cycle arrest driven by PERK (Adamson et al., 2016; Malzer et al., 2010; Zhang et al., 2006).

A master regulator of cell cycle arrest is the tumor suppressor protein p53. Active p53 arrests cell cycle progression in response to genotoxic stress (Thomas et al., 2013). Additionally, ER stress can lead to the accumulation of active canonical p53 at the G_1/S boundary, and accumulation of a different isoform of p53 at the G_2/M transition (Bourougaa et al., 2010a; Zhang et al., 2006). Deletion of p53 and its downstream effector, $p21^{cip}$ overcomes the cell cycle arrest induced by the UPR (Bourougaa et al., 2010a). Mutations in p53 are common in many cancers, highlighting the dysregulation of cell cycle related genes that amplify the proliferative capacity of cancer cells (Muller and Vousden, 2013; Sabapathy and

Lane, 2018). Improper regulation of cell cycle checkpoints by mutations or deletions of p53 also promote gain of oncogenic potential (Brosh and Rotter, 2009; Muller and Vousden, 2013). Cancer cells often accrue other mutations as well, and many of these mutations could impair or impose a burden on proper ER function and activate the UPR (Chevet et al., 2015; Clarke et al., 2014). Therefore, it is conceivable that tumor cells rely on the UPR for growth and survival, and that the UPR could promote tumorigenesis, as occurs in multiple myeloma (Cite Carrasco and depinho, Harnoss). The cancer reliance on the UPR is not restricted to myeloma. For example, a recent study linked different mutants of p53 in triple negative breast cancer cell lines to dampened IRE1 and PERK signaling, but enhanced ATF6 signaling (Sicari et al., 2019). How mutations in p53 leads to the suppression of apoptotic signaling and discrete activation of one UPR branch is unclear. Thus, cancer cells provide a unique model to study the interconnectivity between the cell cycle and the UPR.

The UPR has also been linked to cell cycle progression outside tumorigenesis. *Hac1*, the yeast homolog of *XBP1*, promotes cytokinesis (Bicknell et al., 2007). Moreover, deletion of the cytokinesis controllers *hof1, cyk3,* and *bni* in yeast resulted in an upregulation of the UPR (Bicknell et al., 2007). In support of these findings, an ER stress surveillance (ERSU) pathway has been described in yeast, which ensures proper ER inheritance (Babour et al., 2010). However, no roles for ER surveillance mechanisms or for the UPR have been described in the cell cycle of animal cells.

Different stages of the cell cycle might impact ER function in different ways. A cell that is committed to division must not only duplicate its genome but increase its size. This increase in size is coupled to increased membrane content, organelle number, and a surge in translation and protein folding capacity. Because the UPR is at the interface of protein translation and lipid biogenesis, it is likely to play a fundamental role monitoring ER health during cell cycle progression.

II. ER Chaperone Content Increases during Interphase of the Cell Cycle

Increases in surface area and molecular constituents of the Golgi apparatus and plasma membrane suggest that organellar growth is essential during the cell cycle. However, a causal relationship between ER growth and cell cycle progression has not been established. To investigate changes in ER size and its molecular contents, I generated stable cell lines harboring fluorescent reporters of cell cycle progression known as FAST-FUCCI. FAST-FUCCI cell lines are powerful tools to assess ER chaperone content in G_1 versus S/G_2 stages of the cell cycle without the need for pharmacological agents to synchronize them. FAST-FUCCI cells revealed an increase in ER chaperone content during interphase. To determine whether this increase in chaperone content is coupled to a physical enlargement of the ER (i.e., and increase in volume and surface rea), we established a collaboration with a group at the Telethon Institute of Genetics and Medicine (TIGEM) in Naples, Italy, to conduct transmission electron microscopy (TEM) analysis of FAST-FUCCI cells that had been separated in G_1 or in S/G_2 by cell sorting. TEM data revealed no significant changes in ER surface area or volume. However, I cannot discard the possibility that small changes were underestimated. Further analyses of ER volume will indicate if the ER significantly ER enlarges at the G_1/S transition.

A. Tools to dissect cell cycle dynamics in live cells

1. Fluorescence Ubiquitination Cell Cycle Indicator

DNA content throughout cell cycle progression is typically analyzed in flow cytometry experiments by staining with fluorescent DNA intercalating dyes, such as propidium iodide and DAPI (Darzynkiewicz et al., 2017). To assess the progression of a population of cells through stages of the cell cycle, the population must first be synchronized using one of a number of biochemical methods. These methods include serum starvation to force cells into quiescence, or pharmacological agents that arrest cells at particular stages of the cell cycle (Jackman and O'Connor, 1998). Following treatment, the drugs are removed to allow cells to re-enter the cycle synchronously. Widespread methods include unbalancing nucleotide pools by treatment with excess thymidine, or microtubule destabilization using nocodazole. The commonly used “double thymidine block” alters the deoxynucleotide pool, arresting cells at the G_1/S boundary prior to DNA replication; while nocodazole treatment disrupts microtubule polymerization and is used to arrest cells

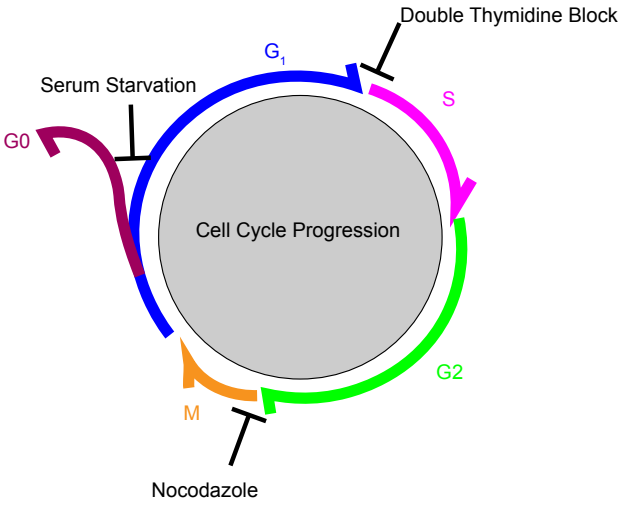

Figure 6. Classic techniques used to synchronize the cell cycle. Schematic of the cell cycle indicating synchronization methods to arrest cell cycle progression.

at the G_2/M transition, prior to mitotic spindle formation (Jackman and O'Connor, 1998) (**Figure 6**).

Alternative methods quantify the incorporation of nucleotide analogs into DNA by staining fixed cells with specific antibodies, for example, labeling with bromo-deoxyuridine (Clarke et al., 2017; Zhu, 2012). Although powerful, this type of immunostaining-based DNA content analysis cannot be deployed for long-term experiments in living cells. In addition to loss of synchrony over time, use of pharmacological tools can affect cell signaling pathways, biasing results (Seyb et al., 2006). To bypass this limitation, Sakaue-Sawano et al. developed a system to track cell cycle progression in living cells, which is referred to as “fluorescent ubiquitination-based cell cycle indicator”, or FUCCI (Sakaue-Sawano et al., 2008). By fluorescently tagging proteins that are naturally degraded during the cell cycle, FUCCI does not require artificial synchronization and it enables visualization and quantification of the fractions of the cell population in different stages of the cell cycle (Sakaue-Sawano et al., 2008). Specifically, FUCCI relies on the natural turnover of cell-cycle licensing factors CDT1 and geminin (Sakaue-Sawano et al., 2008).

CDT1 and geminin are ubiquitylated and targeted for degradation in a cell-cycle dependent manner, with CDT1 being degraded in S/G_2 while Geminin is degraded in G_1 (Benmaamar and Pagano, 2005; Nishitani et al., 2000; Vodermaier, 2004; Wei et al., 2004). In the original FUCCI system, the geminin and CDT1 degrons are fused to fluorescent proteins, a red monomeric Kusibara Orange (mKO2) and a green monomeric Azami Green (mAG), respectively (Sakaue-Sawano et al., 2008)

(**Figure 7**). In this way, G_1 cells are labelled red and S/G_2 cells are labelled green (Sakaue-Sawano et al., 2008). These protein chimeras are integrated into the genome of host cells using a high-titer lentiviral delivery of each transgene in a 1:1 ratio, aiming at introducing both transgenes in the majority of the cells (Sakaue-Sawano et al., 2008). Marketed versions of this reporter system are commercially available. A next-generation version of the FUCCI system, known as "FAST-FUCCI", which couples both of the FUCCI transgenes into a single lentiviral expression system has been recently developed (Koh et al., 2017). I selected the FAST-FUCCI system for this study due to the fact it contained both reporters in a single polycistronic open reading frame separated by a T2A self-cleaving peptide, which ensures equimolar levels of both fluorescent fusion proteins. Additionally, the viral vector also encodes a puromycin resistance gene that enables selection of cells expressing the reporter (Koh et al., 2017). These properties enable the streamlined generation of many cell lines containing the reporter, which was suitable for the analysis of the cell cycle in relation to ER growth in many cell lines.

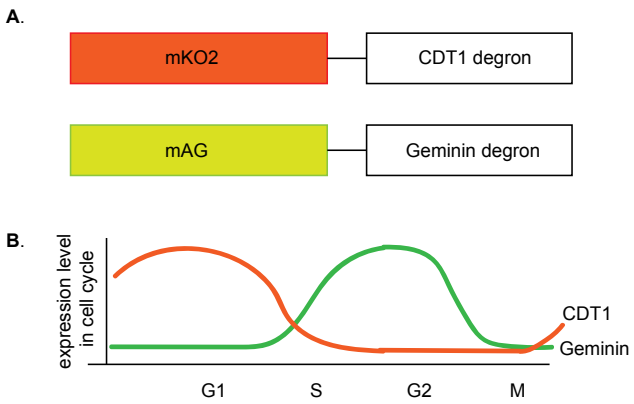

Figure 7. FUCCI reporters rely on the natural turnover of the cell cycle licensing factors CDT1 and Geminin. A) The fusion proteins of the FUCCI reporter are fluorescent proteins fused to cell cycle licensing factors CDT1 and geminin. B) Expression levels of CDT1 (orange) and geminin (green) vary during the cell cycle due to cell-cycle dependent ubiquitylation.

2. Generation of FAST-FUCCI cell lines

FAST-FUCCI KMS11dCas9 (multiple myeloma) and H4dCas9 (neuroglioma) cell lines were generated by standard lentiviral transduction (see Methods). Both cell lines contain a catalytically dead Cas9 protein (dCas9) fused to a KRAB repressor and Pacific-BFP fluorophore (Gilbert et al., 2013). dCas9-KRAB can be guided to gene promoters to by small guide RNAs (sgRNAs) to repress gene expression, enabling single-gene knockdowns (Gilbert et al., 2013). This technology is referred as CRISPR interference, or CRISPRi (Gilbert et al., 2014; Gilbert et al., 2013). I chose to engineer cell lines containing the CRIPSRi machinery so I could study how the loss-of-function of specific genes (e.g., UPR components) affects cell cycle progression in FAST-FUCCI cells.

KMS11dCas9 cells are a multiple myeloma cell line derived from the pleural effusion of a 67 year old female patient (Namba et al., 1989). Multiple myeloma is a cancer of plasma cells, which are secretory cells that produce antibodies for the adaptive immune system (Roth et al., 2014). Plasma cells are terminally differentiated cells that exhibit an extended ER necessary for their high secretory output (Gass, 2004; Kirk et al., 2010). In multiple myeloma patients, several different oncogenic driver mutations, such as *KRAS* and *p53*, lead to a dysregulated cell cycle and uncontrolled cell growth (Fulciniti et al., 2018; Hu et al., 2019; Maes et al., 2017). KMS11dCas9 cells have a deletion of *p53* and no mutations in *KRAS* (Gillardin et al., 2017).The UPR, which oversees protein folding capacity in the ER, is not only required for maintaining secretory function for plasma cells, but also for the differentiation of B-cells into plasma cells (Obeng et al., 2006; Shaffer et al.,

2004; Zhu et al., 2019). IRE1 signaling (see Chapter 1) is dysregulated in multiple myeloma (Harnoss et al., 2019). Therefore, multiple myeloma cells provide a good model system for studying the interconnectivity between ER stress and the cell cycle. H4dCas9 is a non-secretory cell line I used as a comparison outgroup (Arnstein et al., 1974).

After lentiviral transduction, the cells were subjected to puromycin selection to enrich for the cells expressing the transgene. Fluorescence microscopy imaging revealed that puromycin-selected cells were fluorescent in the red and green channels, indicating that the protocol for infection and selection was successful. However, the cells were not clearly separable into red or green subpopulations (data not shown).

3. Optimization and characterization of FAST-FUCCI reporter cell lines

Pilot experiments using fluorescence activated cell sorting (FACS) of the transduced cell lines revealed that the bulk of the population expressed both fluorescent proteins simultaneously, which indicated that the dynamic range of the reporter was too narrow (data not shown). Consequentially, the fraction of the population in G_1 and S/G_2 are underestimated. I reasoned that the high levels of expression of the reporter, which could result

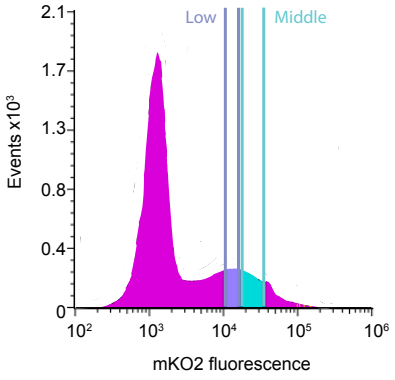

Figure 8. FACS sorting parameters for FAST-FUCCI cells. Histogram of mKO2 fluorescence events with gates to sort “low” and “middle”

from multiple transgene integrations into the host genome, overwhelm the cellular machineries in charge of their turnover. To overcome this limitation, I selected cells expressing low or middle levels of mKO2 by FACS by gating on the distribution of fluorescence intensity for the parent cell population as shown in **Figure 8.** Through microscopy analyses I corroborated that the cells I sorted did not co-express both fluorescent proteins (**Figure 9)**. This result indicated that my strategy yielded new cell lines in which the fluorescent reporters can be efficiently degraded by endogenous cellular machineries.

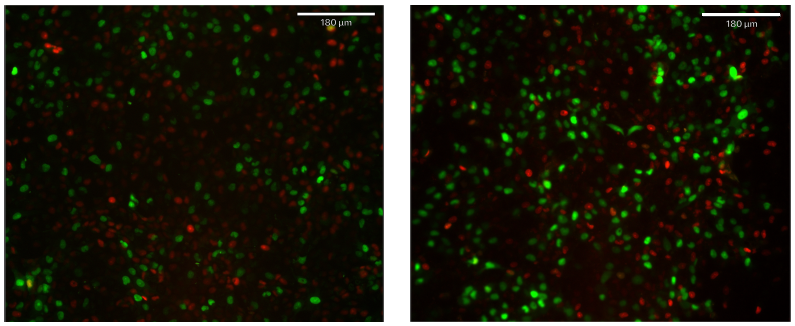

Figure 9. Sorted H4dCas9 FAST-FUCCI cells. H4dCas9 FAST-FUCCI "low" (left) and H4dCas9 FAST-FUCCI "middle" (right).

I sought to characterize cell cycle kinetics and ascertain the dynamic range of the FUCCI reporter system for separating cells in G1 or S/G2 by flow cytometry in the "low" and "middle" expressors. To corroborate the validity of the reporter, I synchronized the "low" and "middle" FUCCI cells with thymidine to arrest at G1/S boundary, nocodazole to arrest at the G2/M boundary or by serum starvation to force cells into quiescence (refer to **Figure 10**). Next, I compared the red/green readout obtained from the FUCCI reporter to the readout obtained by DNA staining with propidium iodide (PI), which informs on DNA content.

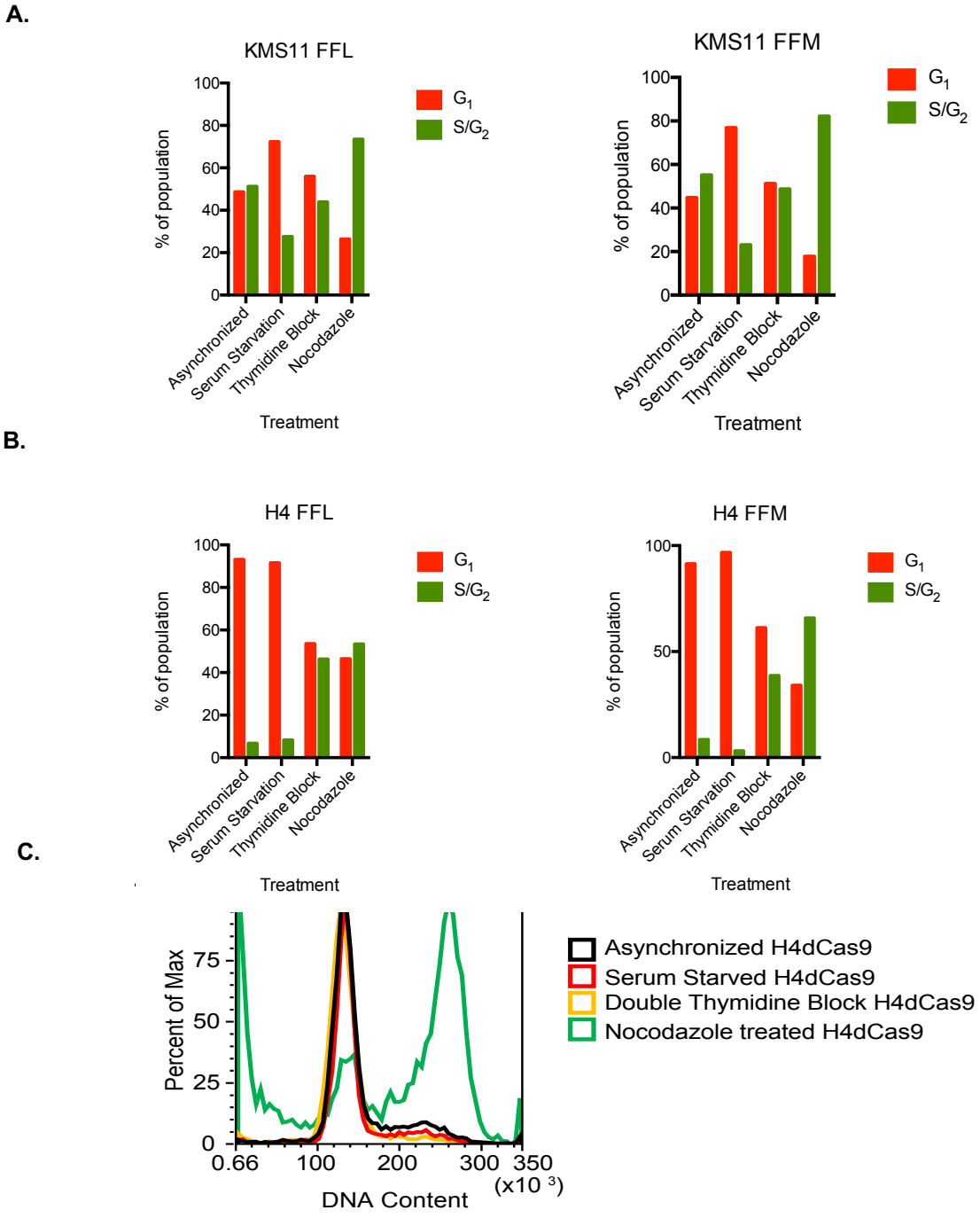

Figure 10. Synchronization of FAST-FUCCI cells confirms reporter activity. A) KMS11dCas9 Fast FUCCI "low" (FFL) and KMS11dCas9 FAST FUCCI "middle" (FFM) synchronization test. B) H4dCas9 Fast FUCCI "low" (FFL) and H4dCas9 FAST FUCCI "middle" (FFM) synchronization test. C) PI staining of H4dCas9 FFL shows synchronization techniques were efficient.

These experiments showed that, expectedly, all synchronization methods worked in our cell lines and that the FAST-FUCCI system reports on G_1 and S/G_2 cell populations with high accuracy (**Figure 10C**). In serum starvation experiments, the FAST-FUCCI system showed a larger proportion of cells expressing mKO2-CDT1 (74.6% for KMS11 cells and 94.2% for H4 cells, on average, for “low” and “middle” FAST-FUCCI; Fig. 6A and 6B). Nocodazole treatment resulted in an increased representation of mAG-geminin cells (77.9% for KMS11 cells and 59.7% for H4 cells, on average, for “low” and “middle” FAST-FUCCI), which correlated with increased PI staining, confirming DNA duplication and arrest at the G_2/M boundary (**Figure 10**). Synchronization using double thymidine block did not allow a clear separation of the red and green populations in the FAST-FUCCI cells (**Figure 10**). This result can be explained by cells being at the boundary of G1 and S phases, wherein the reporter transitions from red to green. For all subsequent experiments I used the “low” population of FAST-FUCCI cells because they show a dynamic range comparable to the “middle” population but without further overexpression of the reporter.

Forward and side scatter (FSC and SSC) data collected in the above experiments indicated that green cells are larger and more granular than red cells (i.e., their FSC and SSC are larger, indicating an increase in volume in organellar content, respectively), which shows that S/G_2 cells are larger and more complex (**Figure 11**). This observation is consistent with S/G_2 cells preparing for division to give rise to two daughter cells (Killander and Zetterberg, 1965a, b).

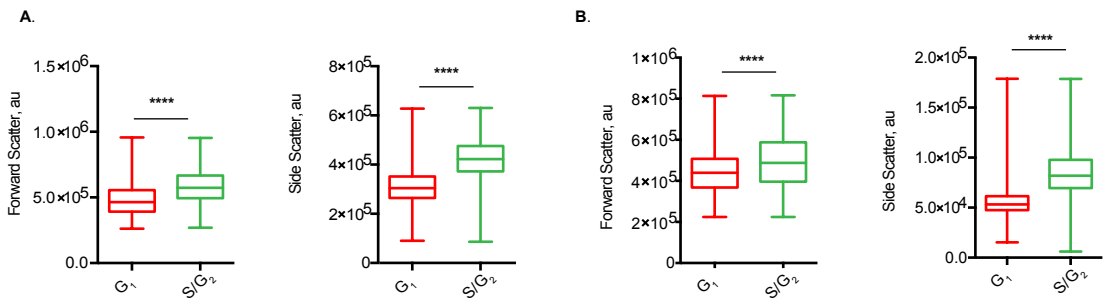

Figure 11. Size and granularity of S/G$_2$ cells are larger than G$_1$ cells. Comparison of FSC and SSC of FAST-FUCCI cells attained by flow cytometry, gating for red and green respectively. A) H4dCas9, N_{G1}=37,077, $N_{S/G2}$=17,202. B) KMS11dCas9, N_{G1}=24,919, $N_{S/G2}$= 27,052. P <0.0001, unpaired t-test.

To analyze if FAST-FUCCI cells accurately report cells in G_1 or G_2 at the molecular level, I sorted red and green H4dCas9 and KMS11dCas9 cells and used the lysates obtained from these cells to analyze cyclin expression by quantitative RT-PCR (RT-qPCR) or by Western blots (**Figure 12)**. These experiments revealed that red cells (G_1) contain less *cyclin B* and *cyclin A* transcripts than green cells (S/G_2), which in turn exhibit higher levels of *cyclin A* and *cyclin B* mRNAs (**Figure 13**). This observation is in agreement with the known levels of these cyclins

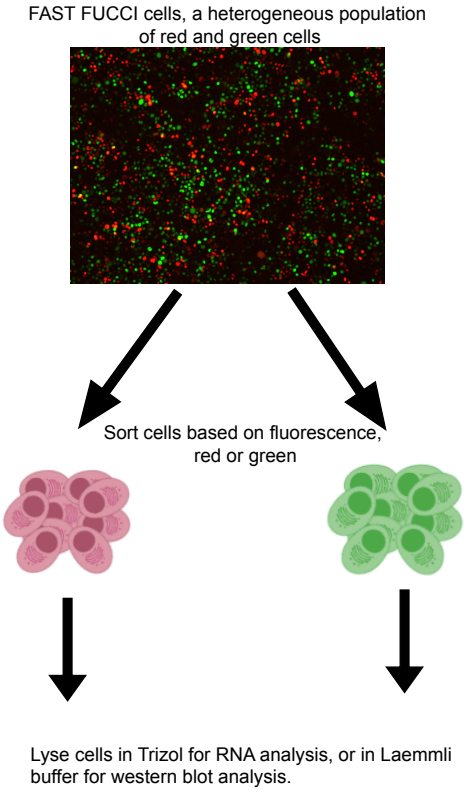

Figure 12. Experimental workflow for sorting FAST-FUCCI cells. Cells were sorted based on red and green fluorescence to separate G1 and S/G2 populations.

throughout the cell cycle and authenticates the reliability of the FAST-FUCCI reporter in these cell lines.

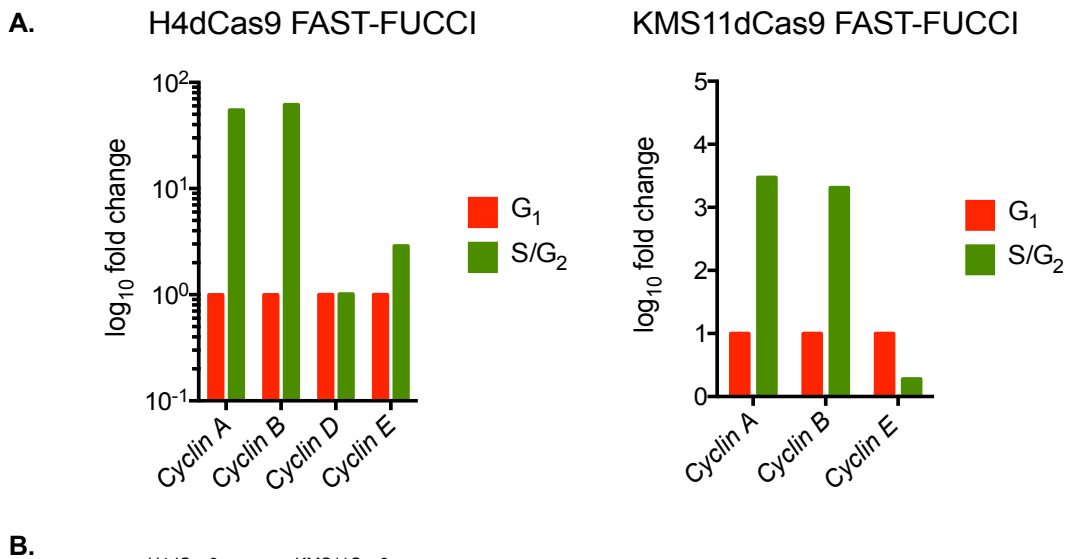

Figure 13. Cyclin expression in FACS sorted FAST-FUCCI cells. Quantification of specific cyclin expression by A) qRT-PCR and B) western blot in the FAST-FUCCI cell lines in the G_1 and S/G_2 stages of the cell cycle. For expression of the cyclins throughout the mammalian cell cycle, refer to Chapter 1.

The mRNA levels of *Cyclin D1*, which is typically a marker for G_1, were similar in red and green cells. However, the protein levels of Cyclin D1 were higher in G1, in accordance with what others have described for Cyclin D1 abundance during the cell cycle (Yang et al., 2006). Because *Cyclin D1* mRNA levels are undetectable by RT-qPCR in KMS11 cells, I performed the abovementioned Cyclin D1 analyses in

H4dCas9 cells only (Specht, 2004). The abundance of the *Cyclin E* mRNA was used as a marker for G1 in KMS11dCas9 FAST-FUCCI cells. Western blots analyses revealed that cyclin B, cyclin A and cyclin E protein expression correlate with their corresponding cell cycle stages in all KMS11dCas9 and H4dCas9 cells (**Figure 13, Figure S1** for loading). Taken together, these experiments indicate that the FAST-FUCCI KMS11dCas9 and H4dCas9 cell lines I generated provide a convenient and accurate system to study cell cycle progression in living cells. Further, FACS sorting of FAST-FUCCI cells provides a powerful method to synchronize cells without the need for pharmacological agents which have the potential to disrupt multiple cellular processes.

B. ER chaperone levels increase during interphase

1. Flow cytometry analysis of protein levels

Recent high throughput transcriptomic, proteomic and phospho-proteomic datasets using FUCCI cell lines have been used to identify genes whose expression levels oscillate in a cell cycle-dependent manner (Ly et al., 2014; Ly et al., 2017). Not surprisingly, these studies revealed that the levels of a large subset of proteins oscillate as a function of the cell cycle. Interestingly, proteomics data in synchronized cells uncovered increases in the levels of ER related proteins at the G_1/S boundary, for example calnexin, glycosyltransferases, components of the Sec61 translocon, and KDEL receptor, suggesting a cell cycle regulation of ER physiology (Olsen et al., 2010). Despite these findings, how the protein folding capacity of the ER during the cell cycle is regulated remains unknonwn. Since the

protein folding capacity of the ER largely depends on the abundance and availability of ER-resident chaperones and foldases, I used my FAST-FUCCI cell lines to compare ER chaperone content in G_1 and S/G_2.

To this end, I fixed asynchronous KMS11dCas9 and H4dCas9 FAST-FUCCI cells and immunostained for ER chaperones and foldases, including BiP, calnexin, and PDI. BiP is the most abundant ER chaperone that assists in folding of newly synthesized proteins as they enter the ER lumen (Ni and Lee, 2007). BiP also has a regulatory role in the UPR (Ni and Lee, 2007). Calnexin is part of the ER protein-folding quality control machinery before their export from the ER (Ni and Lee, 2007). PDI catalyzes rearrangements in disulfide bond formation to ensure correct tertiary and quaternary structure of secretory pathway associated proteins (Ni and Lee, 2007). BiP, calnexin and PDI protein levels were analyzed by flow cytometry in H4dCas9 FAST FUCCI and KMS11dCas9 FAST FUCCI cell lines using specific antibodies. G_1 and S/G_2 cells were gated according to FAST-FUCCI reporter expression, with one gate on red (G_1) cells and one gate on (S/G_2) cells. Next, I measured the mean fluorescence intensity of BiP, calnexin or PDI, which I stained with an Alexa-Fluor 647 secondary antibody, which emits in the far-red spectrum, with the emission peak at 665 nm. Therefore, Alexa-Fluor 647 does not interfere and is not affected by mKO, which emits in the red spectrum, with the emission peak at 565 nm. This analysis revealed that the levels of ER chaperones increased in S/G_2 when compared to G_1 in both FAST-FUCCI cell lines (36.75% in H4dCas9 and 26.7% in KMS11dCas9) (**Figure 14**). These results were corroborated by RT-qPCR analysis in red or green cells, wherein H4dCas9 cells showed an large

increase in mRNA levels of *BIP, Calnexin* and *PDI* in S/G_2 in comparison to G_1 (ranging from ~2 to 4.5-fold), whereas KMS11dCas9 showed a more modest increase of approximate ~1.4 fold for the BiP mRNA, but no increase for neither *PDI*

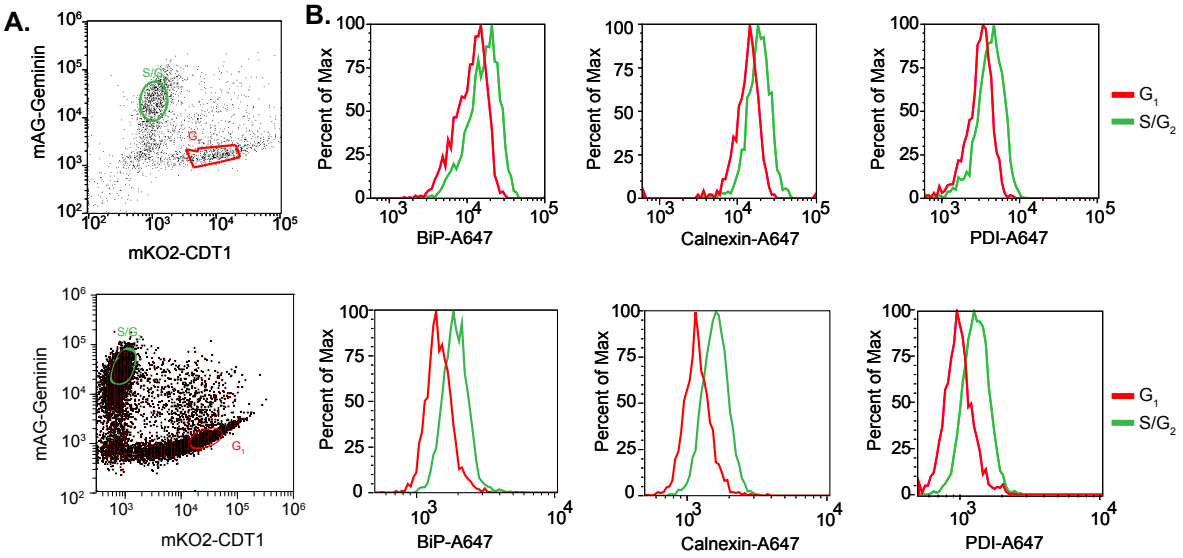

Figure 14. ER chaperone and foldase content increases during interphase. A) Scatter plot for H4dCas9 FAST FUCCI (top) and KMS11dCas9 FAST FUCCI (bottom) with gates drawn. B) Fluorescence intensities of ER chaperones within gates drawn for H4dCas9 FAST FUCCI (top) and KMS11dCas9 FAST FUCCI (bottom).

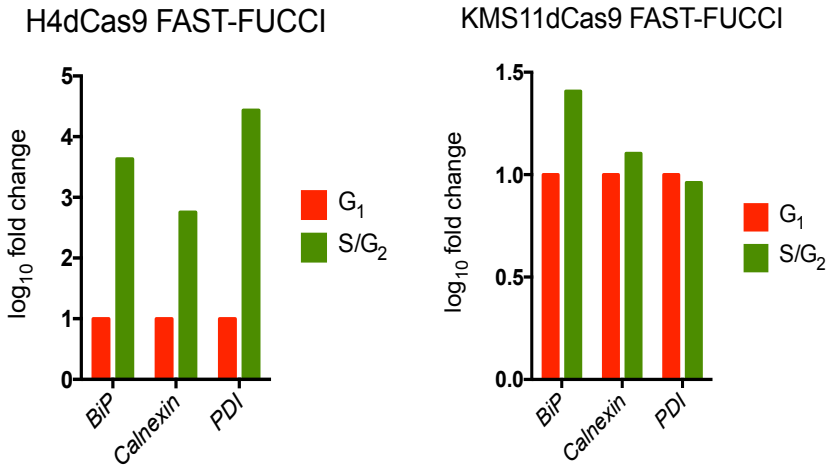

Figure 15. mRNA levels of ER chaperones and foldases increase in non-secretory cell lines. qPCR analysis of ER chaperone mRNA levels in G_1 and S/G_2 cells.

or *Calnexin* mRNA. This discrepancy could be attributed to the secretory nature of KMS11dCas9 cells, which have an extended ER and thus, it is likely they do not require a large upregulation of ER chaperones and foldases prior to division. Taken together these data indicate that the levels of ER chaperones and foldases increase in preparation for cell division (**Figure 15**).

2. Volume and surface area of the endoplasmic reticulum during G_1 and S/G_2

The differences I observed in ER chaperone content during G_1 and S/G_2 of the cell cycle mirror the increase in translation seen for many other proteins (Olsen et al., 2010). One interpretation of this observation is that during the cell cycle, an increase in protein synthesis leads to crowding of the ER lumen, which forces an increase in ER-chaperone levels to accommodate protein folding. It is also possible that this upsurge in ER protein content results in ER swelling which requires an increase in endomembranes. Such increase in organellar volume and surface area during the cell cycle has been described for the Golgi apparatus (Sin and Harrison, 2016). Since membrane biogenesis occurs in the ER (Glick and Nakano, 2009; Nunnari and Walter, 1996), I reasoned that the expansion of Golgi apparatus observed during interphase must be a consequence of an increase in ER surface area and endomembrane biosynthesis. To test this hypothesis, I started a collaboration with the group of Dr. Roman Polishchuk at the Telethon Institute of Genetics and Medicine (TIGEM) in Naples, Italy, to conduct transmission electron microscopy (TEM) on G_1 and S/G_2 FAST-FUCCI cells sorted by FACS. Analysis of H4dCas9 FAST FUCCI and KMS11dCas9 FAST FUCCI cells did not reveal any

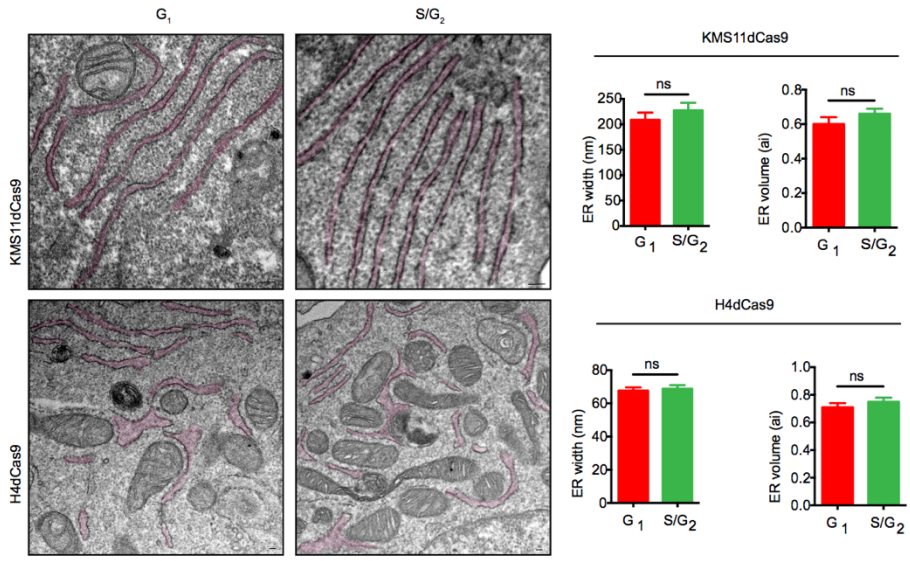

Figure 16. TEM analysis of sorted FAST-FUCCI cells reveals no significant difference in ER size. A) TEM images of KMS11dCas9 and H4dCas9 FAST FUCCI cells. B) Quantification of ER width and volume of TEM images.

significant changes in ER morphology, measured by width and volume of ER cisternae between G_1 and S/G_2 (**Figure 16**). In these experiments, the volume of the ER was calculated using a standard algorithm consisting of applying a grid on the image and counting how many times ER membranes intersect with the grid. This value is normalized to the number of intersections of the grid with the plasma membrane. It is therefore possible that differences in ER volume or surface area could have been underestimated. For instance, if S/G_2 cells have more ER but are also bigger, this algorithm will miss any ER volumetric changes (see Discussion). For this reason, we are currently re-analyzing the images taking in consideration the total cell volume. Using this alternative analysis, I expect to see an increase the ER volume of cells in S/G_2 when compared to G_1.

Increases in ER protein folding capacity and ER volume can be driven by activation of UPR. Therefore, I hypothesize that the UPR might play a physiological role in increasing the ER size and protein folding capacity prior to cell division.

C. Methods

1. Cell culture

KMS11dCas9 and H4dCas9 cells were a kind gift of Dr. Martin Kampmann (UCSF). 293METR virus packing cells were a kind gift of Brian Rabinoivich (formerly at the MD Anderson Cancer Center). KMS11dCas9 cells were maintained in RPMI 1640 media supplemented with 10% fetal bovine serum, 1% penicillin, 1% streptomycin and 1% glutamine. H4dCas9 and 293METR cells were cultured in DMEM supplemented with 11 mg/L sodium pyruvate, 10% fetal bovine serum, 1% penicillin (1U/mL), 1% streptomycin (1U/mL) and 1% glutamine. All cell lines were maintained at 37˚C with 5%CO_2. All cell line derivatives produced from KMS11dCas9 and H4dCas9 cells were cultured in an identical manner to their parent cell line.

2. VSV-G pseudotyped HIV-1 based lentiviral transduction of mammalian cells

293METR cells at 60-70% confluence were co-transfected using Lipofectamine 2000 with pVSV-G and pCMVΔR8.91 helper plasmids, and the lentiviral vector of choice. After 6 hours, the media was replaced with growth media containing no antibiotics. 24 hours post transfection, the media was replaced with viral collection media (DMEM supplemented with pyruvate, 4% fetal bovine serum, 15 mM HEPES, 1% glutamine, 1% penicillin and 1% streptomycin). 48 hours post transfection, the

viral supernatant was collected and filtered through a 0.45μm filter to remove any cell debris.

To infect adherent cells, target cells were seeded in a 6-well plate at a density of 300,000 cells per well 24 hours prior to infection. The day after, the media was replaced with 2 mL of filtered viral supernatant supplemented with 8 μg/mL polybrene and the plates were centrifuged at 700 *x g* for 2 hours at 30 ˚C in a temperature-controlled centrifuge outfitted with a rotor that accommodates aerosol-resistant microplate carriers. The cells are returned to the incubator and the virus-containing media is replaced the following day (~16 hours later) with fresh standard cell growth media. If the cells reach confluence at this point, they are split in a 1:6 ratio.

To infect suspension cells, 2,000,000 cells were resuspended in filtered viral supernatant supplemented with 8 μg/mL polybrene. The cell suspension is then placed in a 6-well plate and the infection is carried out identically as described above. After the spin-infection, the cells are washed twice with 1x PBS and finally resuspended in fresh growth media before returning them to the incubator. Two days after infection, the cells were treated with 0.7 μg/mL (Kms11) or 1 μg/mL (H4) puromycin for 3-4 days to select against cells not expressing the constructs, which encode for puromycin resistance.

3. Fluorescence activated cell sorting (FACS)

Two 15 cm dishes of cells at 70-80% confluence were trypsinized and resuspended in 1x PBS supplemented with 0.5% FBS. To separate cells that express the FAST-

FUCCI construct at a “low” or “middle” level, the sorting gates were set on red fluorescence, with an excitation/emission of 587/610. The gates are indicated in **Figure 4**. Cells were simultaneously sorted into “low” and “middle” expressors on a SONY SH800 cell sorter. A medium flow rate was used so that the sorting efficiency always remained above 80%. The sort was completed when no cells were remaining (approximately 300,000 to 500,000 cells per subpopulation). The sorted cells were centrifuged at 160 *x g* to pellet living cells and resuspended in their respective growth media for subsequent expansion.

To sort for “red” and “green” cells, the gates were set as indicated in **Figure 11**, and the cells were sorted on the same instrument, using the conditions indicated above. Red and green excitation/emission were 587/610 and 488/509, respectively. The sorted cells were then centrifuged at 160 *x g* to pellet and resuspended in 1xPBS to a concentration of 1 million cells per mL. 1mL of cells of each color were subsequently lysed in either Trizol or Laemmli buffer for downstream RT-qPCR or Western blotting analyses, respectively.

4. Cell synchronization

For all synchronization experiments, the cells were seeded so that their confluence the following day is approximately 50-60%. To induce starvation and synchronize cells at G_0, the cells were washed three times with1x PBS, and placed in media devoid of serum for 48h to induce starvation. To arrest cell cycle progression at the G1/S boundary, the cells were treated with 2.5 mM thymidine for 16 hours. After 16

hours, the cells were washed three times with 1x PBS before replacing with fresh media. The cells were allowed to recover for 8 hours before a second treatment with 2.5 mM thymidine for 16 hours prior to collection for analysis. To arrest cell cycle progression at the G2/M boundary, the cells were first treated with 2.5 mM thymidine for 16 hours to initially synchronize at the G_1/S boundary. After 16 hours, the cells were washed three times with 1x PBS before replacing with fresh media. The cells were allowed to recover for an additional 8 hours before treatment with 300 ng/mL nocodazole for 16 hours prior to collection for analysis. This 24 hour time window after thymidine treatment and before nocodazole treatment allows the bulk of the population to synchronously transition to G2.

5. DNA content analysis by propidium iodide staining

Cells were collected in 1.5 mL microcentrifuge tubes and centrifuged at 1,500 *x g* for 5 minutes. The cells were washed three times with 1x PBS and on the last wash, the cells were left in 100 µL PBS and gently resuspended using a micropipette. To fix the cells, 350 µL of chilled 100% ethanol were added drop-wise whilst vortexing. The cells were fixed for 30 minutes at 4˚C and then washed three additional times with 1x PBS. Immediately before analysis, the samples were treated with 50 µg/mL propidium iodide and 100 µg/mL RNase A. The data were collected on an Attune flow cytometer and the fluorescence intensity was plotted as a linear function against normalized events.

6. Fixing and immunostaining for flow cytometry.

One million cells per condition were pelleted in a 1.5 mL microcentrifuge tube at 1,500 *x g* for 5 minutes. The cells were washed three times with 1x PBS. On the last wash, the cells were left in 100 µL PBS and gently resuspended using a micropipette. To fix the cells, 100 µL of 4% paraformaldehyde were added dropwise whilst vortexing. The cells were incubated in PFA at 4˚C for 30 minutes. Following incubation, the cells were washed three times in 1x PBS prior to incubation in blocking and permeabilization buffer (50 mM NH_4Cl, 0.5% BSA, 0.05% saponin, 0.02% NaN_3 in PBS) for one hour at room temperature. After three more washes in 1x PBS, the cells were incubated in 50 µL of primary antibody (appendix **Table S4**) diluted in 1x PBS overnight at 4˚C.

The following day, the cells were washed three times in 1x PBS prior to addition of secondary antibody dilluted in 1x PBS supplemented with and 0.5% FBS. The secondary antibody was incubated at room temperature for one hour, (appendix **Table S5**). The samples were washed three more times in 1x PBS prior to analysis by flow cytometry.

7. Western blot analyses

FACS-sorted cells were lysed in 1x Laemmli buffer at a density of 5,000 cells/µL and sonicated briefly (3 x 20 sec. pulses) at low intensity to shear genomic DNA. Before loading samples on SDS-PAGE gels, 5% BME (v/v) was added to the samples prior to heating at 95˚C for 5 minutes. The samples were collected in the bottom of the tube by brief centrifugation (one pulse) and were loaded on 10% SDS-

PAGE gels and electrophoresed at 120V until the dye front reached the bottom of the gel (approximately 90 minutes). The separated samples were wet-transferred onto a nitrocellulose membrane at 90V for 2 hours at 4 ˚C. Transfer efficiency was assessed by staining the membranes with Ponceau stain. Membranes were blocked in 5% dry milk in 1x TBST for one hour, followed by three five-minute washes with 1x TBST. The membranes were probed with primary antibodies (**Table S4**) diluted in 1x TBST supplemented with 3% BSA overnight at 4˚C on a shaker. Primary antibodies were washed off in three five-minute washes with 1x TBST. Secondary antibodies (**Table S5**) were diluted in 5% dry milk in 1x TBST and were incubated on the membranes for 1 hour. Following three five-minute washes in 1xTBST, the membranes were incubated with the Azure Radiance HRP substrate and peroxide for 2 minutes to reveal immunoreactive bands. Images were acquired using the chemiluminescence function on the Azure Biosystems c300 imager.

8. RNA extraction, cDNA synthesis and gene expression analysis

500,000 to 1 million cells were lysed in Trizol reagent (ThermoFisher) and RNA was extracted according to the manufacturer's protocol. 1 µg of RNA was DNase treated with NEB DNaseI as per manufacturer protocol, and cDNA was synthesized using the iScript cDNA synthesis system (BioRad) according to the manufacturer's recommendations. The cDNA was diluted 10-fold in nuclease free water prior to the PCR with gene-specific primers. All primers used are listed in the **Table S1**. Gene-specific quantitative PCR on template cDNA was carried out using the SYBR Green Select Master Mix (ThermoFisher) as per manufacturer's recommendations

on a BioRad CFX96 Touch qPCR instrument. Cq values were determined using regression fitting on the CFX Maestro software. Changes in gene expression were analyzed using the standard $\Delta\Delta$Cq method.

9. Transmission electron microscopy

150-200 nM sections were obtained using a Leica Ultracut-UCT microtome, transferred onto copper slot grids, stained with Reynold's lead citrate, and imaged in a Tecnai 12 electron microscope setat 120 keV. ER surfaces were rendered with the IMOD software.

III. A physiological UPR controls cell cycle kinetics

The UPR has been shown to be important in many physiological processes in metazoans, such as the differentiation of B-cells into plasma cells (Reimold and Glimcher), development and maintenance of professional secretory tissues (Lee and Glimcher, Ron), and choice of olfactory receptors (Dalton et al, Cell), among others (Gass, 2004). However, potential roles for the UPR in monitoring ER health during the cell cycle of metazoan cells have not been established. In this chapter, I provide evidence of a physiological role for the UPR in the regulating the cell cycle of mammalian cells. Specifically, inhibition of the UPR sensor IRE1 delayed cell growth and induced a specific kinetic delay at the G_1/S boundary, suggesting that IRE1 plays key roles at cell cycle checkpoints

A. IRE1 inhibition negatively impacts cell cycle progression

The UPR has been transcriptionally and translationally linked to cell cycle progression upon induction of ER stress (Adamson et al., 2016; Bourougaa et al., 2010b; Brewer and Diehl, 2000; Brewer et al., 1999; Chen et al., 2011; Zhang et al., 2006). Specifically, these studies show a role for PERK, whose activation by ER stress inducers and the resulting global translation attenuation lead to the downregulation of cyclin D1 and the concomitant delay in cell cycle progression (REF). Classical ER stressors, such as tunicamycin, which prevents N-linked glycosylation in the ER are known to arrest cells at the G_1/S boundary (Han et al., 2013a). However, a role for the UPR in regulating cell cycle progression in the absence of pharmacologically induced ER stress remains unknown. It is conceivable that the UPR could play a physiological role in communicating ER integrity to the cell cycle machinery. This type of communication is important, as peripheral ER and NE remodeling are required for mitosis in animal cells (see Chapter 1). It is thus possible that signaling pathways controlling mitosis communicate with the UPR to oversee ER health during the cell cycle. I hypothesize that the UPR might serve as a link between the ER and cell cycle machinery, and inhibition of the UPR in the absence of stress would impinge on cell cycle progression.

1. Acute induction or blocking of the UPR using pharmacological agents

To study the effects of dampening UPR signaling in cell cycle progression, I used commercially available and validated pharmacological inhibitors of the UPR: 4μ8C,

ISRIB and ceapins, which inhibit IRE1's nuclease activity, block signaling downstream of PERK, or prevent proteolytic processing of ATF6, respectively (**Figure 17**). 4μ8C is an umbelliferone that from a Schiff base with a specific lysine in IRE1's RNase domain, rendering it catalytically dead (Cross et al., 2012). 4μ8C does not affect IRE1 oligomerization or auto-phosphorylation, but it prevents IRE1 from splicing XBP1 or cleaving RNAs in RIDD (Cross et al., 2012). Importantly, 4μ8C does not target the IRE1-related nuclease RNaseL, attesting to its specificity (Cross et al., 2012). ISRIB is a potent drug-like molecule that renders cells insensitive to the effects of any ISR kinase, including PERK (Sidrauski et al., 2013). ISRIB targets eIF2B with low nanomolar affinity (Sidrauski et al., 2013). eIF2B is the guanine nucleotide exchange factor for eIF2 and thus serves to replenish the pools of ternary complex necessary for translation initiation (Zyryanova et al., 2018). One drawback to this approach is that ISRIB does not directly inhibit PERK; however

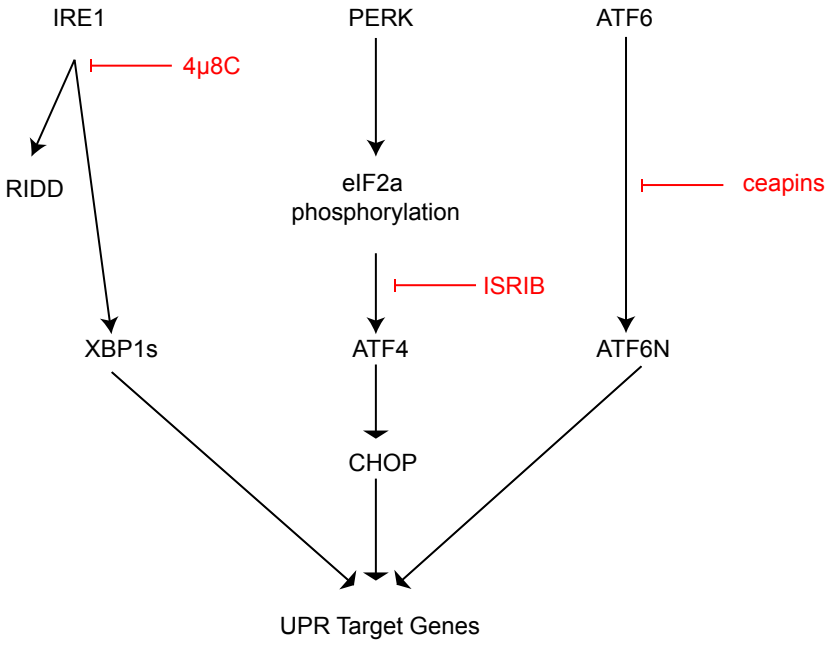

Figure 17. Pharmacological UPR inhibitors block specific branches of the UPR. Schematic of UPR signaling indicating where pharmacological inhibitors act.

other well established- pharmacological inhibitors of PERK are known to have potent off-target effects, primarily targeting the RIP kinases, which are involved on controlling cell death (Rojas-Rivera et al., 2017). Ceapins trap ATF6 in the ER, preventing its translocation to the Golgi apparatus for proteolytic processing (Gallagher et al., 2016; Gallagher and Walter, 2016). The mechanism of action of ceapins remains unclear, but recent CRISPRi genomic screens have revealed that ceapins seem to act by generating a neomorphinc tether between the ER and peroxisomes which prevents ATF6 trafficking to the Golgi apparatus (Torres et al., 2019).

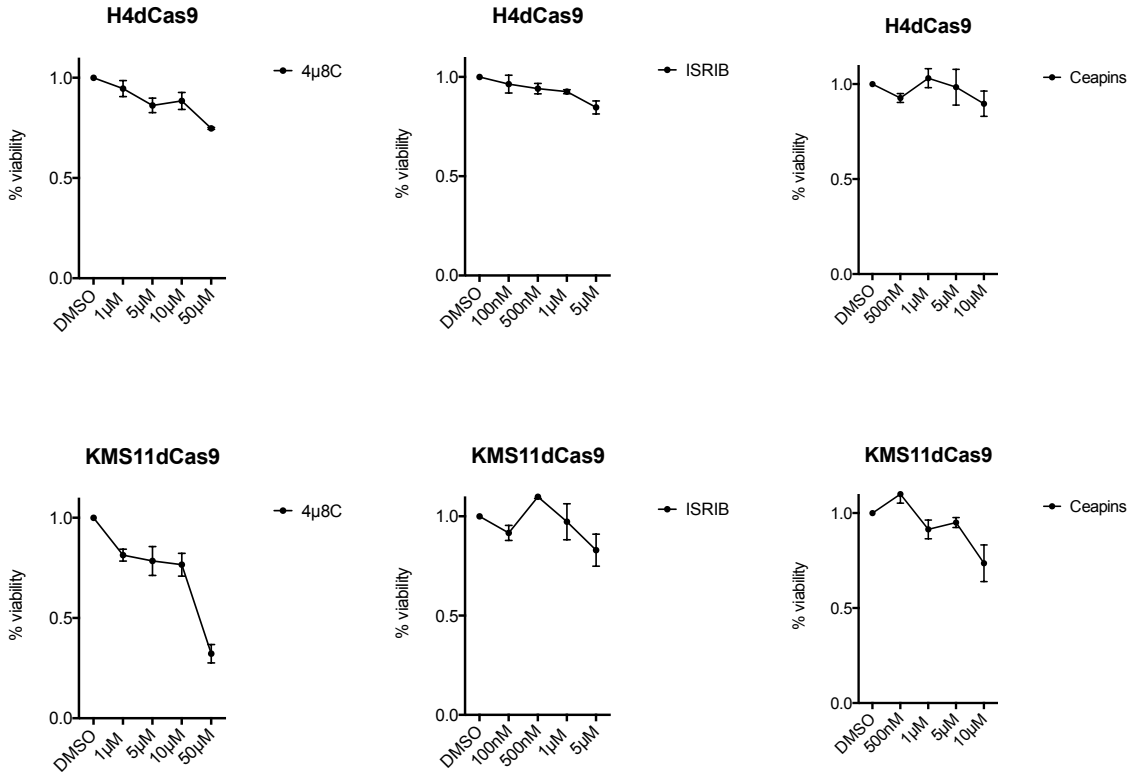

Figure 18. Cell viability upon 24-hour treatment with each UPR inhibitor. Viability of A) H4dCas9 cells and B) KMS11dCas9 cells in response to a 24-hour treatment of the UPR inhibitors 4μ8C (50μM, 10μM, 5μM, 1μM, DMSO), ISRIB (5μM, 1μM, 500nM, 100nM, DMSO) and ceapins (10μM, 5μM, 1μM, 500nM, DMSO). N=2; Error bars are SEM.

To ensure that these pharmacological agents did not alter cellular viability I when dosed in acutely (24-hour period). I established dose-response kill curves using a range of concentrations for each UPR inhibitor (**Figure 18**). From these data, I selected concentrations that do not impact cell viability (measured by ATP content using a luciferase-based assay; Promega CellTiter Glo) for my subsequent experiments. These concentrations are 10μM 4μ8C (data point 4 in both 4μ8C curves), 500 nM ISRIB (data point 3 in both ISRIB curves) and 5 μM ceapins (data point 4 in both ceapins curves.

To test if chronic treatment with UPR inhibitors affects cell growth, I conducted a similar but exposed H4dCas9 and KMS11dCas9 cells to 8-days of treatment as opposed to 24 hours. I quantified cell viability every two days by Trypan blue staining. Treatment with 4μ8C delayed growth in H4dCas9 and in KMS11dCas9 cells, and the effect was much more pronounced in KMS11dCas9 cells than in H4dCas9 cells (**Figure 19**). Multiple myeloma cells are known to be sensitive to IRE1 inhibition and have been shown to die in

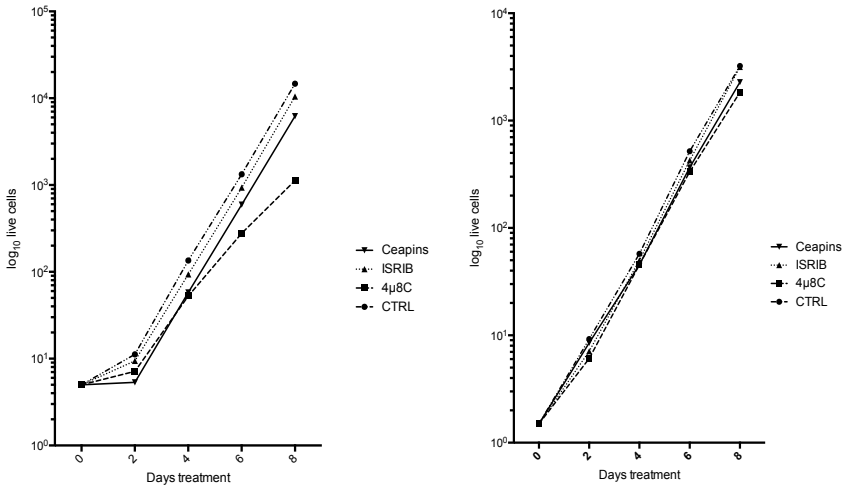

Figure 19. Chronic treatment with UPR inhibitors leads to delayed growth. Chronic treatment of A) H4dCas9 cells and B) KMS11dCas9 cells. with 10μM 4μ8C, 500nM ISRIB, and 5μM

response to IRE1 inhibitors in cell culture and in myeloma animal models (Harnoss et al., 2019; Mimura et al., 2012; Papandreou et al., 2011). I confirmed the sensitivity of multiple myeloma cell lines to IRE1 inhibitors by treating another multiple myeloma cell line, RPMI 8226, with 4μ8C and found that it also displayed reduced growth (**Figure 20**). It is possible that the exacerbated effects observed in myeloma cells, as opposed to the modest effect observed for H4dCas9 cells, reflects the inherent sensitivity of myeloma cells to IRE1 inhibition aforementioned. At the same time, the similar trend in growth inhibition I observed between secretory and non-secretory cells suggests that IRE1 signaling may be universally important for cell growth and the kinetics of cell cycle progression regardless of cellular ontogeny. By contrast, even though treatment with ISRIB and ceapins also impacted cell proliferation upon chronic treatment in both cell lines, neither treatment showed the same magnitude as that of 4μ8C (**Figure 19**). Together, these results suggest that IRE1 signaling might engage in crosstalk with cell-cycle signaling pathways.

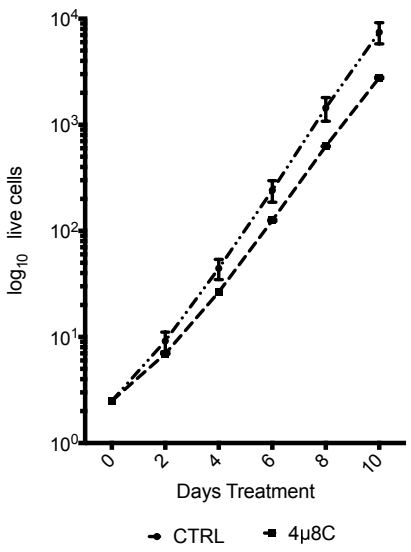

Figure 20. Chronic treatment with 4μ8C leads to delayed growth.
Chronic treatment of RPMI 8226 cells with 10μM 4μ8C for 10 days.

To determine whether this IRE1-cell cycle crosstalk is engaged in cancer cells, I synchronized H4dCas9 and KMS11dCas9 cells at the G_1/S boundary using a double thymidine bock (Chapter 2). I released the block by switching to fresh growth

media and treated the with the UPR inhibitors, or tunicamycin, as a positive control (tunicamycin arrests cell cycle progression). I collected samples 6 hours post-release in the drug-treated cells in order to assess transition through the G_1/S boundary. I observed a delay in progression through the G1/S boundary in cells treated with 4μ8C (**Figure 21** blue and green traces, top panels). No such delay was observed upon treatment with Ceapin A7 or ISRIB (**Figure 21**). Additionally, I was able to observe that treatment with ISRIB rescued the cell cycle arrest imposed by tunicamycin, which is consistent with previously described roles of PERK signaling in suppressing cyclin expression (Adamson et al., 2016; Brewer and Diehl, 2000).

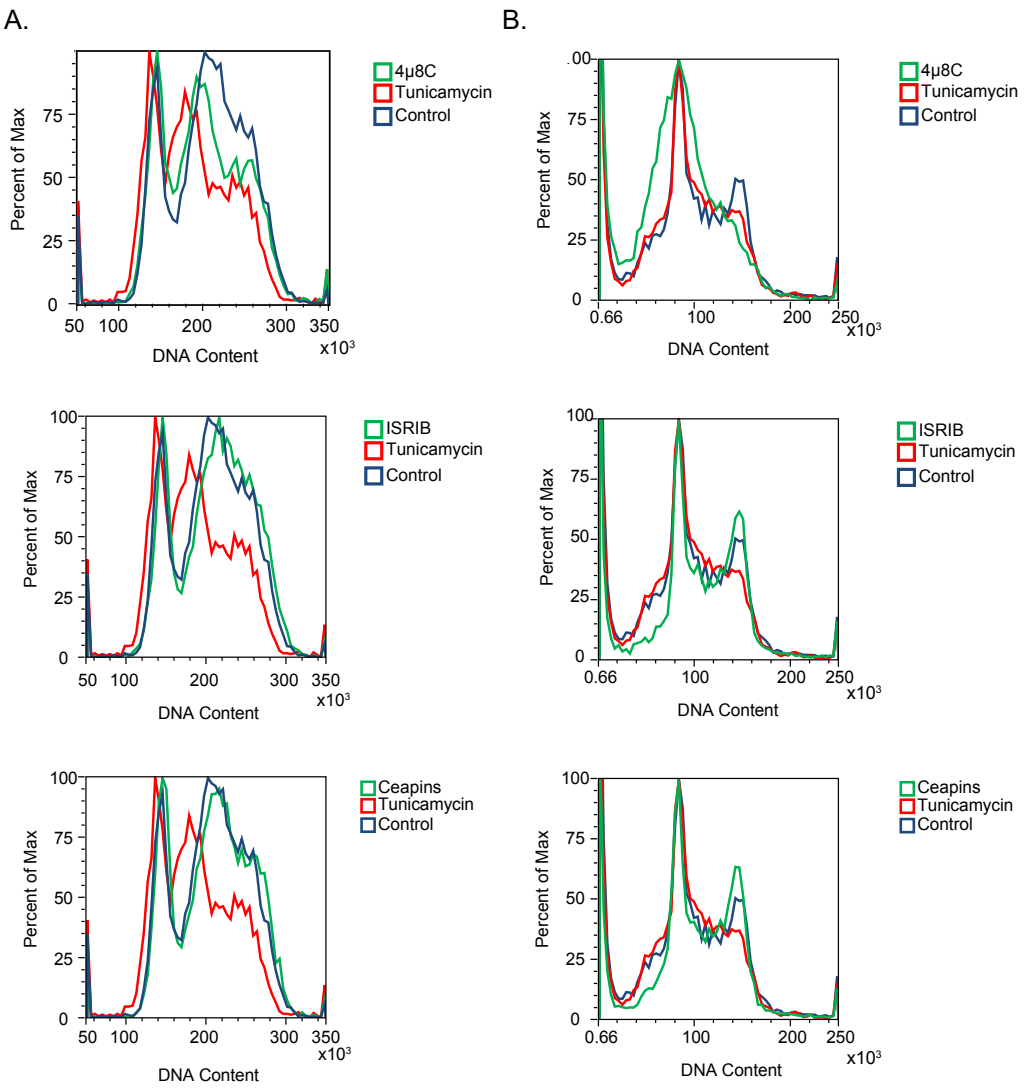

Figure 21. Treatment with 4μ8C stalls cells at the G_1/S boundary. Column A) Treatment of synchronized H4dCas9 cells with UPR inhibitors for 6 hours. Column B) Treatment of synchronized KMS11dCas9 cells with UPR inhibitors for 6 hours.

B. Methods

1. Cell viability assays

Adherent cells were seeded in a 96-well white plate at a density of 10,000 cells per well in 100μL of media the day prior to drug treatment. On the day of the treatment, the media was replaced with media containing drug at the target concentration. The plate was incubated at 37˚C for 24 hours after addition of the drugs. The next day, 50 μL of the CellTiterGlo reagent (Promega) were added to each well and luminescence was measured using a PerkinElmer 1420 Multilabel Counter VICTOR3V plate reader. Data were normalized to no drug controls (cells treated with DMSO).

2. Chronic treatment of H4dCas9, KMS11dCas9 and RPMI 8226 with UPR inhibitors

H4dCas9 cells were seeded 150,000 cells per well in a 6-well plate and treated with DMSO (no drug control), 10 μM 4μ8C, 500 nM ISRIB, or 5μM ceapin A7 for 8 days. Media (with fresh drugs) was replaced every 2 days. Before replacing the media, the cells were trypsinized and collected, and their viability was assessed by Trypan blue staining. The cells were then re-seed at the same initial density in drug-containing media. This procedure was repeated every 2 days for a total of 8 days. KMS11dCas9 and RPMI 8226 cells were seeded at a density of 500,000 cells per mL (2.5 million cells total) in 6 cm dishes and treated as described above. Every two days, the cells were collected, their viability was assessed by trypan blue staining, and they were re-seeded at their original density in drug-containing media. This

procedure was repeated every 2 days for a total of 8 days. All cell counts were conducted in duplicate on a Countess II FL automated cell counter (ThermoFisher). The cell numbers per unit volume obtained every two days were used to extrapolate the overall growth of the population.

3. Cell synchronization and treatment with UPR inhibitors for flow cytometry analysis

Cells were synchronized by double thymidine block as described in Chapter 2.C.5. Upon release, cells were treated with 10 μM 4μ8C, 1 μM ISRIB and 5 μM ceapin A7. After 6 hours, the cells were collected and fixed in ethanol for propidium iodide staining as described in Chapter 2.C.7. All data were collected on an Attune NxT flow cytometer (ThermoFisher) and analyzed using the Attune NxT software.

IV. PKMYT1 regulates IRE1 activity

The data described in chapters 2 and 3 suggests a functional link between the protein folding capacity of the ER, the UPR, and the cell cycle. I therefore hypothesized that interconnectivity between the UPR and the cell cycle machinery might be altered in cancer cells. Because multiple myeloma exhibits a reliance on the UPR and because inhibition of the UPR negatively impacts multiple myeloma cell growth (see Chapter 3), I reasoned that a functional link between cell cycle progression and the UPR could be unearthed by studying multiple myeloma cells. In this chapter, I provide evidence for such connection. I identified the cell cycle G_2/M kinase PKMYT1 as a negative regulator of IRE1. PKMYT1 is the only known membrane-associated cell cycle kinase, and its levels and activity oscillate during the cell cycle (Liu et al., 1997b). This, taken together with my data showing that PKMYT1 negatively influences IRE1 signaling, suggest a dynamic interplay between the UPR and the cell cycle.

A. Background

Cell cycle checkpoint kinases control cell cycle progression upon detection of internal and external signals, for example genome integrity and nutrient availability (see Chapter 1). I hypothesized that the cell monitors the integrity of the ER during cell cycle progression to integrate information at an “ER checkpoint”. In chapters 2 and 3, I showed data suggesting that the UPR might play a physiological role in monitoring cell cycle progression. To find mechanistic links between UPR activity and cell cycle checkpoints, I took a candidate-based approach. One possibility is that specific cell cycle regulators associate with the ER and engage the UPR to monitor ER integrity. Such type of regulation would require the physical association of such putative cell cycle regulators with endomembranes. Of all known cell cycle checkpoint kinases, only PKMYT1, also known as Myt1, localized to the ER and Golgi Apparatus, and it regulates the fragmentation of the latter during cell division (Villeneuve et al., 2013). For these reasons, PKMYT1 emerged as a top candidate that could provide a molecular link between a cell cycle checkpoint kinase and the UPR.

PKMYT1 is a relatively understudied G_2/M checkpoint threonine/tyrosine kinase that phosphorylates the CDK1/cyclin B complex to regulate the G_2/M transition (Booher et al., 1997; Liu et al., 1997b). PKMYT1 is a membrane-associated CDK1 inhibitory kinase that belongs to the same family as the nuclear tyrosine kinase

Figure 22. PKMYT1 and Wee1 are highly similar. An overlay of the PKMYT1 (PDB 3P1A, in orange) and Wee1 (PDB 1X8B, in blue).

Wee1. Structurally, PKMYT1 and Wee1 are highly similar (**Figure 22**) and they share 33.9% overall identity, 34.4% on their kinase domains. Despite such high similarity PKMYT1 and Wee1 exhibit profound biochemical differences. Unlike PKMYT1, Wee1 does not localize to the secretory apparatus, and it is only able to phosphorylate Tyr15 in CDK1 and CDK2, whereas PKMYT1 is able to phosphorylate both Thr14 and Tyr15, but only on CDK1 (Liu et al., 1997b). The biological relevance of this difference in phosphorylation targets remains unknown, but both PKMYT1 and Wee1 block the G2/M transition by inhibiting cyclin B/CDK1. Even though PKMYT1 is thought to be redundant with Wee1, this may not always be the case, as loss of PKMYT1 does not result in compensatory signaling by Wee1 in glioblastoma (Cornwell et al., 2002; Toledo et al., 2015).

Differences in subcellular localization may account for the different functions for Wee1 and PKMYT1. The Golgi apparatus goes through extensive reorganization during mitosis, which is controlled by at least three kinases; the mitogen activating kinase (MEK1), polo-like kinase (PLK) and CDK1 (Acharya et al., 1998; Lowe et al., 1998; Sütterlin et al., 2001). PKMYT1 is a substrate for MEK1 and PLK and

PKMYT1 loss-of-function alters Golgi fragmentation and ER reassembly after mitosis in HeLa cells leading to defects in reassembly of the Golgi apparatus after mitosis in *Drosophila melanogaster* cells (Booher et al., 1997; Cornwell et al., 2002; Nakajima et al., 2003; Nakajima et al., 2008a; Palmer et al., 1998; Villeneuve et al., 2013).

B. PKMYT1 loss-of-function enhances IRE1 signaling

1. Pharmacological inhibition studies

To study the role of PKMYT1 in UPR signaling, I blocked its function with the validated and commercially available PKMYT1 inhibitor PD166285 (Wang et al., 2001). PD166285 targets both PKMYT1 and Wee1, but is more selective towards the former (reported IC50 for PKMYT1 is 7.2nM whereas IC50 for Wee1 is 24nM in cancer cell lines) (Schmidt et al., 2017b). The Wee1 inhibitor MK1775, currently in clinical trials, was used as a control (Hirai et al., 2009). In these experiments, I used multiple myeloma cell lines because of their reliance on the UPR for maintenance of their secretory function. Unpublished dose-response experiments carried out in our lab indicated

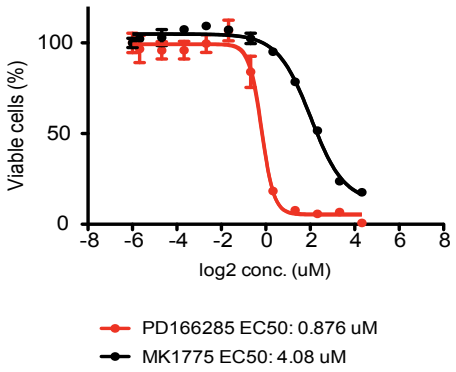

Figure 23. PD166285 shows potent anti-multiple myeloma effects. A 24-hour treatment of RPMI 8226 cells with the PKMYT1 inhibitor PD166285 or Wee1 inhibitor MK1775 reveals increased sensitivity to PKMYT1 inhibition. N=2.

that multiple myeloma cells are much more sensitive to PD166285 than MK1775 (**Figure 23**), suggesting a reliance on PKMYT1 for viability**.**

Since all multiple myeloma cells upregulate the IRE1/XBP1s axis of the UPR and are more sensitive to PKMYT1 inhibition, I hypothesized that the UPR and the G_2/M checkpoint could intersect at the IRE1 signaling arm of the UPR, (**Figure 23** and data from our laboratory)(Harnoss et al., 2019). Previous unpublished data from our laboratory suggest that PKMYT1, but not Wee1, influence IRE1 signaling: PD166285, but not MK1775, protected cells from toxicity induced by IRE1 inhibition with 4u8C in a dose-dependent manner (**Figure 24**). These results suggest an epistatic interaction between IRE1 and PKMYT1.

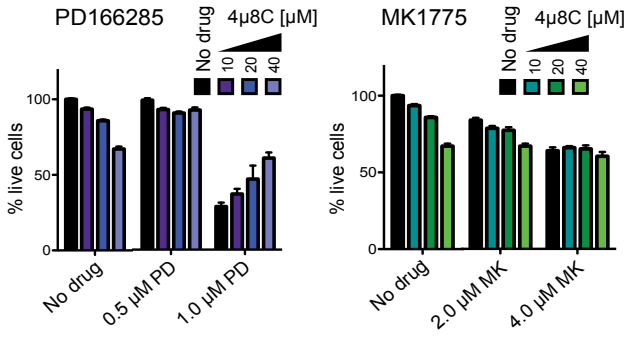

Figure 24. Inhibition of IRE1 blocks the decrease in viability seen with PD166285. Concurrent treatment with both 4μ8C and PD166285, but not with 4μ8C and MK1775, leads to a restoration of cell viability. N=3

2. Genetic depletion studies

Since kinase inhibitors are notorious for their off-target effects, and to rigorously confirm whether epistasis exists between IRE1 and PKMYT1, I knocked down PKMYT1 in multiple myeloma cells using CRSPRi and treated these cells with 4μ8C (**Figure 25**). These gene-drug interaction experiments phenocopied the drug-drug interaction results shown in Figure 23, further substantiating the potential interaction

between IRE1 and PKMYT1 (**Figure 25**). Neither ISRIB nor Ceapin A7 restore viability in PKMYT1 knockdown myeloma cells treated with 4μ8C, which further confirmed the specificity of the interaction.

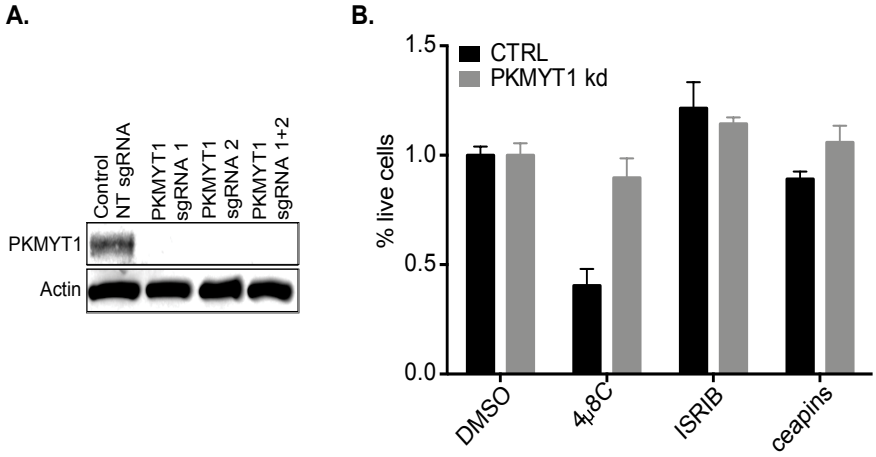

Figure 25. Genetic depletion of PKMYT1 with CRISPRi confirms IRE1-PKMYT1 epistasis in KMS11dCas9 cells. A) CRISPRi was used to knockdown (kd) PKMYT1 with either a non-targeting (NT) control or 2 different targeted sgRNAs. B) Viability of KMS11dCas9cells expressing the control (NT) sgRNA or PKMYT1 sgRNA (indicate 1 or 2) and treated with UPR inhibitors for 48 hours as described in Materials and Methods.

To further examine how PKMYT1 and IRE1 might crosstalk, I treated PKMYT1 knockdown cells with the ER poison tunicamycin (Tm) and investigated whether the loss-of-function of PKMYT1 altered IRE1 signaling. In these experiments, I observed that the loss-of-function of PKMYT1 enhanced IRE1 signaling, as determined by measuring *XBP1* mRNA splicing; recall that *XBP1* mRNA splicing depends on IRE1's RNase activity (**Figure 26**, *XBP1* mRNA splicing increased by ~2.5-fold, compare black bars for WT +Tm and PKMYT kd + Tm). As expected, the double knockdown led to suppressed *XBP1* mRNA splicing (**Figure 26**, splicing decreased by ~1.6-fold, compare black bars for PKMYT kd +Tm and double kd + Tm). However, we note that *XBP1* mRNA splicing in the double KD was still elevated compared to WT by ~1.5-fold (**Figure 26**, compare black bars for WT + Tm and double kd + Tm), which could be attributed to an incomplete knockdown of IRE1.

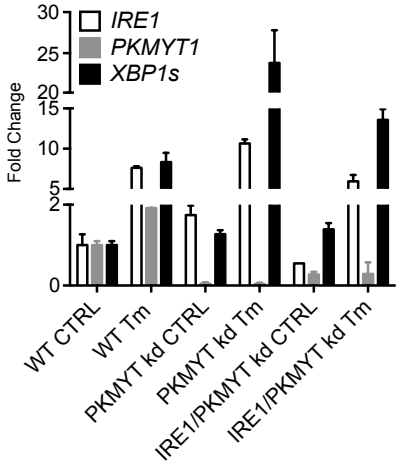

Figure 26. PKMYT1 loss-of-function de-represses IRE1 activity in KMS11dCas9 cells. PKMYT1 kd and IRE1/ PKMYT1 kd cell lines were generated by CRISPRi . All cells were subjected to 2.5 μg/mL tunicamycin (Tm) for 6 hours. Fold changes are normalized to *GAPDH*.

2. Generation of fluorescent tagged PKMYT1

PKMYT1 is not an abundant protein, which can pose a challenge for biochemical analyses. Therefore, to study the roles of PKMYT1 in cell lines, I generated a lentiviral expression construct encoding a doxycycline-inducible, fluorescently labeled version of PKMYT1. I chose an inducible system because overexpression of PKMYT1 leads to cell cycle arrest (Wells et al., 1999). To generate these constructs, I amplified the PKMYT1 coding sequence by PCR from cDNA obtained from KMS11 multiple myeloma cells. Using standard recombinant DNA techniques, I fused an N-terminal EGFP or mCherry coding sequence to the PKMYT1 coding sequence (**Figure 27A**). I tagged the protein on its N-terminus because this location is less likely to interfere with its kinase function and its membrane-association motif, which are located in PKMYT1's C-terminus (**Figure 27B**) (Liu et al., 1997b). Microscopy analyses indicated that GFP- and mCherry-tagged PKMYT1 localize to the ER and Golgi apparatus, as previously observed (Liu et al., 1997b). Interestingly, different cell lines

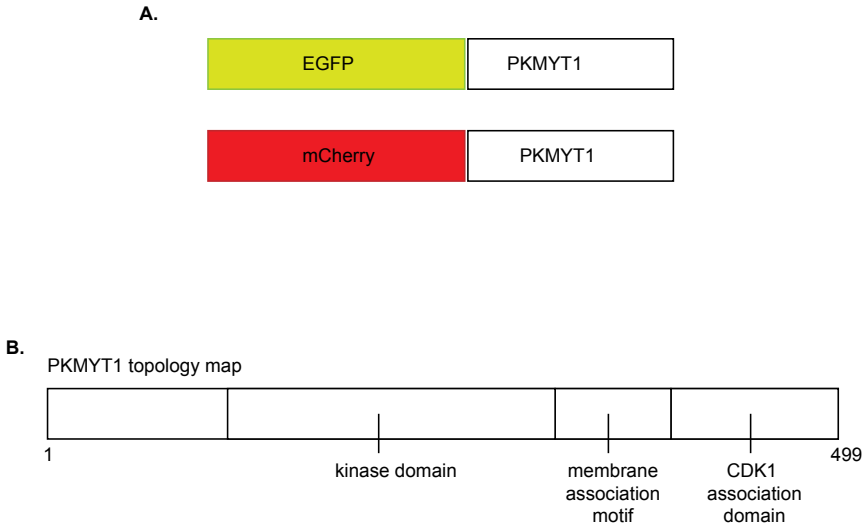

Figure 27. Chimeric PKMYT1 design based on topology of protein. A) Fluorescent-tagged PKMYT1 constructs. B) topology map of PKMYT1 protein.

showed different amounts of PKMYT1 in the ER or in the Golgi apparatus (**Figure 28**). In HeLa cells, I observed a tendency for PKMYT1 to accumulate preferentially in the Golgi apparatus, whereas in U2OS (osteosarcoma cells) and in MEFs (mouse embryonic fibroblasts) PKMYT1 preferentially associates with the ER. I carried out these experiments in well-characterized adherent cell lines because it allowed me to characterize PKMYT1's subcellular localization with more accuracy than in myeloma cells, which grow in suspension.

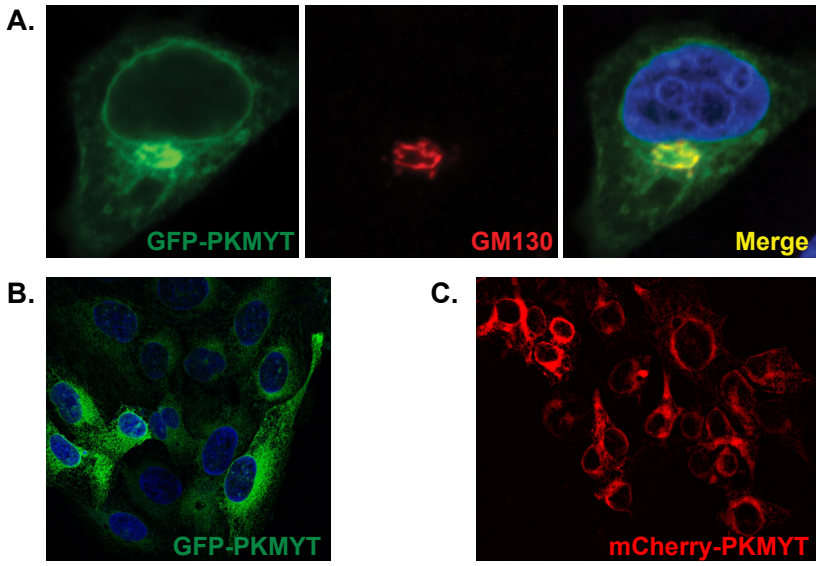

Figure 28. Fluorescently tagged PKMYT1 localizes to the ER and Golgi apparatus. A) Immunofluorescence of GFP-PKMYT in HeLa cells, with Golgi apparatus marker GM130 in red. B) GFP-PKMYT expressed in U2OS cells. C) mCherry-PKMYT1

3. Physical interaction between IRE1 and PKMYT1

To study if PKMYT1 and IRE1 physically interact, I first assessed co-localization by immunofluorescence microscopy. Since the IRE1 antibody we use in our laboratory is known to be challenging for immunofluorescence staining, I generated a stable MEF cell line encoding doxycycline inducible mCherry-PKMYT1 in addition to a doxycycline inducible IRE1-GFP (Karagöz et al., 2017). In steady-state conditions,

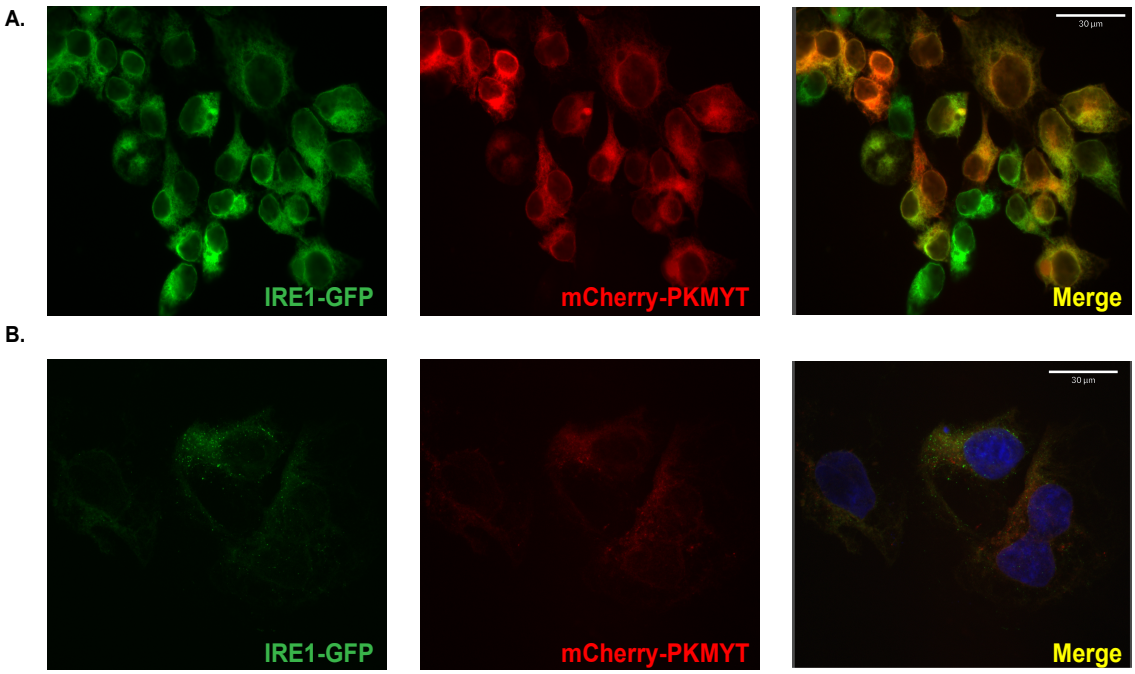

Figure 29. IRE1 and PKMYT1 are not observed to co-localize by immunofluorescence. A) Fluorescence microscopy of IRE1-GFP and mCherry-PKMYT1 in unstressed MEF cells. B) Immunofluorescence of IRE1-GFP and mCherry-PKMYT1 in cells treated with BFA as an ER stressor.

both IRE1 and PKMYT1 primarily localize to the ER (**Figure 29A**). Expectedly, upon ER stress, triggered by tunicamycin treatment, IRE1 forms puncta, which are thought to be dynamic high-order oligomeric assemblies of active IRE1 (Han Li paper). These experiments also revealed that the IRE1 foci do not colocalize with PKMYT1 signals (**Figure 29B**). Further analyses will be required to confirm the dynamic nature of PKMYT1 puncta. Induction of ER stress with other ER poisons (brefeldin A, which collapses the Golgi apparatus onto the ER, or with thapsigargin, which blocks calcium re-uptake into the ER) showed the same results (data not shown). I also carried out co-immunoprecipitation (co-IP) experiments to assess a potential interaction between IRE1 and PKYMT1. Because of PKMYT1's low

abundance, I carried out these experiments in a stable U2OS cell line encoding inducible GFP-PKMYT1 (**Figure 29B**) and pulled l down on GFP in cell lysates collected in conditions of no stress and upon ER stress induction, triggered by tunicamycin. A negative control antibody (mouse IgG) confirmed specificity (**Figure 30**) lanes IP IgG, with and without Tm). Pulldown with an anti-GFP antibody allowed recovery of CDK1 (a known interacting partner of PKMYT1), but not IRE1 (**Figure 30**, lanes IP, GFP, with and without Tm), suggesting that at least in conditions that allow to capture PKMYT1 protein-protein interactions, a physical interaction between IRE1 and PKMYT1 was not detectable. It remains possible that the PKMYT1-IRE1 interaction is transient in nature. Future experiments will be required to determine whether this is the case, for example through the use proximity labeling techniques that allow capturing transient protein-protein interactions by biotinylation (Hannigan et al., 2020).

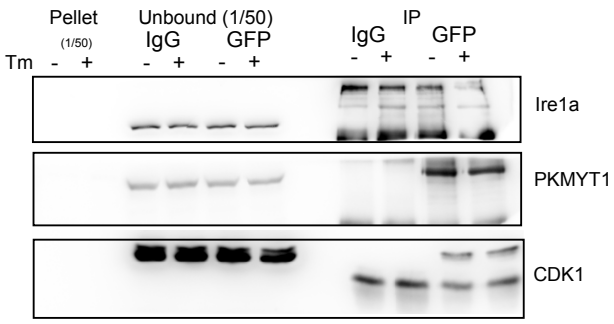

Figure 30. Co-IP of PKMYT1 and IRE1 reveals no detectable interaction between IRE1 and PKMYT1.Using U2OS cells with a Dox inducible EGFP-PKMYT1, I pulled down PKMYT1 using EGFP or IgG (a control) as bait in conditions of stress and no stress. IgG pull down shows specificity of the EGFP to pulldown known PKMYT1 interactor CDK1. However, no pulldown of IRE1a was observed.

C. Methods

1. Drug dose responses

RPMI 8226 multiple myeloma cells were seeded at a density of 20,000 cells per well in 50 µL in 96-well plates the day of experiment. 50 uL of media supplemented with 2X drug were then added to each well for a final volume of 100 uL. All tests were repeated in 3 wells to obtain technical triplicates. For experiments with 2 drugs, 25 uL of media supplemented with 4X the amount of each drug were then added to each well for a final volume of 100 uL. 24 hours after addition of the drugs, cell viability was assessed using CellTiterGlo (Promega), and the data were collected and analyzed as described in Chapter 3.C.1. For gene-drug PKMYT1/IRE1 inhibition experiments, the experimental set-up was identical, but the cell viability measurements were taken 48 hours instead of 24 hours after setting up the experiment.

2. Cloning of lentiviral sgRNAs

All sgRNA sequences and plasmids were a kind gift of Dr. Martin Kampmann (UCSF). The shRNA expression vector contains a mU6 promoter, followed by a sgRNA scaffold sequence containing a cloning site for gene-specific target sequences flanked by two restriction digest sites, BstXI and BlpI. This vector was digested with BstXI and BlpI restriction enzymes overnight, and the fragment was purified on gel. Two ssDNA complementary oligonucleotides (top and bottom)

containing the gene-specific target sequence and flanked by the restriction enzyme overhangs were annealed *in vitro* in 100 mM potassium acetate, 30 mM HEPES-KOH pH 7.4, 2 mM magnesium acetate (**Table S3** for sgRNA sequences). Briefly, the oligonucleotide mixture was heated at 95˚C for five minutes and the allowed to cool gradually to room temperature, and then diluted 1:40 in water. The diluted annealed oligonucleotides were ligated into the backbone with T4 DNA ligase at 16˚C overnight, and transformed into competent DH5a bacteria. All clones screened by sequencing.

3. Lentiviral packaging and transduction of sgRNAs

See detailed protocol in Chapter 2.C.2.

4. Western blot to confirm knockdown of PKMYT1

See detailed protocol in Chapter 2.C.9.

5. RNA extraction and cDNA synthesis

See detailed protocol in Chapter 2.C.10.

6. Gene expression data and analysis

See detailed protocol in Chapter 2.C.11.

7. Cloning of a lentiviral, inducible fluorescently tagged PKMYT1

A forward primer containing a BsrGI recognition site and a reverse primer containing an EcoRI recognition site were used to amplify the PKMYT1 coding sequence by PCR from cDNA obtained from KMS11 cells (**Table S2**). This PCR product was then ligated in frame with the GFP coding sequence in the pEGFP-C1 vector (Clontech) using BsrGI and MfeI restriction digest sites. The entire open reading frame, GFP-PKMYT1 was transferred into a single lentivirus inducible system as described before (Elif paper). All constructs were verified by sequencing. To construct mCherry-PKMYT1, the GFP coding sequence of pEGFP-PKMYT1 was swapped for that encoding mCherry using AfeI and BsrGI restriction digest sites.

8. Immunofluorescence assays

Cells were seeded onto coverslips placed into 24 well plates at a density of 60,000 cells per well. The cells were allowed to attach overnight. The following day, 100 ng/mL doxycycline were added to each well and the cells were incubated for 24 hours at 37C before fixation and immunostaining. When the experimental design called for induction of ER stress, ER poisons were added after doxycycline treatment as follows: 2 µg/mL BFA for 30 minutes, 2.5 ug/mL for 6 hours, or 100 nM thapsigargin for 3 hours. The cells were fixed in 4% PFA for 10 minutes. Following fixation, the cells were washed three times with 1x PBS before blocking/permeabilization in 50mM NH_4Cl, 0.5% BSA, 0.02% NaN_3, 0.05% saponin in PBS for 20 minutes. Coverslips were incubated with primary antibody overnight, diluted in blocking buffer at the concentrations indicated in appendix table S4. After

primary antibody incubation, the cells were washed three times with 1x PBS before incubation with 300 nM DAPI and secondary antibody for one hour. Cells were washed three times with 1x PBS before mounting the coverslips onto glass sides for permanent storage.

9. Co-immunoprecipitation of GFP-PKMYT1

U2OS Dox inducible GFP-PKMYT1 cells were plated in T175 flasks (3 flasks per condition, control or ER stress). When the cells reached 60% confluence, 100 ng/mL doxycycline was added and the cells were incubated overnight. The following day, three flasks were treated with 2.5µg/mL tunicamycin for 6 hours. The remaining three remained untreated. Cells were collected after media aspiration, in 500 µL of ice cold PBS using cell scarpers. The cells were lysed in lysis buffer (25mM Tris pH 7.4, 150 mM NaCl, 1 mM EDTA, 0.1% NP-40, 0.1% Triton X-100, 1mM NaF, 50mM Na_3VO_4, and 1x Roche Protease Inhibitor Cocktail) on ice for 10 minutes, with gentle vortexing every 2-3 minutes. Nuclei were pelleted by centrifugation and the supernatant was placed into a fresh pre-chilled microcentrifuge tube. A 10 uL fraction of this supernatant was used to quantify protein concentration by Bradford assay. 1 mg of protein was used for each IP. Lysates were incubated with control IgG or anti-GFP antibody overnight at 4˚C on a rotator. The following day, Protein G Dynabeads were added and incubated for an additional 45 minutes. Immunoprecipitates were collected on a magnetic stand, washed 3 times with ice-cold lysis buffer, and then resuspended in Laemmli buffer for SDS-PAGE and Western blot analysis.

V. Discussion and Future Directions

Progression through the cell cycle requires the coordination of many interconnected signaling pathways. In this work I provide evidence for interconnectivity between the ER protein folding capacity, the UPR, and cell cycle progression, in mammalian cells. In chapter 2, I found out that the levels of ER chaperones and foldases increase during interphase. In chapter 3, I show that both activation of the UPR and inhibition of IRE1, delay cell cycle progression at the G1/S boundary. Finally, in chapter 4, I show crosstalk between the membrane-localized cell cycle checkpoint kinase PKMYT1, which blocks progression through the G2/M boundary, and IRE1, the most conserved UPR sensor/transducer. Together, these results suggest that cell actively monitors ER integrity and function throughout the cell cycle in an “ER checkpoint” to ensure inheritance of endoplasmic reticulum by daughter cells.

A. The chaperone content of the ER is linked to the cell cycle

Symmetric cell division requires cells to approximately double their organellar content prior to cell division (Chapter 1). For example, mitochondria and peroxisomes increase in numbers prior to division, and the Golgi apparatus enlarges at the G_1 and S/G_2 boundary (Hettema and Motley, 2009; Sin and Harrison, 2016). Following on these observations, I hypothesized that the ER, the single largest organelle in the cell, must grow as well. Both the peripheral ER and the nuclear envelope need to enlarge prior to division in order to re-establish the organelle in daughter cells and maintain nuclear integrity (De Magistris and Antonin, 2018). In line with this notion, I found that the chaperone and foldase content of the ER increases by approximately 37% in non-secretory cells (H4 neuroglioma) and approximately 26% in professional secretory cells (KMS11 multiple myeloma) in S/G_2. This observation aligns with previous reports demonstrating that the contents of the Golgi apparatus increase by approximately 40% in non-secretory HeLa cells (Sin and Harrison, 2016). Together, these data suggest that the protein processing capacity of the secretory apparatus increases in preparation for cell division. Interestingly, multiple myeloma cells showed a less dramatic increase in ER protein content, which could reflect the fact that they already possess an expanded

secretory apparatus, a physiological consequence of their increased secretory burden (Gass, 2004).

It is possible that the increase in protein content of the ER was underestimated because the FAST-FUCCI system cannot separate cells in S from those in G_2. Considering that protein content of the Golgi apparatus steadily increases from G_1 to S to G_2, analyzing a mixed S/G_2 cell population may dilute any effects when measured by flow cytometry (i.e., detecting chaperone and foldase content) (Sin and Harrison, 2016). In addition, it has been reported that that the plasma membrane grows during mitosis prior to cytokinesis (Graham et al., 1973). Moreover, ribosome profiling experiments indicate that the mRNAs encoding lipid metabolism enzymes are translated preferentially during mitosis (Stumpf et al., 2013). Because the source of all membranes in the cell is the ER, it is conceivable that the ER enlarges through endomembrane biosynthesis after G_2 and immediately prior to cytokinesis. Future experiments measuring lipid synthesis and metabolism using sorted FAST-FUCCI cells could help elucidate lipid activity at the ER.

It is plausible that the increase in ER chaperone content I observed (Chapter 2, **Figure 14**) is coupled to a physical enlargement of the ER, as has been described for the Golgi apparatus (Sin and Harrison, 2016). However, TEM data in FAST-FUCCI cells did not provide conclusive evidence of endomembrane growth. The increase in volume of the Golgi apparatus in G_1 versus G_2 is at most 140%, as determined by TEM (Sin and Harrison, 2016). However, when compared to the ER, the Golgi is much smaller, leading to a larger surface area to volume ratio. Thus, further studies are needed to address the possibility that small differences in

endomembrane growth could lead to a small increase in ER volume, relative to those observed for the Golgi apparatus, and that I underestimated these changes in my experiments.

It is also possible that the ER undergoes structural changes prior to cell division. Reticulons and REEPs are ubiquitous wedge-like ER-shaping proteins that regulate whether the ER adopts a more tubular structure by induce membrane curvature (Wang and Rapoport, 2019). Future experiments in FAST-FUCCI cells staining for reticulons and REEPs may reveal whether changes in ER morphology accompany the changes observed in chaperone content observed as cells progress through interphase.

The increase in chaperone content of the ER suggests that its protein folding capacity increases in S/G_2. A main regulator controlling the abundance of ER chaperones is the UPR. The UPR induces chaperones and foldases to adjust the ER protein folding capacity according to the needs of the cell. The increase in ER chaperone content associated with the cell cycle suggests there is a physiological need for the UPR during cell cycle progression. The UPR also regulates the physical expansion of the ER through endomembrane biosynthesis, it induces reticulons and REEPs, and it controls the abundance of ERAD machinery (Lee et al., 2003; Tirasophon et al., 2000; Tirasophon et al., 1998). Therefore, it is possible that the UPR regulates changes in ER volume and structure and fine-tunes the ER's protein degradative capacity during the cell cycle. If this is the case, then the UPR would serve a pivotal role connecting ER physiology and cell cycle progression.

One way in which regulatory control of ER physiology during the cell cycle progression could be enforced is by changing the threshold for UPR activation in different stages of the cell cycle. For example, it is possible that cells in G_1 and in G_2 exhibit differential sensitivity to ER stress. Treating FUCCI cells with classical ER stress inducers will allow me to address this question. If this is the case, it is possible that such differential UPR arises from passive or active mechanisms. For instance, in a passive mechanism, it is possible that G_2 cells are less sensitive to UPR induction upon stimulation with ER stress inducing agents because they upregulate their ER chaperone content, as suggested by our data. In a non-mutually exclusive active mechanism, it is possible that cells suppress UPR signaling in G2 through the actions of other genes and proteins that fine-tune the UPR, as occurs with the interplay between IRE1 and PKMYT1 discussed below. Additional work is required to address these possibilities. For example, CRISPRi-based drop-out and enrichment genetic screens in the background of IRE1 knockdown can be deployed to identify additional key players and delineate alternative mechanisms.

B. Inhibition of IRE1 delays cell cycle at defined boundaries

The UPR plays a pivotal role in homeostatic adjustment upon perturbations to both ER proteostasis and lipid homeostasis. Because my data suggests that the ER protein folding capacity increases as cells progress through the cell cycle, I predicted that inhibition of specific UPR components might alter cell cycle progression. In line with this notion, pharmacological inhibition of IRE1's RNase

activity, but not PERK or ATF6, delayed the kinetics of cell cycle progression. It is possible that IRE1's role in the cell cycle depends on activation of XBP1, which in turn increases the ER biosynthetic capacity (Lee et al., 2003). Future experiments using constructs encoding inducible dominant negative IRE1 and XBP1 versions may help address this possibility. These constructs will also allow bypassing cellular adaptation arising from constitutive CRISPRi knockdown of XBP1 or IRE1.

Assuming cellular adaptation is not a confounding factor, an approach consisting of "co-culture" type experiments based on cell-cell competition models (Bowling et al., 2019), could be deployed to investigate the cell's reliance on specific UPR components to control cell cycle kinetics. an also help pinpoint adaptation. In these experiments, control green fluorescent cells transduced with a nontargeting sgRNA can be col-cultured with red fluorescent cells transduced with specific sgRNAs targeting each UPR sensor. Ratiometric analyses using flow cytometry will tell if the red cells show a competitive disadvantage that could be interpreted as a delayed cell cycle progression.

The delayed cell cycle progression observed upon blockade of IRE1's RNase-activity hints at a fundamental mechanism that interconnects surveillance of ER stress and the cell cycle through IRE1, which is consistent with IRE1 being the most ancestral UPR sensor. A delay at the G_1/S boundary in both secretory and non-secretory cells suggests that even though IRE1 is not required for entrance into S phase, it is involved in a checkpoint. Because the cells transition from G1 to S even in the absence of functional IRE1 signaling, it is possible that this checkpoint is controlled by IRE1 together with other proteins. Such epistatic interactions could be

revealed using CRISPR-based genetic screens in the background of IRE1 loss-of-function (double loss-of-function phenotypes).

Considering that IRE1 signaling plays a role in controlling cytokinesis in yeast, it is conceivable that IRE1 could also plays roles at the G2/M transition in mammalian cells (Bicknell et al., 2007). IF this is the case, one can anticipate that blocking IRE1 delays cell cycle progression through the G2/M boundary. It is possible that PKMYT1 physiologically enforces regulatory control of IRE1 at the G2/M transition to control the kinetics of mitotic entry. The experiments presented in Chapters 2-4, a support a model for the IRE1 signaling in the context of the cell cycle (**Figure 31**). In this model, a set level of physiological IRE1 activity is required to preserve normal kinetics of cell cycle progression whereas over-activation of IRE1 -and other UPR sensors- can lead to cell cycle arrest as a precautionary measure until the stress can be mitigated. Future work will be required to rigorously test this model and establish its molecular circuitry with precision. A recent report suggesting that IRE1 can signal differentially depending on input, proteotoxic stress or lipid bilayer stress (Ho et al., 2020), provides an attractive pivot for the notion that IRE1 might regulate

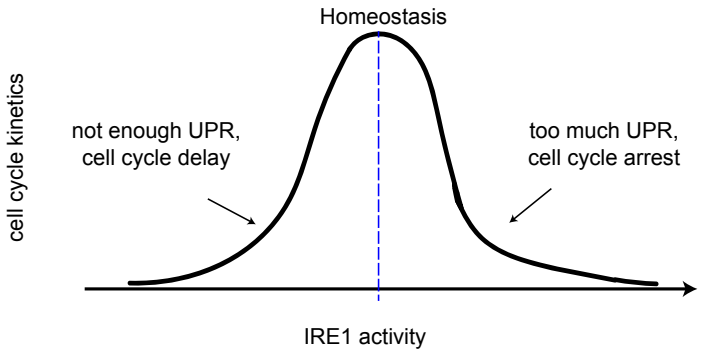

Figure 31. A model for IRE1 signaling as a function of cell cycle kinetics. When there is too much or too little signaling by IRE1, cell cycle kinetics are altered in order to accommodate (by delay if not enough signal, or arrest if overstimulation).

the coupled enlargement of the endomembrane system and chaperone content of the ER during cell cycle progression. It is possible that the additional factors fine tune IRE1 signaling as needed for ER expansion during interphase of the cell cycle.

C. PKMYT1 suppresses IRE1 signaling

PKMYT1, a membrane-localized member of the Wee1 kinase family is a negative regulator of cell cycle progression at the G2/M transition and has been linked to fragmentation and assembly of the secretory apparatus pre and post-mitosis (see Chapter 4). My data suggest that PKMYT1 suppresses IRE1 signaling, but the precise mechanism is not known. Co-localization and co-immunoprecipitation experiments did not reveal a physical interaction between the two proteins. However, it is possible that the interaction exists and is transient in nature as levels and activity of PKMYT1 oscillate during the cell cycle. Proximity labeling experiment could be deployed to address this possibility. Proximity labeling experiments to define ER “interactomes” identified PKMYT1 as an interactor of the Sec61b translocon, and given that interactions between Sec61 and IRE1 have been recently described it is plausible that the Sec61 translocon provides a hub in which IRE1 and PKMYT1 could interact (Hannigan et al., 2020; Plumb et al., 2015; Sundaram et al., 2018). Future work using different co-IP conditions coupled to genetic loss-of-function experiments will elucidate if this is a plausible mechanism for IRE1 suppression by PKMYT1. However, it is also possible that the interaction between

PKMYT1 and IRE1 is indirect and that PKMYT1 and IRE1 engage each other through regulatory feedback loops with yet-to-de-described intermediates.

PKMYT1 and IRE1 could also potentially crosstalk via non protein-protein interaction mechanisms, for example, the *PKMYT1* mRNA could be a substrate of RIDD. In this way IRE1 and PKMYT1 could engage each other in a futile cycle, until one mechanism supersedes the other, for example in G2 where PKMYT1 suppresses IRE1. An alternative hypothesis could hinge on the transcription factor activity of XBP1s; it is conceivable that XBP1s is able to upregulate other targets that could impact PKMYT1 levels or activity. RNA-seq experiments in wild type and IRE1 knockdown cells could reveal differences in transcriptional state of cells in different stages of the cell cycle subjected to ER stress. This work could help to elucidate new players that could bridge interconnectivity between PKMYT1 and IRE1.

PKMYT1 was identified originally as a Wee1 family kinase that is able to activate under conditions of genotoxic stress (Chow and Poon, 2013). The integrity and duplication of the genome is known to be actively regulated throughout the cell cycle, and these regulatory activities often constitute checkpoints that allow cells to pass through cell cycle stage boundaries (G1/S, G2/M) (Alberts et al., 2004). On first principles, similar checkpoints exist to monitor the integrity and growth of organelles prior to cell division. A “Golgi mitotic checkpoint” has been described that ensures organelle inheritance post-mitosis (Corda et al., 2012). However, no such checkpoint has been described for the ER, which is a large contiguous organelle that must be partitioned, as ER cannot be generated *de novo*. The UPR

provides a central homeostatic mechanism that is able to oversee and modulate ER structure and function, including proteostatic and lipidic readjustment. My data support a model in which PKMYT1, by suppressing IRE1, might serve as a non-compulsory temporal break on the cell cycle that allows monitoring ER integrity (Fig. 2). Releasing the break would require a healthy ER that is competent for cell division. In this way, one can envision that a cell cycle "ER checkpoint" relies on IRE1-PKMYT1 crosstalk. Future work, such as substituting kinase deficient or mis-localized mutants of PKMYT1 could reveal the functional and contextual importance of PKMYT1 during activation of the UPR.

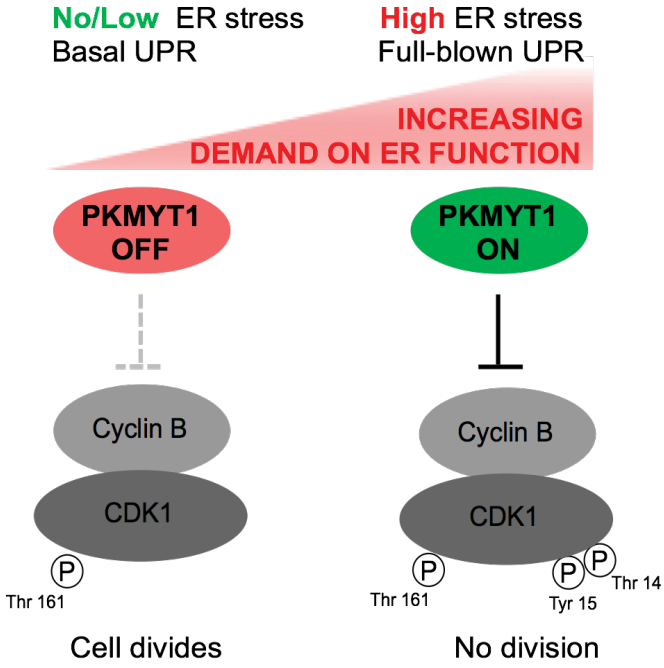

Figure 32. A model for PKMYT1 signaling during ER stress. In conditions of activation of the UPR, PKMYT1 is able to suppress progression through the cell cycle by inhibiting the CDK1/cyclin B complex.

Taken together, my data provide strong evidence that the UPR might play a physiological role in an "ER checkpoint" that is able to monitor and fine-tune ER health throughout the cell cycle.

References

Acharya, U., Mallabiabarrena, A., Acharya, J.K., and Malhotra, V. (1998). Signaling via mitogen-activated protein kinase kinase (MEK1) is required for Golgi fragmentation during mitosis. Cell *92*, 183-192.

Acosta-Alvear, D., Zhou, Y., Blais, A., Tsikitis, M., Lents, N.H., Arias, C., Lennon, C.J., Kluger, Y., and Dynlacht, B.D. (2007). XBP1 controls diverse cell type- and condition-specific transcriptional regulatory networks. Mol Cell *27*, 53-66.

Adamson, B., Norman, T.M., Jost, M., Cho, M.Y., Nuñez, J.K., Chen, Y., Villalta, J.E., Gilbert, L.A., Horlbeck, M.A., Hein, M.Y.*, et al.* (2016). A Multiplexed Single-Cell CRISPR Screening Platform Enables Systematic Dissection of the Unfolded Protein Response. Cell *167*, 1867-1882.e1821.

Alberts, B., Johnson, A., Lewis, J., Raff, M., Roberts, K., and Walter, P. (2004). Molecular Biology of the Cell, 4th edition (New York: Garland Science).

Anderson, D.J., and Hetzer, M.W. (2008). Reshaping of the endoplasmic reticulum limits the rate for nuclear envelope formation. *182*, 911-924.

Appenzeller-Herzog, C. (2006). The ER-Golgi intermediate compartment (ERGIC): in search of its identity and function. Journal of Cell Science *119*, 2173-2183.

Arnstein, P., Taylor, D.O.N., Nelson-Rees, W.A., Huebner, R.J., and Lennette, E.H. (1974). Propagation of Human Tumors in Antithymocyte Serum-Treated Mice2. JNCI: Journal of the National Cancer Institute *52*, 71-84.

Assoian, R.K., and Schwartz, M.A. (2001). Coordinate signaling by integrins and receptor tyrosine kinases in the regulation of G1 phase cell-cycle progression. Current Opinion in Genetics & Development *11*, 48-53.

Babour, A., Bicknell, A.A., Tourtellotte, J., and Niwa, M. (2010). A Surveillance Pathway Monitors the Fitness of the Endoplasmic Reticulum to Control Its Inheritance. *142*, 256-269.

Bae, D., Moore, K.A., Mella, J.M., Hayashi, S.Y., and Hollien, J. (2019). Degradation of Blos1 mRNA by IRE1 repositions lysosomes and protects cells from stress. J Cell Biol *218*, 1118-1127.

Bakunts, A., Orsi, A., Vitale, M., Cattaneo, A., Lari, F., Tadè, L., Sitia, R., Raimondi, A., Bachi, A., and Van Anken, E. (2017). Ratiometric sensing of BiP-client versus BiP levels by the unfolded protein response determines its signaling amplitude. eLife *6*.

Benmaamar, R., and Pagano, M. (2005). Involvement of the SCF Complex in the Control of Cdh1 Degradation in S-phase. Cell Cycle *4*, 1230-1232.

Bergeland, T., Widerberg, J., Bakke, O., and Nordeng, T.W. (2001). Mitotic partitioning of endosomes and lysosomes. *11*, 644-651.

Besson, A., Dowdy, S.F., and Roberts, J.M. (2008). CDK Inhibitors: Cell Cycle Regulators and Beyond. Developmental Cell *14*, 159-169.

Bicknell, A.A., Babour, A., Federovitch, C.M., and Niwa, M. (2007). A novel role in cytokinesis reveals a housekeeping function for the unfolded protein response. J Cell Biol *177*, 1017-1027.

Birky, C.W. (1983). The Partitioning of Cytoplasmic Organelles at Cell Division. In Aspects of Cell Regulation, J.F. Danielli, ed. (Academic Press), pp. 49-89.

Blobel, G., and Dobberstein, B. (1975). Transfer of proteins across membranes. I. Presence of proteolytically processed and unprocessed nascent immunoglobulin light chains on membrane-bound ribosomes of murine myeloma. Journal of Cell Biology *67*, 835-851.
Booher, R.N., Holman, P.S., and Fattaey, A. (1997). Human Myt1 Is a Cell Cycle-regulated Kinase That Inhibits Cdc2 but Not Cdk2 Activity. Journal of Biological Chemistry *272*, 22300-22306.
Bourougaa, K., Naski, N., Boularan, C., Mlynarczyk, C., Candeias, M.M., Marullo, S., and Fahraeus, R. (2010a). Endoplasmic reticulum stress induces G2 cell-cycle arrest via mRNA translation of the p53 isoform p53/47. Mol Cell *38*, 78-88.
Bourougaa, K., Naski, N., Boularan, C., Mlynarczyk, C., Candeias, M.M., Marullo, S., and Fåhraeus, R. (2010b). Endoplasmic Reticulum Stress Induces G2 Cell-Cycle Arrest via mRNA Translation of the p53 Isoform p53/47. *38*, 78-88.
Bowling, S., Lawlor, K., and Rodríguez, T.A. (2019). Cell competition: the winners and losers of fitness selection. Development *146*, dev167486.
Braakman, I., and Hebert, D.N. (2013). Protein Folding in the Endoplasmic Reticulum. Cold Spring Harbor Perspectives in Biology *5*, a013201-a013201.
Brewer, J.W., and Diehl, J.A. (2000). PERK mediates cell-cycle exit during the mammalian unfolded protein response. Proc Natl Acad Sci U S A *97*, 12625-12630.
Brewer, J.W., Hendershot, L.M., Sherr, C.J., and Diehl, J.A. (1999). Mammalian unfolded protein response inhibits cyclin D1 translation and cell-cycle progression. Proceedings of the National Academy of Sciences of the United States of America *96*, 8505-8510.
Brosh, R., and Rotter, V. (2009). When mutants gain new powers: news from the mutant p53 field. Nature Reviews Cancer *9*, 701-713.
Cadart, C., Monnier, S., Grilli, J., Saez, P.J., Srivastava, N., Attia, R., Terriac, E., Baum, B., Cosentino-Lagomarsino, M., and Piel, M. (2018). Size control in mammalian cells involves modulation of both growth rate and cell cycle duration. Nat Commun *9*, 3275.
Calfon, M., Zeng, H., Urano, F., Till, J.H., Hubbard, S.R., Harding, H.P., Clark, S.G., and Ron, D. (2002). IRE1 couples endoplasmic reticulum load to secretory capacity by processing the XBP-1 mRNA. Nature *415*, 92-96.
Campisi, J., and D'Adda Di Fagagna, F. (2007). Cellular senescence: when bad things happen to good cells. Nature Reviews Molecular Cell Biology *8*, 729-740.
Cánepa, E.T., Scassa, M.E., Ceruti, J.M., Marazita, M.C., Carcagno, A.L., Sirkin, P.F., and Ogara, M.F. (2007). INK4 proteins, a family of mammalian CDK inhibitors with novel biological functions. IUBMB Life *59*, 419-426.
Carreras-Sureda, A., Pihán, P., and Hetz, C. (2018). Calcium signaling at the endoplasmic reticulum: fine-tuning stress responses. Cell Calcium *70*, 24-31.
Chemaly, E.R., Troncone, L., and Lebeche, D. (2018). SERCA control of cell death and survival. Cell Calcium *69*, 46-61.
Chen, M., Gutierrez, G.J., and Ronai, Z.A. (2011). Ubiquitin-recognition protein Ufd1 couples the endoplasmic reticulum (ER) stress response to cell cycle control. Proc Natl Acad Sci U S A *108*, 9119-9124.
Chevet, E., Hetz, C., and Samali, A. (2015). Endoplasmic Reticulum Stress-Activated Cell Reprogramming in Oncogenesis. Cancer Discovery *5*, 586-597.

Chow, J.P., and Poon, R.Y. (2013). The CDK1 inhibitory kinase MYT1 in DNA damage checkpoint recovery. Oncogene *32*, 4778-4788.
Clarke, H.J., Chambers, J.E., Liniker, E., and Marciniak, S.J. (2014). Endoplasmic Reticulum Stress in Malignancy. Cancer Cell *25*, 563-573.
Clarke, S.T., Calderon, V., and Bradford, J.A. (2017). Click Chemistry for Analysis of Cell Proliferation in Flow Cytometry. Current Protocols in Cytometry *82*, 7.49.41-47.49.30.
Colanzi, A., Carcedo, C.H., Persico, A., Cericola, C., Turacchio, G., Bonazzi, M., Luini, A., and Corda, D. (2007). The Golgi mitotic checkpoint is controlled by BARS-dependent fission of the Golgi ribbon into separate stacks in G2. *26*, 2465-2476.
Collins, K., Jacks, T., and Pavletich, N.P. (1997). The cell cycle and cancer. Proceedings of the National Academy of Sciences *94*, 2776.
Conlon, I., and Raff, M. (2003). Differences in the way a mammalian cell and yeast cells coordinate cell growth and cell-cycle progression. J Biol *2*, 7-7.
Corda, D., Barretta, M.L., Cervigni, R.I., and Colanzi, A. (2012). Golgi complex fragmentation in G2/M transition: An organelle-based cell-cycle checkpoint. IUBMB Life *64*, 661-670.
Cornwell, W.D., Kaminski, P.J., and Jackson, J.R. (2002). Identification of Drosophila Myt1 kinase and its role in Golgi during mitosis. Cellular Signalling *14*, 467-476.
Costa-Mattioli, M., and Walter, P. (2020). The integrated stress response: From mechanism to disease. Science *368*, eaat5314.
Coverley, D., Laman, H., and Laskey, R.A. (2002). Distinct roles for cyclins E and A during DNA replication complex assembly and activation. Nature Cell Biology *4*, 523-528.
Cox, J.S., Shamu, C.E., and Walter, P. (1993). Transcriptional induction of genes encoding endoplasmic reticulum resident proteins requires a transmembrane protein kinase. Cell *73*, 1197-1206.
Credle, J.J., Finer-Moore, J.S., Papa, F.R., Stroud, R.M., and Walter, P. (2005). On the mechanism of sensing unfolded protein in the endoplasmic reticulum. Proceedings of the National Academy of Sciences *102*, 18773-18784.
Cross, B.C.S., Bond, P.J., Sadowski, P.G., Jha, B.K., Zak, J., Goodman, J.M., Silverman, R.H., Neubert, T.A., Baxendale, I.R., Ron, D.*, et al.* (2012). The molecular basis for selective inhibition of unconventional mRNA splicing by an IRE1-binding small molecule. Proceedings of the National Academy of Sciences *109*, E869.
Darzynkiewicz, Z., Huang, X., and Zhao, H. (2017). Analysis of Cellular DNA Content by Flow Cytometry. Current Protocols in Cytometry *82*, 7.5.1-7.5.20.
De Magistris, P., and Antonin, W. (2018). The Dynamic Nature of the Nuclear Envelope. Curr Biol *28*, R487-r497.
Denz, M., Chiantia, S., Herrmann, A., Mueller, P., Korte, T., and Schwarzer, R. (2017). Cell cycle dependent changes in the plasma membrane organization of mammalian cells. Biochimica et Biophysica Acta (BBA) - Biomembranes *1859*, 350-359.

Dewhirst, M.W., Cao, Y., and Moeller, B. (2008). Cycling hypoxia and free radicals regulate angiogenesis and radiotherapy response. Nature Reviews Cancer *8*, 425-437.
Dreier, L., and Rapoport, T.A. (2000). In Vitro Formation of the Endoplasmic Reticulum Occurs Independently of Microtubules by a Controlled Fusion Reaction. The Journal of Cell Biology *148*, 883-898.
Ducommun, B., Brambilla, P., Félix, M.A., Franza, B.R., Karsenti, E., and Draetta, G. (1991). cdc2 phosphorylation is required for its interaction with cyclin. The EMBO Journal *10*, 3311-3319.
Dufey, E., Bravo-San Pedro, J.M., Eggers, C., Gonzalez-Quiroz, M., Urra, H., Sagredo, A.I., Sepulveda, D., Pihan, P., Carreras-Sureda, A., Hazari, Y.*, et al.* (2020). Genotoxic stress triggers the activation of IRE1alpha-dependent RNA decay to modulate the DNA damage response. Nat Commun *11*, 2401.
Duran-Aniotz, C., Martínez, G., and Hetz, C. (2014). Memory loss in Alzheimer's disease: are the alterations in the UPR network involved in the cognitive impairment? *6*.
Ellenberg, J., Siggia, E.D., Moreira, J.E., Smith, C.L., Presley, J.F., Worman, H.J., and Lippincott-Schwartz, J. (1997). Nuclear Membrane Dynamics and Reassembly in Living Cells: Targeting of an Inner Nuclear Membrane Protein in Interphase and Mitosis. The Journal of Cell Biology *138*, 1193-1206.
Fantes, P., and Nurse, P. (1977). Control of cell size at division in fission yeast by a growth-modulated size control over nuclear division. *107*, 377-386.
Fesquet, D., Labbé, J.C., Derancourt, J., Capony, J.P., Galas, S., Girard, F., Lorca, T., Shuttleworth, J., Dorée, M., and Cavadore, J.C. (1993). The MO15 gene encodes the catalytic subunit of a protein kinase that activates cdc2 and other cyclin-dependent kinases (CDKs) through phosphorylation of Thr161 and its homologues. The EMBO Journal *12*, 3111-3121.
Franke, W.W., Scheer, U., Krohne, G., and Jarasch, E.D. (1981). The nuclear envelope and the architecture of the nuclear periphery. The Journal of Cell Biology *91*, 39s-50s.
Friedman, J.R., Lackner, L.L., West, M., Dibenedetto, J.R., Nunnari, J., and Voeltz, G.K. (2011). ER Tubules Mark Sites of Mitochondrial Division. Science *334*, 358-362.
Fulciniti, M., Lin, C.Y., Samur, M.K., Lopez, M.A., Singh, I., Lawlor, M.A., Szalat, R.E., Ott, C.J., Avet-Loiseau, H., Anderson, K.C.*, et al.* (2018). Non-overlapping Control of Transcriptome by Promoter- and Super-Enhancer-Associated Dependencies in Multiple Myeloma. Cell Rep *25*, 3693-3705 e3696.
Gallagher, C.M., Garri, C., Cain, E.L., Ang, K.K.-H., Wilson, C.G., Chen, S., Hearn, B.R., Jaishankar, P., Aranda-Diaz, A., Arkin, M.R.*, et al.* (2016). Ceapins are a new class of unfolded protein response inhibitors, selectively targeting the ATF6α branch. Elife *5*.
Gallagher, C.M., and Walter, P. (2016). Ceapins inhibit ATF6α signaling by selectively preventing transport of ATF6α to the Golgi apparatus during ER stress. Elife *5*.
Gartel, A.L., and Tyner, A.L. (1999). Transcriptional Regulation of the p21(WAF1/CIP1)Gene. Experimental Cell Research *246*, 280-289.

Gass, J. (2004). Stressed-out B cells? Plasma-cell differentiation and the unfolded protein response. *25*, 17-24.
Gerace, L., Blum, A., and Blobel, G. (1978). Immunocytochemical localization of the major polypeptides of the nuclear pore complex-lamina fraction. Interphase and mitotic distribution. The Journal of Cell Biology *79*, 546-566.
Gerace, L., and Burke, B. (1988). Functional Organization of the Nuclear Envelope. Annual Review of Cell Biology *4*, 335-374.
Gerard, C., and Goldbeter, A. (2009). Temporal self-organization of the cyclin/Cdk network driving the mammalian cell cycle. *106*, 21643-21648.
Gérard, C., and Goldbeter, A. (2014). The balance between cell cycle arrest and cell proliferation: control by the extracellular matrix and by contact inhibition. Interface Focus *4*, 20130075.
Gilbert, L.A., Horlbeck, M.A., Adamson, B., Villalta, J.E., Chen, Y., Whitehead, E.H., Guimaraes, C., Panning, B., Ploegh, H.L., Bassik, M.C.*, et al.* (2014). Genome-Scale CRISPR-Mediated Control of Gene Repression and Activation. Cell *159*, 647-661.
Gilbert, Luke A., Larson, Matthew H., Morsut, L., Liu, Z., Brar, Gloria A., Torres, Sandra E., Stern-Ginossar, N., Brandman, O., Whitehead, Evan H., Doudna, Jennifer A.*, et al.* (2013). CRISPR-Mediated Modular RNA-Guided Regulation of Transcription in Eukaryotes. Cell *154*, 442-451.
Gillardin, P.-S., Descamps, G., Maiga, S., Tessoulin, B., Djamai, H., Lucani, B., Chiron, D., Moreau, P., Le Gouill, S., Amiot, M.*, et al.* (2017). Decitabine and Melphalan Fail to Reactivate p73 in p53 Deficient Myeloma Cells. Int J Mol Sci *19*, 40.
Ginzberg, M.B., Chang, N., D'Souza, H., Patel, N., Kafri, R., and Kirschner, M.W. (2018). Cell size sensing in animal cells coordinates anabolic growth rates and cell cycle progression to maintain cell size uniformity. eLife *7*.
Glick, B.S., and Nakano, A. (2009). Membrane traffic within the Golgi apparatus. Annu Rev Cell Dev Biol *25*, 113-132.
Gonzalez, T.N., Sidrauski, C., Dörfler, S., and Walter, P. (1999). Mechanism of non-spliceosomal mRNA splicing in the unfolded protein response pathway. *18*, 3119-3132.
Graham, J.M., Sumner, M.C.B., Curtis, D.H., and Pasternak, C.A. (1973). Sequence of Events in Plasma Membrane Assembly during the Cell Cycle. *246*, 291-295.
Güttinger, S., Laurell, E., and Kutay, U. (2009). Orchestrating nuclear envelope disassembly and reassembly during mitosis. Nature Reviews Molecular Cell Biology *10*, 178-191.
Halbleib, K., Pesek, K., Covino, R., Hofbauer, H.F., Wunnicke, D., Hanelt, I., Hummer, G., and Ernst, R. (2017). Activation of the Unfolded Protein Response by Lipid Bilayer Stress. Mol Cell *67*, 673-684 e678.
Han, C., Jin, L., Mei, Y., and Wu, M. (2013a). Endoplasmic reticulum stress inhibits cell cycle progression via induction of p27 in melanoma cells. Cellular Signalling *25*, 144-149.
Han, J., Back, S.H., Hur, J., Lin, Y.-H., Gildersleeve, R., Shan, J., Yuan, C.L., Krokowski, D., Wang, S., Hatzoglou, M.*, et al.* (2013b). ER-stress-induced

transcriptional regulation increases protein synthesis leading to cell death. Nature Cell Biology *15*, 481-490.
Hanahan, D., and Robert (2011). Hallmarks of Cancer: The Next Generation. Cell *144*, 646-674.
Hannigan, M.M., Hoffman, A.M., Thompson, J.W., Zheng, T., and Nicchitta, C.V. (2020). Quantitative proteomics links the LRRC59 interactome to mRNA translation on the ER membrane. bioRxiv, 2020.2003.2004.975474.
Harding, H.P., Zhang, Y., and Ron, D. (1999). Protein translation and folding are coupled by an endoplasmic-reticulum-resident kinase. Nature *397*, 271-274.
Harnoss, J.M., Le Thomas, A., Shemorry, A., Marsters, S.A., Lawrence, D.A., Lu, M., Chen, Y.-C.A., Qing, J., Totpal, K., Kan, D.*, et al.* (2019). Disruption of IRE1α through its kinase domain attenuates multiple myeloma. Proceedings of the National Academy of Sciences *116*, 16420-16429.
Hashida, K., Kitao, Y., Sudo, H., Awa, Y., Maeda, S., Mori, K., Takahashi, R., Iinuma, M., and Hori, O. (2012). ATF6alpha Promotes Astroglial Activation and Neuronal Survival in a Chronic Mouse Model of Parkinson's Disease. *7*, e47950.
Haze, K., Yoshida, H., Yanagi, H., Yura, T., and Mori, K. (1999). Mammalian Transcription Factor ATF6 Is Synthesized as a Transmembrane Protein and Activated by Proteolysis in Response to Endoplasmic Reticulum Stress. *10*, 3787-3799.
Hernandez-Segura, A., Nehme, J., and Demaria, M. (2018). Hallmarks of Cellular Senescence. Trends in Cell Biology *28*, 436-453.
Hettema, E.H., and Motley, A.M. (2009). How peroxisomes multiply. Journal of cell science *122*, 2331-2336.
Hetz, C., and Mollereau, B. (2014). Disturbance of endoplasmic reticulum proteostasis in neurodegenerative diseases. Nature Reviews Neuroscience *15*, 233-249.
Hetzer, M.W., Walther, T.C., and Mattaj, I.W. (2005). PUSHING THE ENVELOPE: Structure, Function, and Dynamics of the Nuclear Periphery. *21*, 347-380.
Hirai, H., Iwasawa, Y., Okada, M., Arai, T., Nishibata, T., Kobayashi, M., Kimura, T., Kaneko, N., Ohtani, J., Yamanaka, K.*, et al.* (2009). Small-molecule inhibition of Wee1 kinase by MK-1775 selectively sensitizes p53-deficient tumor cells to DNA-damaging agents. Mol Cancer Ther *8*, 2992-3000.
Ho, N., Yap, W.S., Xu, J., Wu, H., Koh, J.H., Goh, W.W.B., George, B., Chong, S.C., Taubert, S., and Thibault, G. (2020). Stress sensor Ire1 deploys a divergent transcriptional program in response to lipid bilayer stress. J Cell Biol *219*.
Hoffmann, I. (2000). The role of Cdc25 phosphatases in cell cycle checkpoints. *211*, 8-11.
Hollien, J., Lin, J.H., Li, H., Stevens, N., Walter, P., and Weissman, J.S. (2009). Regulated Ire1-dependent decay of messenger RNAs in mammalian cells. Journal of Cell Biology *186*, 323-331.
Hollien, J., and Weissman, J.S. (2006). Decay of Endoplasmic Reticulum-Localized mRNAs During the Unfolded Protein Response. Science *313*, 104-107.
Hu, Y., Chen, W., and Wang, J. (2019). Progress in the identification of gene mutations involved in multiple myeloma. Onco Targets Ther *12*, 4075-4080.

Hunter, T., and Pines, J. (1994). Cyclins and cancer II: Cyclin D and CDK inhibitors come of age. Cell *79*, 573-582.
Ishikawa K., I.H., Saito T. (2007). Damage-Dependent Cell Cycle Checkpoints and Genomic Stability. DNA and Cell Biology.
Jackman, J., and O'Connor, P.M. (1998). Methods for Synchronizing Cells at Specific Stages of the Cell Cycle. Current Protocols in Cell Biology *00*, 8.3.1-8.3.20.
Jacquemyn, J., Cascalho, A., and Goodchild, R.E. (2017). The ins and outs of endoplasmic reticulum-controlled lipid biosynthesis. EMBO Rep *18*, 1905-1921.
Jeffrey, P.D., Russo, A.A., Polyak, K., Gibbs, E., Hurwitz, J., Massagué, J., and Pavletich, N.P. (1995). Mechanism of CDK activation revealed by the structure of a cyclinA-CDK2 complex. Nature *376*, 313-320.
Jelsema, C.L., and Morré, D.J. (1978). Distribution of phospholipid biosynthetic enzymes among cell components of rat liver. Journal of Biological Chemistry *253*, 7960-7971.
Jonikas, M.C., Collins, S.R., Denic, V., Oh, E., Quan, E.M., Schmid, V., Weibezahn, J., Schwappach, B., Walter, P., Weissman, J.S.*, et al.* (2009). Comprehensive Characterization of Genes Required for Protein Folding in the Endoplasmic Reticulum. Science *323*, 1693-1697.
Kabachinski, G., and Schwartz, T.U. (2015). The nuclear pore complex - structure and function at a glance. Journal of Cell Science *128*, 423-429.
Karagöz, G.E., Acosta-Alvear, D., Nguyen, H.T., Lee, C.P., Chu, F., and Walter, P. (2017). An unfolded protein-induced conformational switch activates mammalian IRE1. eLife *6*.
Karagoz, G.E., Acosta-Alvear, D., and Walter, P. (2019). The Unfolded Protein Response: Detecting and Responding to Fluctuations in the Protein-Folding Capacity of the Endoplasmic Reticulum. Cold Spring Harb Perspect Biol *11*.
Kato, J., Matsushime, H., Hiebert, S.W., Ewen, M.E., and Sherr, C.J. (1993). Direct binding of cyclin D to the retinoblastoma gene product (pRb) and pRb phosphorylation by the cyclin D-dependent kinase CDK4. *7*, 331-342.
Killander, D., and Zetterberg, A. (1965a). A quantitative cytochemical investigation of the relationship between cell mass and initiation of DNA synthesis in mouse fibroblasts in vitro. *40*, 12-20.
Killander, D., and Zetterberg, A. (1965b). Quantitative cytochemical studies on interphase growth. *38*, 272-284.
Kirk, S.J., Cliff, J.M., Thomas, J.A., and Ward, T.H. (2010). Biogenesis of secretory organelles during B cell differentiation. *87*, 245-255.
Knoblach, B., Sun, X., Coquelle, N., Fagarasanu, A., Poirier, R.L., and Rachubinski, R.A. (2013). An ER-peroxisome tether exerts peroxisome population control in yeast. EMBO J *32*, 2439-2453.
Kobayashi, H., Stewart, E., Poon, R., Adamczewski, J.P., Gannon, J., and Hunt, T. (1992). Identification of the domains in cyclin A required for binding to, and activation of, p34cdc2 and p32cdk2 protein kinase subunits. *3*, 1279-1294.
Koch, G.L.E. (1990). The endoplasmic reticulum and calcium storage. BioEssays *12*, 527-531.

Koh, S.-B., Mascalchi, P., Rodriguez, E., Lin, Y., Jodrell, D.I., Richards, F.M., and Lyons, S.K. (2017). A quantitative FastFUCCI assay defines cell cycle dynamics at a single-cell level. Journal of Cell Science *130*, 512-520.
Kopp, M.C., Larburu, N., Durairaj, V., Adams, C.J., and Ali, M.M.U. (2019). UPR proteins IRE1 and PERK switch BiP from chaperone to ER stress sensor. Nature Structural & Molecular Biology *26*, 1053-1062.
Korennykh, A.V., Egea, P.F., Korostelev, A.A., Finer-Moore, J., Zhang, C., Shokat, K.M., Stroud, R.M., and Walter, P. (2009). The unfolded protein response signals through high-order assembly of Ire1. Nature *457*, 687-693.
Korennykh, A.V., Korostelev, A.A., Egea, P.F., Finer-Moore, J., Stroud, R.M., Zhang, C., Shokat, K.M., and Walter, P. (2011). Structural and functional basis for RNA cleavage by Ire1. BMC Biology *9*, 47.
Kornmann, B., Currie, E., Collins, S.R., Schuldiner, M., Nunnari, J., Weissman, J.S., and Walter, P. (2009). An ER-Mitochondria Tethering Complex Revealed by a Synthetic Biology Screen. Science *325*, 477-481.
Kosmaczewski, S.G., Edwards, T.J., Han, S.M., Eckwahl, M.J., Meyer, B.I., Peach, S., Hesselberth, J.R., Wolin, S.L., and Hammarlund, M. (2014). The R tc B RNA ligase is an essential component of the metazoan unfolded protein response. EMBO reports *15*, 1278-1285.
Lee, A.H., Iwakoshi, N.N., and Glimcher, L.H. (2003). XBP-1 Regulates a Subset of Endoplasmic Reticulum Resident Chaperone Genes in the Unfolded Protein Response. Molecular and Cellular Biology *23*, 7448-7459.
Lee, J.E., Cathey, P.I., Wu, H., Parker, R., and Voeltz, G.K. (2020). Endoplasmic reticulum contact sites regulate the dynamics of membraneless organelles. Science *367*, eaay7108.
Lee, K. (2002). IRE1-mediated unconventional mRNA splicing and S2P-mediated ATF6 cleavage merge to regulate XBP1 in signaling the unfolded protein response. *16*, 452-466.
Lees, E.M., and Harlow, E. (1993). Sequences within the conserved cyclin box of human cyclin A are sufficient for binding to and activation of cdc2 kinase. *13*, 1194-1201.
Liu, F., Stanton, J.J., Wu, Z., and Piwnica-Worms, H. (1997a). The human Myt1 kinase preferentially phosphorylates Cdc2 on threonine 14 and localizes to the endoplasmic reticulum and Golgi complex. *17*, 571-583.
Liu, F., Stanton, J.J., Wu, Z., and Piwnica-Worms, H. (1997b). The human Myt1 kinase preferentially phosphorylates Cdc2 on threonine 14 and localizes to the endoplasmic reticulum and Golgi complex. Molecular and cellular biology *17*, 571-583.
Lloyd, A.C. (2013). The Regulation of Cell Size. Cell *154*, 1194-1205.
Loud, A.V. (1968). A quantitative stereological description of the ultrastructure of normal rat liver parenchymal cells. The Journal of cell biology *37*, 27-46.
Lowe, M., Rabouille, C., Nakamura, N., Watson, R., Jackman, M., Jämsä, E., Rahman, D., Pappin, D.J., and Warren, G. (1998). Cdc2 kinase directly phosphorylates the cis-Golgi matrix protein GM130 and is required for Golgi fragmentation in mitosis. Cell *94*, 783-793.

Lu, L., Ladinsky, M.S., and Kirchhausen, T. (2009). Cisternal Organization of the Endoplasmic Reticulum during Mitosis. Molecular Biology of the Cell *20*, 3471-3480.
Lu, L., Ladinsky, M.S., and Kirchhausen, T. (2011). Formation of the postmitotic nuclear envelope from extended ER cisternae precedes nuclear pore assembly. *194*, 425-440.
Lu, M., Lawrence, D.A., Marsters, S., Acosta-Alvear, D., Kimmig, P., Mendez, A.S., Paton, A.W., Paton, J.C., Walter, P., and Ashkenazi, A. (2014a). Opposing unfolded-protein-response signals converge on death receptor 5 to control apoptosis. Science *345*, 98-101.
Lu, Y., Liang, F.-X., and Wang, X. (2014b). A Synthetic Biology Approach Identifies the Mammalian UPR RNA Ligase RtcB. *55*, 758-770.
Ly, T., Ahmad, Y., Shlien, A., Soroka, D., Mills, A., Emanuele, M.J., Stratton, M.R., and Lamond, A.I. (2014). A proteomic chronology of gene expression through the cell cycle in human myeloid leukemia cells. *3*.
Ly, T., Whigham, A., Clarke, R., Brenes-Murillo, A.J., Estes, B., Madhessian, D., Lundberg, E., Wadsworth, P., and Lamond, A.I. (2017). Proteomic analysis of cell cycle progression in asynchronous cultures, including mitotic subphases, using PRIMMUS. Elife *6*, e27574.
Macip, S., Kosoy, A., Lee, S.W., O'Connell, M.J., and Aaronson, S.A. (2006). Oxidative stress induces a prolonged but reversible arrest in p53-null cancer cells, involving a Chk1-dependent G2 checkpoint. Oncogene *25*, 6037-6047.
Maes, A., Menu, E., Veirman, K.D., Maes, K., Vand Erkerken, K., and De Bruyne, E. (2017). The therapeutic potential of cell cycle targeting in multiple myeloma. Oncotarget *8*, 90501-90520.
Maller, J.L., Gautier, J., Langan, T.A., Lohka, M.J., Shenoy, S., Shalloway, D., and Nurse, P. (1989). Maturation-promoting factor and the regulation of the cell cycle. *1989*, 53-63.
Malumbres, M., and Barbacid, M. (2001). To cycle or not to cycle: a critical decision in cancer. Nature Reviews Cancer *1*, 222-231.
Malzer, E., Daly, M.L., Moloney, A., Sendall, T.J., Thomas, S.E., Ryder, E., Ryoo, H.D., Crowther, D.C., Lomas, D.A., and Marciniak, S.J. (2010). Impaired tissue growth is mediated by checkpoint kinase 1 (CHK1) in the integrated stress response. Journal of Cell Science *123*, 2892-2900.
Manford, A.G., Stefan, C.J., Yuan, H.L., MacGurn, J.A., and Emr, S.D. (2012). ER-to-Plasma Membrane Tethering Proteins Regulate Cell Signaling and ER Morphology. Developmental Cell *23*, 1129-1140.
Marchi, S., Patergnani, S., Missiroli, S., Morciano, G., Rimessi, A., Wieckowski, M.R., Giorgi, C., and Pinton, P. (2018). Mitochondrial and endoplasmic reticulum calcium homeostasis and cell death. Cell Calcium *69*, 62-72.
Marciniak, S.J., Garcia-Bonilla, L., Hu, J., Harding, H.P., and Ron, D. (2006). Activation-dependent substrate recruitment by the eukaryotic translation initiation factor 2 kinase PERK. *172*, 201-209.
Matus, S., Valenzuela, V., Medinas, D.B., and Hetz, C. (2013). ER Dysfunction and Protein Folding Stress in ALS. *2013*, 1-12.
McIntosh, J.R. (2016). Mitosis. Cold Spring Harbor Perspectives in Biology *8*, a023218.

Meyerson, M., and Harlow, E. (1994). Identification of G1 kinase activity for cdk6, a novel cyclin D partner. *14*, 2077-2086.
Mimura, N., Fulciniti, M., Gorgun, G., Tai, Y.T., Cirstea, D., Santo, L., Hu, Y., Fabre, C., Minami, J., Ohguchi, H.*, et al.* (2012). Blockade of XBP1 splicing by inhibition of IRE1α is a promising therapeutic option in multiple myeloma. Blood *119*, 5772-5781.
Morgan, D.O. (1995). Principles of CDK regulation. Nature *374*, 131-134.
Mulkey, R.M., and Zucker, R.S. (1991). Action potentials must admit calcium to evoke transmitter release. *350*, 153-155.
Muller, P.A.J., and Vousden, K.H. (2013). p53 mutations in cancer. Nature Cell Biology *15*, 2-8.
Munro, S. (2003). Lipid Rafts. Cell *115*, 377-388.
Nadanaka, S., Okada, T., Yoshida, H., and Mori, K. (2007). Role of Disulfide Bridges Formed in the Luminal Domain of ATF6 in Sensing Endoplasmic Reticulum Stress. Molecular and Cellular Biology *27*, 1027-1043.
Nakajima, H., Toyoshima-Morimoto, F., Taniguchi, E., and Nishida, E. (2003). Identification of a consensus motif for Plk (Polo-like kinase) phosphorylation reveals Myt1 as a Plk1 substrate. J Biol Chem *278*, 25277-25280.
Nakajima, H., Yonemura, S., Murata, M., Nakamura, N., Piwnica-Worms, H., and Nishida, E. (2008a). Myt1 protein kinase is essential for Golgi and ER assembly during mitotic exit. Journal of Cell Biology *181*, 89-103.
Nakajima, H., Yonemura, S., Murata, M., Nakamura, N., Piwnica-Worms, H., and Nishida, E. (2008b). Myt1 protein kinase is essential for Golgi and ER assembly during mitotic exit. J Cell Biol *181*, 89-103.
Namba, M., Ohtsuki, T., Mori, M., Togawa, A., Wada, H., Sugihara, T., Yawata, Y., and Kimoto, T. (1989). Establishment of five human myeloma cell lines. In Vitro Cellular & Developmental Biology *25*, 723-729.
Naveau, M., Lazennec-Schurdevin, C., Panvert, M., Dubiez, E., Mechulam, Y., and Schmitt, E. (2013). Roles of yeast eIF2 and eIF2 subunits in the binding of the initiator methionyl-tRNA. *41*, 1047-1057.
Newport, J.W., and Forbes, D.J. (1987). The Nucleus: Structure, Function, and Dynamics. *56*, 535-565.
Ni, M., and Lee, A.S. (2007). ER chaperones in mammalian development and human diseases. FEBS Lett *581*, 3641-3651.
Nishitani, H., Lygerou, Z., Nishimoto, T., and Nurse, P. (2000). The Cdt1 protein is required to license DNA for replication in fission yeast. Nature *404*, 625-628.
Nunnari, J., and Walter, P. (1996). Regulation of Organelle Biogenesis. *84*, 389-394.
Nurse, P. (1994). Ordering S phase and M phase in the cell cycle. *79*, 547-550.
Obeng, E.A., Carlson, L.M., Gutman, D.M., Harrington, W.J., Jr., Lee, K.P., and Boise, L.H. (2006). Proteasome inhibitors induce a terminal unfolded protein response in multiple myeloma cells. Blood *107*, 4907-4916.
Olsen, J.V., Vermeulen, M., Santamaria, A., Kumar, C., Miller, M.L., Jensen, L.J., Gnad, F., Cox, J., Jensen, T.S., Nigg, E.A.*, et al.* (2010). Quantitative Phosphoproteomics Reveals Widespread Full Phosphorylation Site Occupancy During Mitosis. Science Signaling *3*, ra3.

Olzmann, J.A., and Carvalho, P. (2019). Dynamics and functions of lipid droplets. Nature Reviews Molecular Cell Biology *20*, 137-155.
Palmer, A., Gavin, A.C., and Nebreda, A.R. (1998). A link between MAP kinase and p34(cdc2)/cyclin B during oocyte maturation: p90(rsk) phosphorylates and inactivates the p34(cdc2) inhibitory kinase Myt1. EMBO J *17*, 5037-5047.
Papandreou, I., Denko, N.C., Olson, M., Van Melckebeke, H., Lust, S., Tam, A., Solow-Cordero, D.E., Bouley, D.M., Offner, F., Niwa, M.*, et al.* (2011). Identification of an Ire1alpha endonuclease specific inhibitor with cytotoxic activity against human multiple myeloma. Blood *117*, 1311-1314.
Pardee, A.B. (1974). A Restriction Point for Control of Normal Animal Cell Proliferation. Proceedings of the National Academy of Sciences *71*, 1286.
Periasamy, M., and Kalyanasundaram, A. (2007). SERCA pump isoforms: Their role in calcium transport and disease. Muscle & Nerve *35*, 430-442.
Peschek, J., Acosta-Alvear, D., Mendez, A.S., and Walter, P. (2015). A conformational RNA zipper promotes intron ejection during non-conventional XBP1 mRNA splicing. EMBO reports *16*, 1688-1698.
Pincus, D., Chevalier, M.W., Aragon, T., van Anken, E., Vidal, S.E., El-Samad, H., and Walter, P. (2010). BiP binding to the ER-stress sensor Ire1 tunes the homeostatic behavior of the unfolded protein response. PLoS Biol *8*, e1000415.
Plumb, R., Zhang, Z.R., Appathurai, S., and Mariappan, M. (2015). A functional link between the co-translational protein translocation pathway and the UPR. Elife *4*.
Prostko, C.R., Brostrom, M.A., and Brostrom, C.O. (1993). Reversible phosphorylation of eukaryotic initiation factor 2? in response to endoplasmic reticular signaling. *127-128*, 255-265.
Puhka, M., Vihinen, H., Joensuu, M., and Jokitalo, E. (2007). Endoplasmic reticulum remains continuous and undergoes sheet-to-tubule transformation during cell division in mammalian cells. *179*, 895-909.
Qi, L., Tsai, B., and Arvan, P. (2017). New Insights into the Physiological Role of Endoplasmic Reticulum-Associated Degradation. Trends in Cell Biology *27*, 430-440.
Rohde, J., Heitman, J., and Cardenas, M.E. (2001). The TOR Kinases Link Nutrient Sensing to Cell Growth. *276*, 9583-9586.
Rojas-Rivera, D., Delvaeye, T., Roelandt, R., Nerinckx, W., Augustyns, K., Vandenabeele, P., and Bertrand, M.J.M. (2017). When PERK inhibitors turn out to be new potent RIPK1 inhibitors: critical issues on the specificity and use of GSK2606414 and GSK2656157. Cell Death & Differentiation *24*, 1100-1110.
Roth, K., Oehme, L., Zehentmeier, S., Zhang, Y., Niesner, R., and Hauser, A.E. (2014). Tracking plasma cell differentiation and survival. Cytometry Part A *85*, 15-24.
Roussel, B.D., Kruppa, A.J., Miranda, E., Crowther, D.C., Lomas, D.A., and Marciniak, S.J. (2013). Endoplasmic reticulum dysfunction in neurological disease. *12*, 105-118.
Rowland, A.A., Chitwood, P.J., Phillips, M.J., and Voeltz, G.K. (2014). ER Contact Sites Define the Position and Timing of Endosome Fission. Cell *159*, 1027-1041.
Russell, P., and Nurse, P. (1987). Negative regulation of mitosis by wee1+, a gene encoding a protein kinase homolog. *49*, 559-567.

Sabapathy, K., and Lane, D.P. (2018). Therapeutic targeting of p53: all mutants are equal, but some mutants are more equal than others. Nature Reviews Clinical Oncology *15*, 13-30.
Sakaue-Sawano, A., Kurokawa, H., Morimura, T., Hanyu, A., Hama, H., Osawa, H., Kashiwagi, S., Fukami, K., Miyata, T., Miyoshi, H.*, et al.* (2008). Visualizing Spatiotemporal Dynamics of Multicellular Cell-Cycle Progression. Cell *132*, 487-498.
Satyanarayana, A., and Kaldis, P. (2009). Mammalian cell-cycle regulation: several Cdks, numerous cyclins and diverse compensatory mechanisms. Oncogene *28*, 2925-2939.
Scheuner, D., Song, B., McEwen, E., Liu, C., Laybutt, R., Gillespie, P., Saunders, T., Bonner-Weir, S., and Kaufman, R.J. (2001). Translational Control Is Required for the Unfolded Protein Response and In Vivo Glucose Homeostasis. Molecular Cell *7*, 1165-1176.
Schlaitz, A.-L., Thompson, J., Catherine, John, and Heald, R. (2013). REEP3/4 Ensure Endoplasmic Reticulum Clearance from Metaphase Chromatin and Proper Nuclear Envelope Architecture. *26*, 315-323.
Schmidt, M., Rohe, A., Platzer, C., Najjar, A., Erdman, F., and Sippl, W. (2017a). Regulation of G2/M Transition by Inhibition of WEE1 and PKMYT1 Kinases. Molecules *22*, 2045.
Schmidt, M., Rohe, A., Platzer, C., Najjar, A., Erdmann, F., and Sippl, W. (2017b). Regulation of G2/M Transition by Inhibition of WEE1 and PKMYT1 Kinases. Molecules *22*.
Schwartz, M.A., and Assoian, R.K. (1996). Cytoskeletal integrity is required throughout the mitogen stimulation phase of the cell cycle and mediates the anchorage-dependent expression of cyclin D1. Molecular Biology of the Cell *7*, 101-111.
Seyb, K.I., Ansar, S., Bean, J., and Michaelis, M.L. (2006). beta-Amyloid and endoplasmic reticulum stress responses in primary neurons: effects of drugs that interact with the cytoskeleton. J Mol Neurosci *28*, 111-123.
Shaffer, A.L., Shapiro-Shelef, M., Iwakoshi, N.N., Lee, A.-H., Qian, S.-B., Zhao, H., Yu, X., Yang, L., Tan, B.K., Rosenwald, A.*, et al.* (2004). XBP1, Downstream of Blimp-1, Expands the Secretory Apparatus and Other Organelles, and Increases Protein Synthesis in Plasma Cell Differentiation. Immunity *21*, 81-93.
Shahriyari, L., and Komarova, N.L. (2013). Symmetric vs. Asymmetric Stem Cell Divisions: An Adaptation against Cancer? PLoS ONE *8*, e76195.
Shen, J., Snapp, E.L., Lippincott-Schwartz, J., and Prywes, R. (2005). Stable Binding of ATF6 to BiP in the Endoplasmic Reticulum Stress Response. Molecular and Cellular Biology *25*, 921-932.
Sherr, C.J. (1994). G1 phase progression: Cycling on cue. Cell *79*, 551-555.
Sherr, C.J. (1996). Cancer Cell Cycles. Science *274*, 1672-1677.
Sherr, C.J., and Roberts, J.M. (1999). CDK inhibitors: positive and negative regulators of G1-phase progression. Genes & Development *13*, 1501-1512.
Shibata, Y., Shemesh, T., Prinz, W.A., Palazzo, A.F., Kozlov, M.M., and Rapoport, T.A. (2010). Mechanisms Determining the Morphology of the Peripheral ER. *143*, 774-788.

Shibata, Y., Voeltz, G.K., and Rapoport, T.A. (2006). Rough Sheets and Smooth Tubules. Cell *126*, 435-439.
Shima, D.T., Cabrera-Poch, N., Pepperkok, R., and Warren, G. (1998). An Ordered Inheritance Strategy for the Golgi Apparatus: Visualization of Mitotic Disassembly Reveals a Role for the Mitotic Spindle. Journal of Cell Biology *141*, 955-966.
Shoulders, M.D., Ryno, L.M., Genereux, J.C., Moresco, J.J., Tu, P.G., Wu, C., Yates III, J.R., Su, A.I., Kelly, J.W., and Wiseman, R.L. (2013). Stress-Independent Activation of XBP1s and/or ATF6 Reveals Three Functionally Diverse ER Proteostasis Environments. *3*, 1279-1292.
Sicari, D., Fantuz, M., Bellazzo, A., Valentino, E., Apollonio, M., Pontisso, I., Di Cristino, F., Dal Ferro, M., Bicciato, S., Del Sal, G.*, et al.* (2019). Mutant p53 improves cancer cells' resistance to endoplasmic reticulum stress by sustaining activation of the UPR regulator ATF6. Oncogene *38*, 6184-6195.
Sidrauski, C., Acosta-Alvear, D., Khoutorsky, A., Vedantham, P., Hearn, B.R., Li, H., Gamache, K., Gallagher, C.M., Ang, K.K.H., Wilson, C.*, et al.* (2013). Pharmacological brake-release of mRNA translation enhances cognitive memory. Elife *2*.
Sin, A.T., and Harrison, R.E. (2016). Growth of the Mammalian Golgi Apparatus during Interphase. Mol Cell Biol *36*, 2344-2359.
Smits, V.A.J., and Medema, R.H. (2001). Checking out the G2/M transition. *1519*, 1-12.
Solimini, N.L., Luo, J., and Elledge, S.J. (2007). Non-Oncogene Addiction and the Stress Phenotype of Cancer Cells. *130*, 986-988.
Soullam, B., and Worman, H.J. (1995). Signals and structural features involved in integral membrane protein targeting to the inner nuclear membrane. The Journal of Cell Biology *130*, 15-27.
Specht, K. (2004). Different mechanisms of cyclin D1 overexpression in multiple myeloma revealed by fluorescence in situ hybridization and quantitative analysis of mRNA levels. *104*, 1120-1126.
Sriburi, R., Jackowski, S., Mori, K., and Brewer, J.W. (2004). XBP1: a link between the unfolded protein response, lipid biosynthesis, and biogenesis of the endoplasmic reticulum. J Cell Biol *167*, 35-41.
Stumpf, C.R., Moreno, M.V., Olshen, A.B., Taylor, B.S., and Ruggero, D. (2013). The translational landscape of the mammalian cell cycle. Mol Cell *52*, 574-582.
Sundaram, A., Appathurai, S., Plumb, R., and Mariappan, M. (2018). Dynamic changes in complexes of IRE1alpha, PERK, and ATF6alpha during endoplasmic reticulum stress. Mol Biol Cell *29*, 1376-1388.
Sütterlin, C., Lin, C.Y., Feng, Y., Ferris, D.K., Erikson, R.L., and Malhotra, V. (2001). Polo-like kinase is required for the fragmentation of pericentriolar Golgi stacks during mitosis. Proc Natl Acad Sci U S A *98*, 9128-9132.
Terasaki, M. (1986). Microtubules and the endoplasmic reticulum are highly interdependent structures. *103*, 1557-1568.
Terasaki, M., Shemesh, T., Kasthuri, N., Klemm, R.W., Schalek, R., Hayworth, K.J., Hand, A.R., Yankova, M., Huber, G., Lichtman, J.W.*, et al.* (2013). Stacked endoplasmic reticulum sheets are connected by helicoidal membrane motifs. Cell *154*, 285-296.

Thomas, S.E., Malzer, E., Ordonez, A., Dalton, L.E., van 't Wout, E.F., Liniker, E., Crowther, D.C., Lomas, D.A., and Marciniak, S.J. (2013). p53 and translation attenuation regulate distinct cell cycle checkpoints during endoplasmic reticulum (ER) stress. J Biol Chem *288*, 7606-7617.
Tirasophon, W., Lee, K., Callaghan, B., Welihinda, A., and Kaufman, R.J. (2000). The endoribonuclease activity of mammalian IRE1 autoregulates its mRNA and is required for the unfolded protein response. Genes Dev *14*, 2725-2736.
Tirasophon, W., Welihinda, A.A., and Kaufman, R.J. (1998). A stress response pathway from the endoplasmic reticulum to the nucleus requires a novel bifunctional protein kinase/endoribonuclease (Ire1p) in mammalian cells. Genes Dev *12*, 1812-1824.
Toledo, C.M., Ding, Y., Hoellerbauer, P., Davis, R.J., Basom, R., Girard, E.J., Lee, E., Corrin, P., Hart, T., Bolouri, H.*, et al.* (2015). Genome-wide CRISPR-Cas9 Screens Reveal Loss of Redundancy between PKMYT1 and WEE1 in Glioblastoma Stem-like Cells. Cell Rep *13*, 2425-2439.
Torres, S.E., Gallagher, C.M., Plate, L., Gupta, M., Liem, C.R., Guo, X., Tian, R., Stroud, R.M., Kampmann, M., Weissman, J.S.*, et al.* (2019). Ceapins block the unfolded protein response sensor ATF6α by inducing a neomorphic inter-organelle tether. eLife *8*.
Travers, K.J., Patil, C.K., Wodicka, L., Lockhart, D.J., Weissman, J.S., and Walter, P. (2000). Functional and Genomic Analyses Reveal an Essential Coordination between the Unfolded Protein Response and ER-Associated Degradation. Cell *101*, 249-258.
Uemura, A., Oku, M., Mori, K., and Yoshida, H. (2009). Unconventional splicing of XBP1 mRNA occurs in the cytoplasm during the mammalian unfolded protein response. *122*, 2877-2886.
Uhlén, M., Fagerberg, L., Hallström, B.M., Lindskog, C., Oksvold, P., Mardinoglu, A., Sivertsson, Å., Kampf, C., Sjöstedt, E., Asplund, A.*, et al.* (2015). Tissue-based map of the human proteome. Science *347*, 1260419.
Urra, H., Henriquez, D.R., Canovas, J., Villarroel-Campos, D., Carreras-Sureda, A., Pulgar, E., Molina, E., Hazari, Y.M., Limia, C.M., Alvarez-Rojas, S.*, et al.* (2018). IRE1alpha governs cytoskeleton remodelling and cell migration through a direct interaction with filamin A. Nat Cell Biol *20*, 942-953.
van Vliet, A.R., Giordano, F., Gerlo, S., Segura, I., Van Eygen, S., Molenberghs, G., Rocha, S., Houcine, A., Derua, R., Verfaillie, T.*, et al.* (2017). The ER Stress Sensor PERK Coordinates ER-Plasma Membrane Contact Site Formation through Interaction with Filamin-A and F-Actin Remodeling. Mol Cell *65*, 885-899 e886.
Vattem, K.M., and Wek, R.C. (2004). Reinitiation involving upstream ORFs regulates ATF4 mRNA translation in mammalian cells. Proceedings of the National Academy of Sciences *101*, 11269-11274.
Vedrenne, C. (2005). Phosphorylation Controls CLIMP-63-mediated Anchoring of the Endoplasmic Reticulum to Microtubules. *16*, 1928-1937.
Vidal, R.L., and Hetz, C. (2012). Crosstalk between the UPR and autophagy pathway contributes to handling cellular stress in neurodegenerative disease. *8*, 970-972.

Villeneuve, J., Scarpa, M., Ortega-Bellido, M., and Malhotra, V. (2013). MEK1 inactivates Myt1 to regulate Golgi membrane fragmentation and mitotic entry in mammalian cells. EMBO J *32*, 72-85.
Vitale, M., Bakunts, A., Orsi, A., Lari, F., Tadè, L., Danieli, A., Rato, C., Valetti, C., Sitia, R., Raimondi, A.*, et al.* (2019). Inadequate BiP availability defines endoplasmic reticulum stress. eLife *8*.
Vodermaier, H.C. (2004). APC/C and SCF: Controlling Each Other and the Cell Cycle. Curr Biol *14*, R787-R796.
Volmer, R., Van Der Ploeg, K., and Ron, D. (2013). Membrane lipid saturation activates endoplasmic reticulum unfolded protein response transducers through their transmembrane domains. Proceedings of the National Academy of Sciences *110*, 4628-4633.
Walter, P., and Blobel, G. (1981). Translocation of proteins across the endoplasmic reticulum III. Signal recognition protein (SRP) causes signal sequence-dependent and site-specific arrest of chain elongation that is released by microsomal membranes. The Journal of Cell Biology *91*, 557-561.
Walter, P., and Blobel, G. (1982). Signal recognition particle contains a 7S RNA essential for protein translocation across the endoplasmic reticulum. *299*, 691-698.
Walter, P., and Ron, D. (2011). The Unfolded Protein Response: From Stress Pathway to Homeostatic Regulation. Science *334*, 1081-1086.
Wang, N., and Rapoport, T.A. (2019). Reconstituting the reticular ER network – mechanistic implications and open questions. Journal of Cell Science *132*, jcs227611.
Wang, Y., Li, J., Booher, R.N., Kraker, A., Lawrence, T., Leopold, W.R., and Sun, Y. (2001). Radiosensitization of p53 mutant cells by PD0166285, a novel G(2) checkpoint abrogator. Cancer Res *61*, 8211-8217.
Warren, G., and Wickner, W. (1996). Organelle Inheritance. *84*, 395-400.
Waterman-Storer, C.M., and Salmon, E.D. (1998). Endoplasmic reticulum membrane tubules are distributed by microtubules in living cells using three distinct mechanisms. Curr Biol *8*, 798-807.
Wei, W., Ayad, N.G., Wan, Y., Zhang, G.-J., Kirschner, M.W., and Kaelin, W.G. (2004). Degradation of the SCF component Skp2 in cell-cycle phase G1 by the anaphase-promoting complex. Nature *428*, 194-198.
Weinberg, R.A. (1995). The retinoblastoma protein and cell cycle control. Cell *81*, 323-330.
Wells, N.J., Watanabe, N., Tokusumi, T., Jiang, W., Verdecia, M.A., and Hunter, T. (1999). The C-terminal domain of the Cdc2 inhibitory kinase Myt1 interacts with Cdc2 complexes and is required for inhibition of G(2)/M progression. Journal of Cell Science *112*, 3361.
West, M., Zurek, N., Hoenger, A., and Voeltz, G.K. (2011). A 3D analysis of yeast ER structure reveals how ER domains are organized by membrane curvature. The Journal of Cell Biology *193*, 333-346.
Wilson, E. (1947). The cell in development and heredity (New York Macmillan Co).
Yamamoto, K., Sato, T., Matsui, T., Sato, M., Okada, T., Yoshida, H., Harada, A., and Mori, K. (2007). Transcriptional Induction of Mammalian ER Quality Control

Proteins Is Mediated by Single or Combined Action of ATF6α and XBP1. *13*, 365-376.
Yang, K., Hitomi, M., and Stacey, D.W. (2006). Variations in cyclin D1 levels through the cell cycle determine the proliferative fate of a cell. Cell Div *1*, 32-32.
Ye, J., Rawson, R.B., Komuro, R., Chen, X., Davé, U.P., Prywes, R., Brown, M.S., and Goldstein, J.L. (2000). ER Stress Induces Cleavage of Membrane-Bound ATF6 by the Same Proteases that Process SREBPs. Molecular Cell *6*, 1355-1364.
Yoshida, H. (1998). Identification of the cis-Acting Endoplasmic Reticulum Stress Response Element Responsible for Transcriptional Induction of Mammalian Glucose-regulated Proteins. INVOLVEMENT OF BASIC LEUCINE ZIPPER TRANSCRIPTION FACTORS. *273*, 33741-33749.
Zhang, F., Hamanaka, R.B., Bobrovnikova-Marjon, E., Gordan, J.D., Dai, M.-S., Lu, H., Simon, M.C., and Diehl, J.A. (2006). Ribosomal Stress Couples the Unfolded Protein Response to p53-dependent Cell Cycle Arrest. *281*, 30036-30045.
Zhu, H. (2012). Cell Proliferation Assay by Flow Cytometry (BrdU and PI Staining). Bio-protocol *2*, e198.
Zhu, H., Bhatt, B., Sivaprakasam, S., Cai, Y., Liu, S., Kodeboyina, S.K., Patel, N., Savage, N.M., Sharma, A., Kaufman, R.J.*, et al.* (2019). Ufbp1 promotes plasma cell development and ER expansion by modulating distinct branches of UPR. Nat Commun *10*, 1084-1084.
Zyryanova, A.F., Weis, F., Faille, A., Alard, A.A., Crespillo-Casado, A., Sekine, Y., Harding, H.P., Allen, F., Parts, L., Fromont, C.*, et al.* (2018). Binding of ISRIB reveals a regulatory site in the nucleotide exchange factor eIF2B. Science *359*, 1533.

Appendix

Figure S1. Ponceau stains on blots used for G_1 and S/G_2 sort data. Cell lysates were normalized by cell numbers attained at the FACS. 1 million cells were lysed in 200µL Laemmli buffer for subsequent analysis. Lanes 1, 2 are H4dCas9. Lanes 3,4 are KMS11dCas9

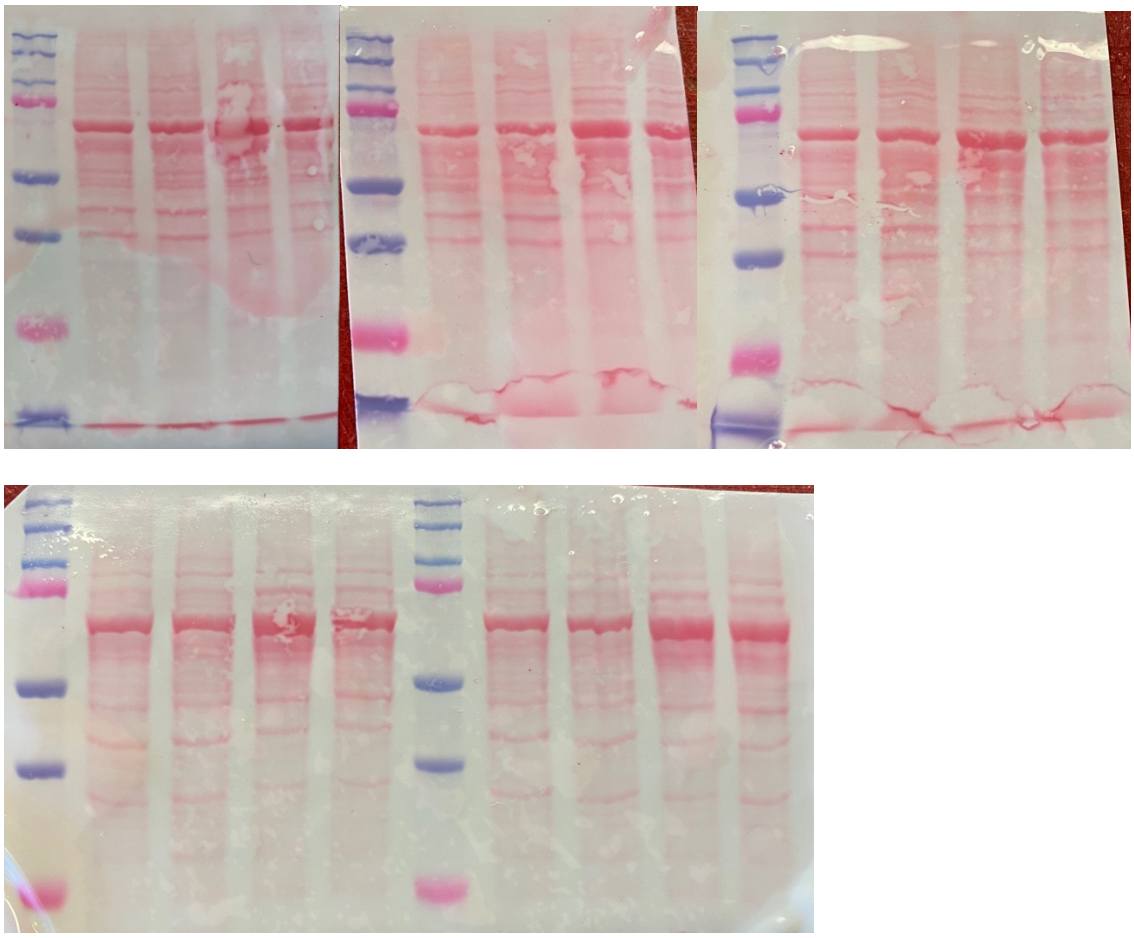

Table S1. Primers used for qPCR

Primer Name	Primer sequence, 5’ to 3’
Hs_28S F	AAACTCTGGTGGAGGTCCGT
HS_28S R	CTTACCAAAAGTGGCCCACTA
Hs_ATF6_RT_L	CCTGCTGTTACCAGCTACCAC
Hs_ATF6_RT_R	CCAAAGAAGGTGTTGGTTTGA
Hs_BLOC1S1_ex3-3'UTR_RT_L	AGCTGGACCATGAGGTGAAG
Hs_BLOC1S1_ex3-3'UTR_RT_R	CTGCAGCTGCCCTTTGTAG
Hs_CANX_RT_L	TCAACCGGATGTGAAGGAA
Hs_CANX_RT_R	CACTCTCTTCGTGGCTTTCTG
Hs_CCNA2_3'UTR_RT_L	CATGGACCTTCACCAGACCT
Hs_CCNA2_3'UTR_RT_R	TGTACTTGGCCACAACTTCTGT
Hs_CCNB1_ex3-4_RT_L	TACCTATGCTGGTGCCAGTG
Hs_CCNB1_ex3-4_RT_R	GGATCAGCTCCATCTTCTGC
Hs_CCND1_3'UTR_RT_L	CTGAGGAGCCCCAACAACT
Hs_CCND1_3'UTR_RT_R	TGGGGTCCATGTTCTGCT
Hs_CCNE1_3'UTR_RT_L	CCCACAGAGACAGCTTGGAT
Hs_CCNE1_3'UTR_RT_R	TCTTTGGTGGAGAAGGATGG
Hs_DDIT3_RT_L3	TTAAGTCTAAGGCACTGAGCGTATC
Hs_DDIT3_RT_R3	TGCTTTCAGGTGTGGTGATG
Hs_EIF2AK3_RT_L	CCATTCAGCACTCAGATGGA
Hs_EIF2AK3_RT_R	GTTCCCGATGAACTCAAGGA

Hs_ERN1_RT_L	CGTGGTGAAGATGGACTGG
Hs_ERN1_RT_R	GTAGGTGTGTGCGAGGAGGT
Hs_GAPDH_RT_L	AGCCACATCGCTCAGACAC
Hs_GAPDH_RT_R	TGGAAGATGGTGATGGGATT
Hs_HSPA5_RT_L	TGCAGCAGGACATCAAGTTC
Hs_HSPA5_RT_R	AGTTCCAGCGTCTTTGGTTG
Hs_PKMYT1_1.2.3_RT_L	GGAGGAACTTACCGTCTACCG
Hs_PKMYT1_1.2.3_RT_R	CACGTGAATCCAGGGTGTC
Hs_XBP1_both_RT_L	GGAGTTAAGACAGCGCTTGG
Hs_XBP1_both_RT_R	ACTGGGTCCAAGTTGTCCAG
Hs_XBP1s_RT_L	AGCTTTTACGAGAGAAAACTCAT
Hs_XBP1s_RT_R	CCTGCACCTGCTGCG

Table S2. Primers used for cloning

Primer Name	Primer sequence, 5’ to 3’
BsrGI-PKMYT1 Fwd	ATGGACGAGCTGTACAAGATGCTAGAACGGCCTCCTGCACT
EcoRI-PKMYT1 Rev	TGAGTGAATTCTCAGGTTGGGTCTAGGGTGTCCTCAAACAGGCT

Table S3. sgRNA sequences for CRISPRi cell lines

Target	Sequence, 5’ to 3’

PKMYT1_1	CCACCTTGTTGGGGGCGTCCGGAACAGTCGAGTTTAAGAGC TAAGCTG
PKMYT1_2	CCACCTTGTTGGTCACGGGAGTCCTCCGCCCGTTTAAGAGCT AAGCTG
ERN1_1	CCACCTTGTTGGGGCGGTGACCGAGCCTCAGGTTTAAGAGC TAAGCTG

Table S4. Primary antibodies used

Antibody Name	Company, Catalog number	Working dilution, WB	Working dilution, flow cytometry or immunofluorescence
ATF4	Cell Signaling Technology,11815S	1:1,000	
ATF6	Imgenex, IMG273	1:1,000	
BiP	Cell Signaling Technology, 3177S	1:1,000	1:500
Calnexin	Cell Signaling Technology, 2679S	1:1,000	1:500
CHOP	Cell Signaling Technology, 2895S	1:1,000	
Cyclin A2	Cell Signaling Technology, 4656T	1:1,000	

Cyclin B1	Cell Signaling Technology,12231T	1:1,000	
Cyclin D1	Cell Signaling Technology, 2926	1:1,000	
Cyclin E2	Cell Signaling Technology, 4132T	1:1,000	
eIF2alpha	Cell Signaling Technology, 9722S	1:1,000	
GFP	Invitrogen, A-11122	1:1,000	
GM130	BD Biosciences, 610822		1:1,000
IRE1alpha	Cell Signaling Technology, 3294S	1:1,000	1:500
PDI	Cell Signaling Technology, 3501P	1:1,000	1:500
PERK	Cell Signaling Technology, 5683S	1:1,000	
phosphorylated eIF2alpha	Cell Signaling Technology, 9721S	1:1,000	
PKMYT1	Cell Signaling Technology, 4282S	1:1,000	
XBP1s	Cell Signaling Technology, 12782S	1:1,000	

Table S5. Secondary Antibodies used

Name	Company, Catalog Number	Western Blot dilution	IFA dilution or flow cytometry dilution
Mouse-HRP	BioRad, 1706516	1:4,000	
Rabbit-HRP	BioRad, 1706515	1:4,000	
AlexaFluor 588 anti-mouse	Invitrogen, A-11004		1:1,000
AlexaFluor 647 anti-rabbit	Invitrogen, A-21245		1:1,000